The mechanical properties of prostatic tissue: the relationship to morphology and the response to alpha blocker therapy

By

Steve Ken Wing Leung

Doctor of Medicine

University of Edinburgh

2013

Declaration

I, Steve Ken Wing Leung, hereby declare that the thesis has been composed by me and that the work is as a result of my own independent investigation unless otherwise stated. This work has not been submitted for any other degree or professional qualification. This is in accordance with regulation 2.5 of the University of Edinburgh postgraduate assessment regulations for research degrees.

.....

Steve Ken Wing Leung

15/08/2013

Date

Abstract

Benign prostatic hyperplasia (BPH) is a common disease of aging men and the development of lower urinary tract symptoms (LUTS) secondary to BPH is believed to be caused by both a static and dynamic component to bladder outflow obstruction (BOO). The static component is attributed to the mass effect of the enlarged adenoma, whereas the dynamic component is related to the smooth muscle tone within the prostate. The prostate is a heterogeneous organ and comprises three distinct anatomical "zones". The formation of stromal and glandular nodules is the histological hallmarks of BPH and occurs in the transition zone. The mechanical properties of benign prostate tissue obtained from transurethral resection (TURP) have been shown to reflect the underlying morphology with respect to smooth muscle content. To further investigate the structure-property relationship in benign prostate tissue, specimens from TURP and whole prostates from cystoprostatectomy were examined. The use of transverse sections of the whole gland allowed morphometric and mechanical studies to be performed in all regions of the prostate. A novel method of morphometric analysis representative of the local area of tissue that was subjected to mechanical testing was developed. Significant correlations were shown between the mechanical and morphological properties of glandular and stromal nodules. Glandular nodules may contribute to the pathophysiology of BPH by altering the dynamic characteristics of the prostate in addition to producing a mass effect.

In parallel to the above aforementioned work in whole prostates, the effect of quinazoline and non-quinazoline based alpha-blockers upon prostate tissue obtained

from TURP was examined. This work also investigated whether alpha blocker therapy influenced the mechanical measurements by their action within the prostate tissue. Significant correlations were shown between alpha blocker therapy and the underlying morphology and this is reflected in the mechanical measurements.

These studies provide a greater understanding of the structure-property relationships within prostate tissue and it is likely that assessment of the mechanical properties of the prostate will be useful in the clinical evaluation and management of patients with benign prostate disease.

Abstract: 333 words.

To my wife, Gillian

Acknowledgments

I was fortunate enough to be given the opportunity to be part of a strong multidisciplinary team of engineers, urologists, cell biologists and physicists all striving to understand the mechanical and morphological aspects of prostate disease. The project grew from an idea between Alan McNeill and Bob Reuben in developing novel approaches to assess this disease.

I would like to thank my supervisor, Fouad Habib, who has provided a lot of his time, knowledge and enthusiasm to ensure that I completed this project. He was always available at short notice to discuss teething problems or just to provide ideas to ensure I was going in the right direction. I would also like to thank Dr Ken Grigor who was always on hand to ensure that I obtained the tissue specimens that I required for the project. He was also an invaluable source of knowledge regarding the pathology of the prostate. Despite his busy schedule, he managed to make time to discuss important aspects of my work.

I have been fortunate enough to work with a fellow researcher, Jimmy Yang, who has been invaluable in terms of carrying out the mechanical testing of prostate tissue and for providing scientific, mathematical and technical advice about areas of the project that I was unsure about.

I also want to thank Prof. Bob Reuben who always provided valuable advice and ideas at our regular steering group meetings. His explanations of the principles of mechanical engineering has been invaluable to a clinician like myself in understanding this other side of the project.

Finally I would like to thank Alan McNeill who has constantly provided support and encouragement and enthusiasm. Despite having a busy clinical schedule, he was always at hand to provide advice on the clinical aspects of the project.

Contents

APPENDICES

List of Figures

List of Tables

Abbreviations

BPH	Benign Prostatic Hyperplasia
BAUS	British Association of Urological Surgeons
BOO	Bladder Outflow Obstruction
BPO	Benign Prostatic Obstruction
CI	Collagen Type I
CIII	Collagen Type III
CT	Computed Tomography
CZ	Central Zone
DAB	Diaminobenzidine
DHT	Dihydrotestosterone
EGF	Epidermal Growth Factor
|E*|	Amplitude Ratio
ERSPC	European Randomized Study of Screening for Prostate Cancer
ET	Epithelial Tissue
Fcrit	Critical F Value
FGF	Fibroblast Growth Factor
FSH	Follicle Stimulating Hormone
GAG	Glycosaminoglycan
HCl	Hydrochloric Acid
HIER	Heat Induced Epitope Retrieval
H2O2	Hydrogen Peroxide
IGF	Insulin-like Growth Factor
IHC	Immunohistochemistry
IPSS	International Prostate Symptom Score
LH	Lutenizing Hormone
LH-RH	Lutenizing Hormone Releasing Hormone
LREC	Lothian Research Ethic Committee
LUTS	Lower Urinary Tract Symptoms
MRI	Magnetic Resonance Imaging

MTOPS	Medical Therapy of Prostatic Symptoms
NaOH	Sodium Hydroxide
PBS	Phosphate Buffered Saline
PCa	Prostate Cancer
PCAR	Presumed Circle Area Ratio
PDGF	Platelet Derived Growth Factor
PLESS	Proscar Long Term Efficacy Study
PREDICT	Prospective European Doxazosin and Combination Therapy Trial
PSA	Prostate Specific Antigen
PVR	Post Void Residual
PZ	Peripheral Zone
Qmax	Maximum Flow Rate
QOL	Quality of Life
SM	Smooth Muscle
Tan δ	Phase Lag
TBS	Tris Buffered Saline
TCC	Transitional Cell Carcinoma
TGF-α	Transforming Growth Factor-alpha
TGF-β	Transforming Growth Factor-beta
TRUS	Transrectal Ultrasound Scan
TURP	Transurethral Resection of the Prostate
TZ	Transition Zone
TZI	Transition Zone Index
UTI	Urinary Tract Infection
VA	Veterans Affairs Study
WW	Watchful Waiting

Chapter One

Introduction

1. The Prostate

The prostate gland is part of the male reproductive system. The prostate produces alkaline fluid that is secreted into the urethra at the time of emission of semen, providing an added medium for the life and motility of sperm.

1.1.1. Embryology and Development of the prostate

The prostate develops from the urogenital sinus, a subdivision of the cloaca. The urogenital sinus arises during the 7^{th} week of gestation but prostatic morphogenesis, under the influence of circulating dihydrotestosterone (DHT), does not occur until the 10^{th} to 12^{th} week. The initial event of prostatic morphogenesis is the outgrowth and branching of epithelial buds from the urogenital epithelium into the surrounding urogenital mesenchyme. The upper epithelial buds form the inner zone of the prostate and are of mesodermal origin whereas the lower buds form the outer zone and are of endodermal origin [1]. The different zones are affected by differing pathology later in life.

Throughout the development of the prostate, there are close interactions between the stromal and the epithelial elements. Classic tissue recombination studies by Cunha *et al* have demonstrated that the androgen receptors within the mesenchyme and not the epithelium are required for normal prostate development [2, 3]. Morphogenesis of the epithelial cells and homeostasis is driven, in part, by the stromal cells in response to DHT induction of several specific soluble growth factors in addition to alterations

in the insoluble extracellular matrix [4, 5]. There are a wide variety of genes and cellular pathways identified in the regulation of prostate development. These have been recently reviewed by Leong *et al* [6] and Matusik *et al* [7].

1.1.2. Gross Anatomy of the prostate

The normal prostate weighs around 20g and resides in the pelvis. The prostate is ovoid in shape and has anterior, posterior and lateral surfaces with a broad base superiorly, which is continuous with the bladder neck and a narrowed apex inferiorly, which is continuous with the urethral sphincter (see figure 1.1). The prostate is enclosed by a thin capsule, which on the anterior and anterolateral aspects, blends with the visceral continuation of the endopelvic fascia. At the apex of the gland, this capsule is absent and superiorly, there is no capsule between the prostate and bladder neck. The prostate is a relatively fixed organ with the puboprostatic ligaments extending anteriorly to anchor the prostate to the pelvic bone. Microscopic bands of smooth muscle extend from the posterior surface to fuse with Denonvilliers' fascia.

The urethra traverses the whole length of the prostate and at the midpoint, the urethra angles anteriorly by approximately 35 degrees. This angle divides the prostatic urethra into proximal and distal segments where the majority of the glands within the prostate open out into.

The arterial supply to the prostate arises from the inferior vesical artery and the venous drainage from the periprostatic venous plexus. The prostate receives

sympathetic and parasympathetic innervation from the pelvic plexus via the cavernous nerves.

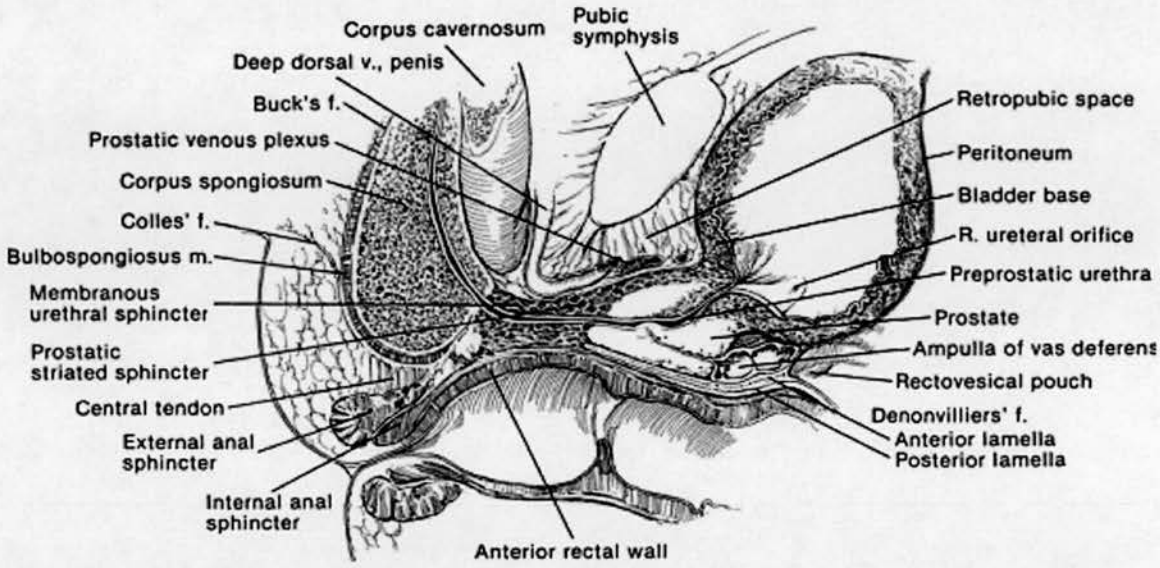

Figure 1.1: Saggital section through the prostatic and membranous urethra, demonstrating the midline relations of the pelvic structures

1.1.3. Zonal anatomy of the prostate

The glandular elements of the prostate are tubuloalveolar epithelial glands showing simple branching and lined with simple or columnar epithelium. The flattened basal cells line each acinar and are the stem cells for the secretory epithelium. The stromal elements consist predominantly of connective tissue, smooth muscle cells and fibroblasts and serves as a structural support for the epithelial glands. The prostate can be considered as three zones as described by McNeal [8]. Figure 1.2 shows a graphical representation of the zonal anatomy of prostate. The transition zone (TZ) surrounds the urethra proximal to the ejaculatory ducts and only accounts for 5-10%

of the glandular tissue in a normal prostate. McNeal demonstrated that benign prostatic hyperplasia (BPH) first develops in the periurethral transition zone of the prostate [9]. The central zone (CZ) surrounds the ejaculatory ducts and accounts for 20% of the prostate volume and peripheral zone (PZ) accounts for the majority of the volume of the normal prostate in the apical, posterior and lateral aspects of the gland. 70% of prostate cancers arise within the peripheral zone. The anterior fibromuscular stroma (AFS) is contiguous with the bladder neck to the striated external sphincter.

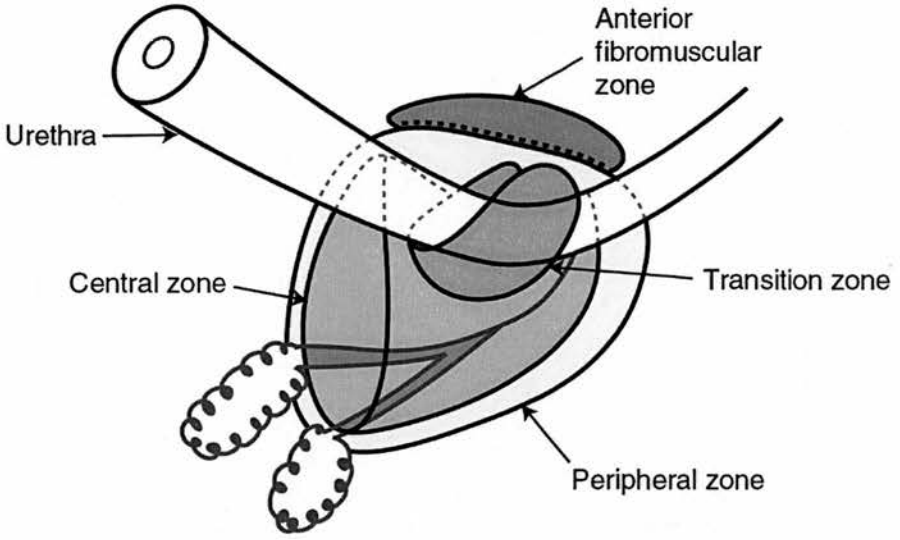

Figure 1.2: Zonal anatomy of the prostate as described by McNeal.

1.1.4. Regulation of normal growth of the prostate

Once the normal prostate reaches its maximal adult size, it enters a maintenance phase. During this phase, cell proliferation and programmed cell death (apoptosis) occur continuously in a balanced fashion so that the size of the gland remains constant [10]. The systems involved in this regulation of growth include steroid hormones such as testosterone and oestrogen, growth factors, and their interactions with the extracellular matrix. These are briefly considered below.

Steroid hormones

The testes produce 95% of the circulating serum androgen, testosterone. The remaining 5% is from the conversion of adrenal steroids dehydroepiandrosterone and androstenedione. With the majority of testosterone bound to sex hormone binding globulin (SHBG), only the free testosterone is able to enter the prostate by diffusion. Within the cell, it is converted to DHT by the enzyme, 5 α-reductase. DHT then binds to the androgen receptor and stimulates, via a series of intracellular events, the expression of specific genes and therefore, translation of proteins. These steps occur both in the prostate epithelial cells but also within the stromal cells.

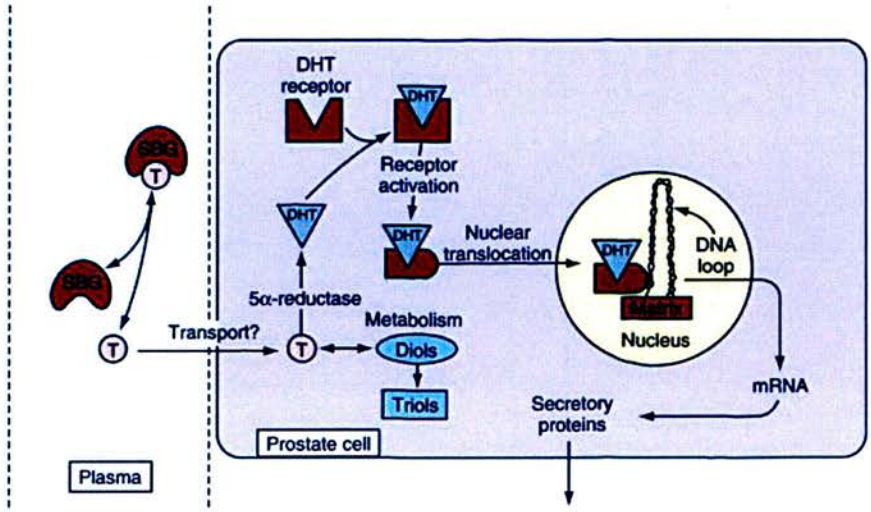

Figure 1.3: Schematic diagram illustrating the intra-cellular effects of testosterone in an epithelial cell.

Oestrogens are formed from the metabolism of circulating androgens within and out with the cell. In canine prostate studies, oestrogens do not antagonise the androgen effects upon the prostate, but instead have synergistic effects [11]. In human studies, it has been shown that oestrogens have a stimulatory effect on prostatic stroma whilst causing involution of the epithelial component [12]. Distribution of oestrogen receptors (ER) and oestrogen binding are heterogeneous within the prostate. ER-α is found predominantly within the stromal compartment and ER-β is mainly found within the epithelial compartment and it seems that oestrogens have their main effects upon the stromal compartment [13, 14]. However, the mechanisms of androgen and oestrogen synergism are not well understood and it is not clear whether anti-oestrogens could play a role in the treatment of abnormal prostate growth [15].

Stromal and epithelial interactions

As discussed in section 1.1.1, the organogenesis of the prostate is dependent on the important mesenchymal-epithelial interactions. The extracellular matrix, which itself has growth factor-like properties, provides the necessary scaffolding for this two-way flow of paracrine signals between the epithelial and stromal compartments. Cell to cell and extracellular matrix interactions are increasingly studied to understand how the phenotype of a cell is regulated. Getzenberg *et al* demonstrated that the interactions of the extracellular matrix regulate many aspects of DNA functions involved in cellular growth and differentiation [16].

Growth Factors

Growth factors are small polypeptides that promote or inhibit cellular proliferation but also have other multifunctional roles in cellular regulation [17]. The cell is prompted to synthesise a growth factor by signals such as paracrine communication or hormonal levels. Figure 1.4 demonstrates a schematic diagram of the complex interactions between androgens and various growth factors upon both stroma and epithelial cells.

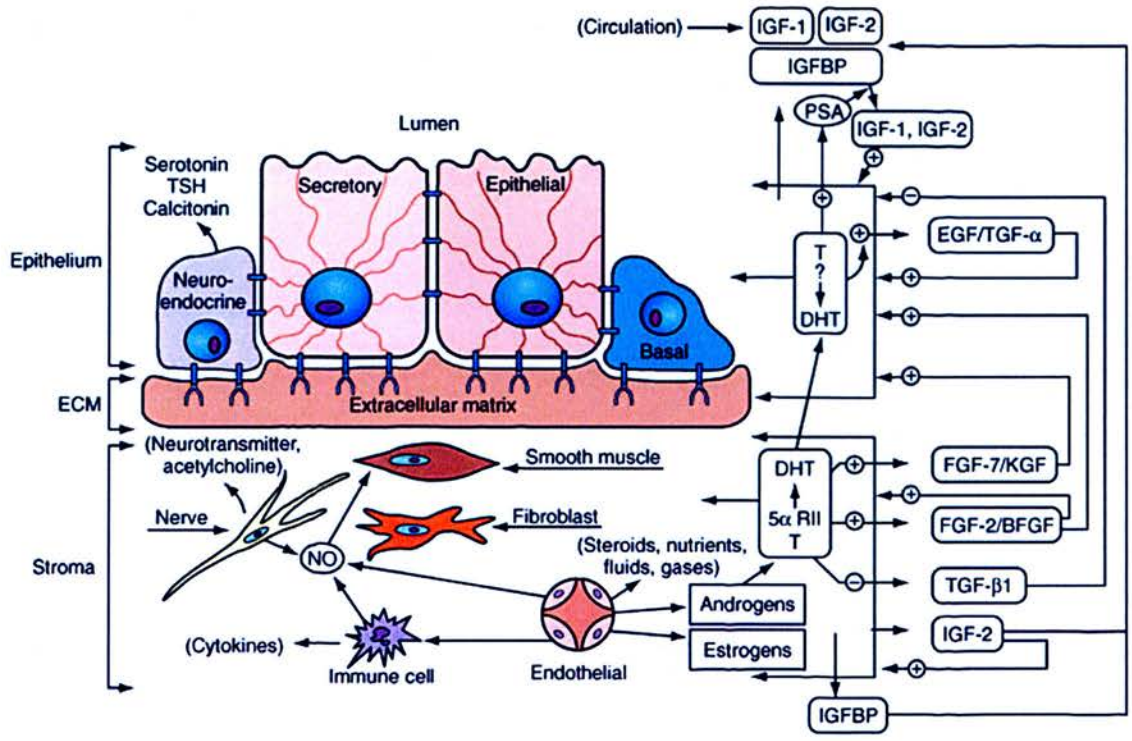

Figure 1.4: Schematic diagram illustrating the complex interactions between androgens and growth factors upon stroma and epithelial cells. The action of various growth factors can be inhibited or stimulated by androgens.

There is no proven growth factor that is unique to the prostate but many growth factors have been studied in detail. Table 1.1 summarises the growth factors that are common to the prostate.

Abbreviation	Name	Comment
bFGF	Basic fibroblast growth factor (prostate growth factor, endothelial growth factor, FGF-2)	Present in normal prostate Elevated in BPH
EGF	Epidermal growth factor	Over expression produces prostate epithelial hyperplasia
TGF-α	Transforming growth factor - α	Low levels in human prostate
TGF-β	Transforming growth factor - β	Inhibitor of epithelial growth
MIS	Müllerian-inhibiting substance	Causes repression of müllerian ducts
IGF	Insulin-like growth factor 1 & 2	Related to proinsulin
PDGF	Platelet-derived growth factor	Mitogen for connective tissue cells

Table 1.1 – A summary of growth factors common to the prostate.

At least 22 family members of fibroblast growth factors (FGFs) have been characterised and studied extensively [18]. There is recent evidence that FGF pathways are involved in postnatal development of prostate ductal and branching morphogenesis [19]. Androgens may work on epithelial cells via paracrine stimulation from stromal cells [20]. Sherwood *et al* reviewed the importance of epidermal growth factor (EGF) in the development of normal and abnormal prostate [21] and postulated that in conjunction with TGF-α , EGF maintains the structural and functional integrity of BPH. Transforming growth factor β (TGF-β) may function as a braking system in negatively regulated normal prostate epithelial cell growth while being a positive factor in stimulating normal stromal cell growth [22].

Müllerian-inhibiting substance is related to the TGF-β family and causes regression of the müllerian ducts. Insulin-like growth factors (IGFs), 1 and 2, are related in sequence to insulin. IGFs exert a strong mitogenic effect on the growth of the prostate [23]. Platelet-derived growth factor (PDGF) is expressed in many tissues and is mainly derived from platelets. PDGF has a strong mitogenic effect on mesenchymal and connective tissue cells and cause cells to respond to other growth factors. PDGF is postulated to be a mediator of the effects of inflammation upon prostate growth [24]; however, these effects have not been fully elucidated.

1.2. Benign prostate hyperplasia

Benign prostate hyperplasia (BPH) is a benign pathologic process of the prostate that is a common, but not exclusive cause, for lower urinary tract symptoms (LUTS) in aging men.

1.2.1. Aetiology of benign prostate hyperplasia

The underlying aetiology of the development of BPH has not been clearly defined. However, it is likely to involve several factors such as the disordered interactions between stroma and epithelial elements and their response to androgens, oestrogens and growth factors. The histopathologic process of enlargement of the gland is characterised by cellular hyperplasia of epithelial and stromal cells which is a process seen in the embryological development of the prostate. This observation

suggests that stromal and epithelial hyperplasia in later life may be as a result of "reawakening" of these early processes [25, 26]. Cellular growth within the prostate is dependent upon a fine balance between cellular proliferation and cellular death (apoptosis) [27]. In the early phases of BPH, cellular proliferation may be seen but in established disease, there is an increase in expression of anti-apoptotic pathway genes such as *bcl-2* [10, 28] rather than a increase in cellular proliferation. Also, androgens are required for the normal development of the prostate but has also been shown to actively inhibit apoptosis [29].

1.2.2. Pathophysiology of Benign prostatic hyperplasia

Histological features

Early work by Franks showed that the development of "fibromyoepithelial nodules" is the morphological hallmark of BPH. The nodules were classified into 5 types based on the morphological appearance and the relative amount of glandular and smooth muscle content. His work highlighted, in detailed drawings, the heterogeneity of histological composition of these nodules but concluded that the most common type of large nodules were mainly epithelial in composition [30]. McNeal's autopsy studies demonstrated that BPH develops in the periurethral transition zone of the prostate (see section 1.1.3). This work also noted that diffuse enlargement of the transition zone, independent of nodule formation, was the most common change noted with age [25]. These findings are confirmed in a later study by Arenas *et al* [31]. The majority of early periurethral nodules were shown to be

purely stromal nodules which were similar to embryonic mesenchyme. However, the early transition zone nodules were mainly composed of glandular epithelium with a reduction in stromal content. This is accompanied by hypertrophy of the epithelial cells with an observed increase in height of the lining epithelium. This glandular proliferative process leads to tight packing of epithelial glands within a given area (see figure 1.5).

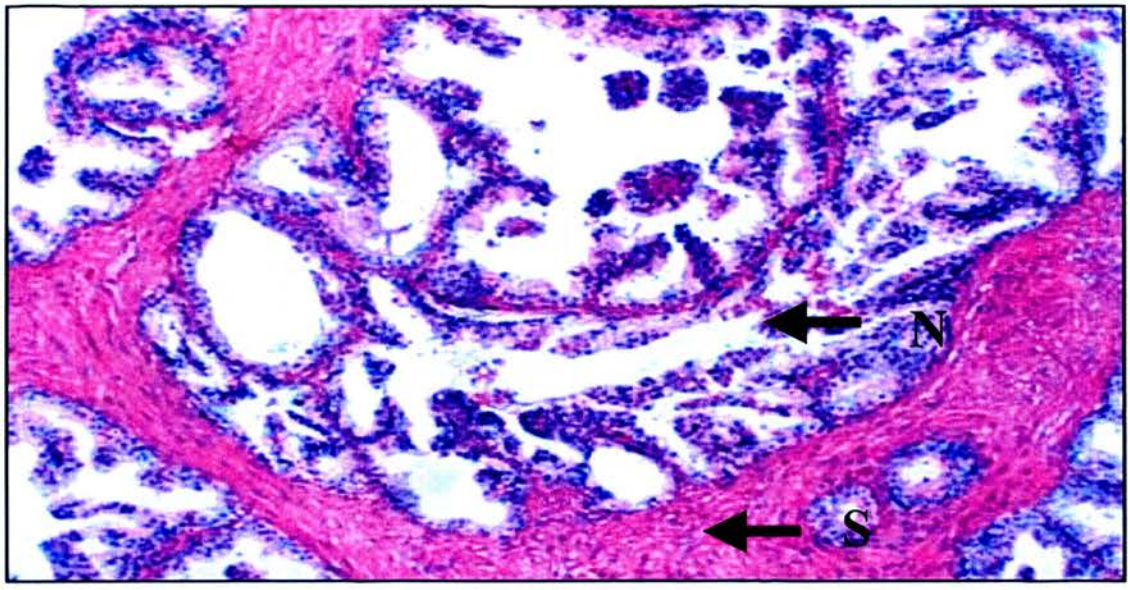

Figure 1.5: Photomicrograph of a glandular nodule (N) surrounded by stroma (S) at ×200 magnification

McNeal further described two chronological phases of nodular development. The earlier and more common phase was characterised by an increase in small stromal nodules within the periurethral and transitional zones. Decades later, many prostates with BPH entered a second phase characterised by marked enlargement of glandular nodules mainly in the transitional zone (see figure 1.6).

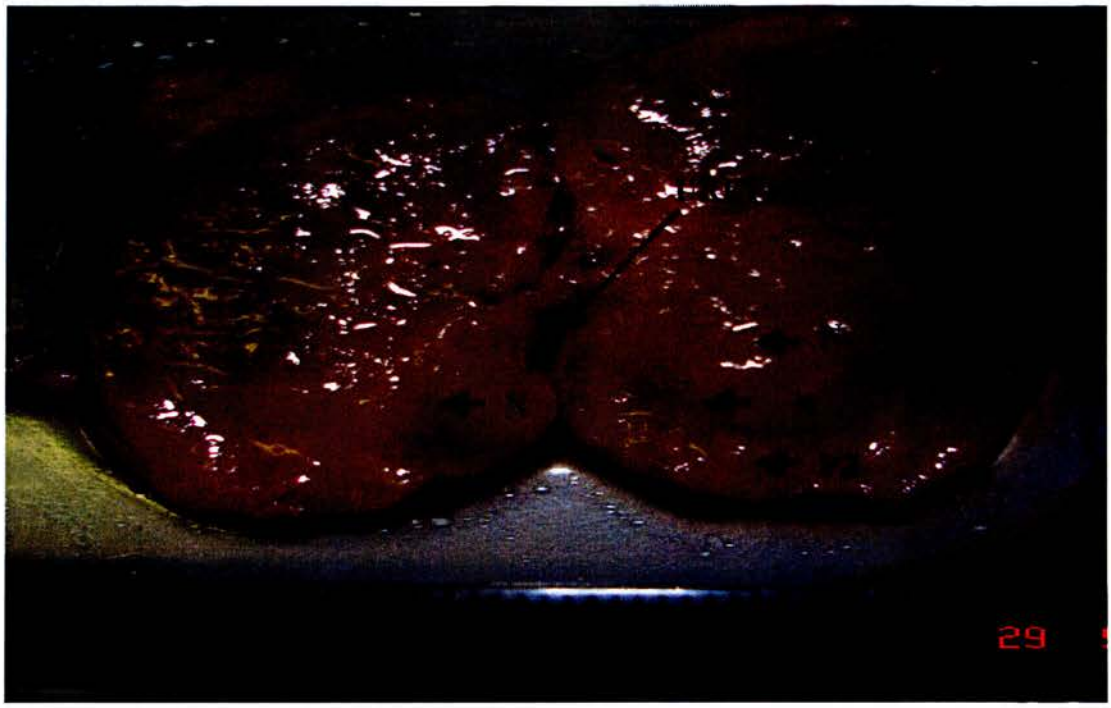

Figure 1.6: Photograph depicting a transverse section of a whole prostate clearly showing the nodular hyperplasia (N) which is a morphological hallmark of BPH. The peripheral zone (PZ) of the prostate does not show nodular formation. The urethra is highlighted on the image.

Following this work, many studies sought to quantitatively analyse the morphometric composition of prostate tissue in both normal and in BPH prostates. Price *et al* quantitatively examined the tissue composition from transurethral resection (TUR) specimens and prostate enucleations. The weights of the TUR resections were measured and it was observed that in the smaller resections (<10g in weight), bladder neck and anterior fibromuscular tissue comprised more than half of the specimen.

Non nodular prostatic tissue from the transition zone represented most of the resected specimens that weighed less than 50g but greater than 10g. However, in the specimens weighing greater than 50g, glandular nodules were found to be the dominant component with a high epithelial to stromal (ET:SM) ratio with the purely stromal nodules being poorly represented. The number of nodules with an ET:SM ratio greater than one were more numerous than those with a lower ET:SM ratio, and therefore it was suggested that these glandular nodules were more important than stromal nodules in the pathogenesis of symptomatic BPH [32]. Work by Schuster *et al* confirmed that resections of larger prostates are comprised mainly of epithelial rather than stroma tissue [33]. However, in other morphometric studies, resected tissues from small glands were shown to be comprised of mainly stromal tissue [34, 35]. Chagas *et al* compared the histological components of the transition zone in normal and BPH prostates. Smooth muscle, glandular acini and connective tissue were quantified using computerised morphometric analysis. In BPH prostates, the smooth muscle and connective tissue content were significantly increased compared to the control prostates and concluded that BPH may be a predominantly stromal disease process [36]. It is clearly evident that the prostate is a heterogeneous organ and has anatomical regions with distinct embryological origins and specific histological composition and these studies reflect this observation. Furthermore, an increase in stromal to epithelial ratios may not necessarily suggest that this is a predominantly "stromal disease". Stromal proliferation may well be due to "epithelial disease" as a result of disordered stromal to epithelial interactions.

The role of prostatic smooth muscle

Historically, the mass effect of prostate enlargement was thought to be the main cause for bothersome lower urinary tract symptoms, as this was based upon epidemiological data suggesting that the prevalence of BPH and clinical BPH is age dependent and therefore causally related [37]. This hypothesis was supported by the clinical evidence that surgical removal of prostate bulk improved LUTS in many patients [38]. However, Caine *et al*, first postulated that adrenergic mediated tone within the prostate musculature, may explain the variations in severity of obstructive symptoms in patients with BPH [39]. The level of sympathetic stimulation of prostatic adrenergic receptors alters smooth muscle tone in the periurethral region and therefore affects urethral resistance [40, 41]. In addition to the increase stimulation of smooth muscle tone in the prostate, Shapiro *et al* have shown that patients with symptomatic BPH have a higher stromal to epithelial ratio compared with asymptomatic patients [35]. This group further demonstrated that the response to alpha adrenergic blockers is proportional to the amount of smooth muscle within the prostate [42]. These early findings have led to the widespread use of alpha adrenergic blockers to address the dynamic aspect of bladder outlet obstruction. However, later studies have demonstrated that quinazoline-based alpha adrenergic blockers increase apoptosis within the glandular and stromal elements of the prostate and this mechanism has been suggested as an explanation for the durability of the response in long term users of alpha adrenergic blockers [43]. The pharmacological and functional aspects of adrenergic receptors and their blockade are considered further in section 1.3.

1.2.3. Epidemiology and natural history of BPH

The histological or autopsy prevalence of BPH was reported in a landmark study by Berry *et al* [44]. In this study the authors summarised the data from ten studies to show that greater than 50% of men aged 50 years or over demonstrate histological evidence of BPH, with this figure rising to 90% by the age of 85.

There is currently no universally accepted epidemiological definition of clinical BPH. In the past decade, the definition of BPH has undergone several changes. Historically, urinary symptoms associated with BPH were termed *prostatism* as it was thought that the prostate was the sole cause. However, it was observed by Tage Hald that there are at least three inter-related phenomena that can be assessed independently. These are the symptoms, histological BPH and bladder outlet obstruction (BOO) and in a given patient, all three, two of the three or only one of the three entities may be present (see figure 1.7).

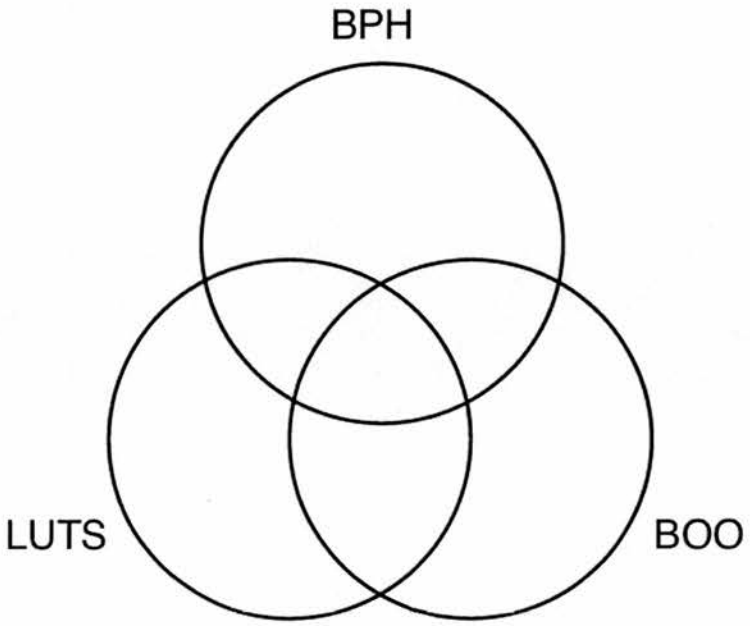

Figure 1.7: Hald's rings depicting the relationship between histologic hyperplasia of the prostate (BPH), lower urinary tract symptoms (LUTS) and bladder outlet obstruction (BOO).

Paul Abrams coined the term *lower urinary tract symptoms* (LUTS) to replace the inappropriate term of *prostatism* [45]. Therefore studies examining the prevalence of clinical BPH may apply one or several of these terms in their definition of the disease condition. The Olmsted County study showed a prevalence of moderate to severe urinary symptoms in 13% of men aged 40-49 years and rising to 28% in men over the age of 70 years [46]. In the UK, a study by Garraway, defined clinical BPH as the presence of an enlarged prostate (>20g) with symptoms or reduced urinary flow rate (Qmax <15ml/s). The BPH prevalence in this study were 13.8% of men aged 40-49 years and 43% of men aged 60-69 years [47]. Despite the significantly

different proportion of men with moderate to severe symptoms in many studies, there is a clear trend toward an increase in symptom scores with increasing age.

The natural history of the disease refers to the prognosis of the disease over time. The natural history of BPH can be obtained from two main sources, namely cross-sectional longitudinal studies of community-dwelling men and the placebo arms of several clinical trials. The most informative longitudinal study is the Olmsted County Study. Recently, 92-month data which showed an annual AUA symptom score deterioration of 0.34/year was observed across the study with the fastest rate of deterioration in men aged 60-69 years. In addition, 6 year follow up data on uroflowmetery measurements showed a median peak urinary flow rate decrease of -2.1% per year. The peak flow declined more rapidly with an increasing baseline age, prostate volume and symptom severity. The prostate growth (as measured with transrectal ultrasound) in this cohort of men was estimated to be 0.6ml per year. Prostate growth showed an exponential growth pattern with the growth rate of 0.4ml per year in men aged 40-59 and of 1.2ml per year in men aged 60-79 years [48, 49]. Acute urinary retention (AUR) is a significant complication resulting from BPH. The patient presents with the inability to void with increasing discomfort and the requirement for catheterisation. The aetiology of AUR is still poorly understood but obstructive, myogenic and neurogenic causes may play a role [50]. Of the 2115 men aged 40 to 79 years in the Olmsted County study, 57 had a first episode of AUR during 8344 patient-years of follow up giving an incidence of 6.8/1000 patient-years [51]. In the placebo arm of the PLESS trial, 1376 men with enlarged prostates and moderate symptoms were followed up for four years. 99 of these men experienced a

first episode of AUR giving an incidence rate of 1.8/1000 patient-years [52]. In the placebo arm of the MTOPS trial the incidence rate of AUR was 0.6/1000 patient-years [53]. In these two studies it was observed that the risk of AUR increases with increasing serum PSA (PSA >1.4 ng/l conferred an eightfold increase in risk) and well as prostate volume (>40mls conferred a threefold increase in risk).

The need for BPH-related surgery has been studied in the Olmsted County cohort. The overall incidence of this event is 16/1000 patient-years with a strong age-related increase in patients 70 years old or older (rising to 30/1000 patient-years) [51]. From the placebo arms of PLESS, the rates of surgery increased from 6.2% to 14.6% for patients in the lowest (1.4-3.9 ng/l) to the highest PSA (>4.0 ng/l) tertile [52].

Many relevant parameters associated with BPH have been shown to worsen with increasing age. The natural history of the disease suggests a worsening of LUTS and BPH with time. However, there are several key baseline parameters allowing an individual's patient's risk of progression to be stratified. Age, symptom severity, prostate size and serum PSA are useful predictors of the risk of progression.

1.2.4. Assessment and diagnosis of clinical BPH

The assessment of LUTS in men leading to a diagnosis of clinical BPH is a challenge for urologists as there are many non-prostatic causes of LUTS. Many tests and investigations are available to the urologist for the assessment of these patients. However, the correlation between the symptoms, clinical parameters and bladder

outlet obstruction is variable and inconsistent [54, 55]. Taken own their own, these assessment tools cannot be used to select the optimum therapy for a given patient and they cannot predict the response to treatment. The investigations available to the urologist are considered below.

Urinalysis

Urinalysis is considered to be a first line investigation and can be performed using dipsticks. These can identify haematuria, glycosuria, proteinuria, pyuria, specific gravity and the presence of urinary nitrites and leucocyte esterase. Abnormal dipstick findings need to be confirmed by microscopy and culture of a mid stream specimen of urine [56].

Structured questionnaires

Several structured symptom questionnaires have been developed but the most widely used is the International Prostate Symptom Score (IPSS) [57]. The questionnaire consists of seven questions relating to the symptoms of BPH and a final question to assess the quality of life. By using this system, the patient's symptoms can be classified as mild (0-7), moderate (8-19) or severe (20-35). However, many studies have demonstrated a poor correlation between symptom score severity and other indices of lower urinary tract dysfunction such as urodynamic parameters, uroflowmetery and prostate size [58].

Serum Creatinine

The recently published National Institute of Clinical Excellence (NICE) guidelines on the management of LUTS do not recommend the routine measurement of serum creatinine [59]. If there are signs and symptoms suggestive of renal impairment such as a palpable bladder, nocturnal enuresis and recurrent urinary tract infections, serum creatinine measurements is appropriate. Patients with renal impairment have a higher rate of post-operative complications following transurethral resection of the prostate (TURP) [60]. An elevated serum creatinine in a patient with BPH is an indication for imaging of the upper urinary tracts.

Serum Prostate Specific Antigen (PSA)

Prostate cancer may arise in patients with LUTS suggestive of BPH. NICE guideline on the management of LUTS recommend a measurement of serum PSA in patients with an abnormal rectal examination, symptoms suggestive of bladder outflow obstruction and in patients concerned about prostate cancer [59].

Serum PSA is organ specific but not disease specific and may be elevated in men with BPH. Serum PSA has been shown to be closely related to prostate volume (PV) and this relationship is dependent on age [61]. Furthermore, several large scale clinical trials such as Medical Therapy of Prostatic Symptoms (MTOPS), Proscar Long-term Efficacy and Safety Study (PLESS) demonstrate that PSA is an independent predictor of both prostate volume (PV) and BPH progression [53, 62,

63]. Further analysis from the MTOPS study demonstrates that patients with a PSA serum level of >1.6 ng/ml are at risk of clinically significant BPH progression. These patients are more likely to have an enlarged prostate >30mls in volume and therapy should be directed at reducing the size of the prostate [64].

Urinary flow rates

Uroflowmetery is the measurement of urinary flow rate with an electronic flowmeter. The flow rate is measured in millilitres per second and peak flow rate (Qmax) has been shown to identify patients with BPH more specifically than average flow rate (Qave) [65]. Due to test-retest variability, there is not a specific rate of flow which can be used to determine the course of therapy. Furthermore, flow rate cannot distinguish between BOO and impaired detrusor contractility as the cause for a low peak flow rate [66].

Post-void residual volume

Post-void residual volume (PVR) is the amount of urine remaining in the bladder after micturition. This can be measured using ultrasound or, invasively by the passage of a urinary catheter. Large variations in PVR measurements have been reported [67]. PVR has been shown that used alone, it could not predict BOO [68].

Pressure flow studies

The measurement of detrusor pressure whilst the bladder is filled and emptied is made using a small suprapubic or urethral catheter. This investigation differentiates patients with detrusor failure and those with BOO [69]. Pressure flow studies should be considered in complicated cases, such as young men with neurological disease or those who have not responded favourably to treatment [59].

Urethrocystoscopy

Endoscopic evaluation of the lower urinary tract is recommended in patients in whom other pathologies are suspected such as bladder cancer or urethral strictures.

Transrectal ultrasound of the prostate

Ultrasound examination of the prostate may be used to assess the size and shape of the prostate. This may identify patients with large volume prostates who may be treated effectively with an open procedure. However, the most common application for transrectal ultrasound is for the guidance of systematic needle biopsies of the prostate.

1.2.5. Non-surgical management of BPH

Watchful waiting

Watchful waiting is a strategy for monitoring for the progression of symptoms or signs. Advice regarding decreasing fluid and caffeine intake late in the day may be given and patients should be encouraged to promptly report any changes in symptoms. Recent studies have shown that self-management, as part of watchful waiting, reduces both symptoms and progression [70, 71].

Alpha adrenergic blockers

The use of alpha adrenergic blockers in the medical management of BPH is based upon the hypothesis that the increase of smooth muscle tone in the prostate is mediated by alpha adrenergic receptors (α ARs) [72]. Adrenergic receptors are transmembrane glycoproteins that mediate catecholaminergic actions within the sympathetic nervous system [73]. This family of receptors are subdivided into α_1, α_2, and β subtypes [74]. It has been shown that the α_{1a} subtype predominates in the prostate and is localised to the stromal compartment [75-77] and is the subtype that mediates contraction of prostatic smooth muscle [41].

Three generations of alpha adrenergic antagonists have been used in the treatment of LUTS suggestive of BPH. The first generation agents such as phenoxybenzamine, antagonised both α_1 and α_2 receptors within the prostate and vasculature. As a consequence of this non-selective blockade, this generation of agents were associated

with many dose-related adverse events such as first dose syncope, orthostatic hypotension and reflex tachycardia [78, 79].

To improve the adverse events profile of these agents, the second generation of agents selectively antagonised the α_1 AR subtype and not the α_2 AR subtype in the doses used in clinical practice. These agents include prazosin, terazosin and doxasoin [80]. Alfuzosin is considered a second generation agent as affinity studies on human-cloned α_1 AR subtypes demonstrate that it does not show significant receptor subtype specificity [81]. However, animals studies have shown that receptor subtype selectivity does not correlate with functional selectivity of α_1 adrenegic antagonists [82].

Third generation agents are pharmacologically selective for prostatic α_{1A} AR subtype receptors [83]. Tamsulosin is a third generation agent and pharmacologic studies have shown that tamsulosin has a 10-fold greater affinity for α_{1A} AR subtype than for the α_{1B} AR subtype [84]. As tamsulosin has low affinity for α_{1B} AR subtypes, which are predominantly found in the vasculature, cardiovascular adverse effects are uncommon [85]. The clinical advantages of this pharmacologic selectivity are that titration doses are not required and patients may begin at the usual treatment dose.

A recent meta-analysis of placebo-controlled and direct comparison studies of alpha adrenergic blockers demonstrated that as a group, these agents are comparably effective in terms of symptom control, urinary flow rate improvement and quality of life measures [86].

Alpha adrenergic receptor antagonists and the induction of apoptosis in the prostate

The clinical efficacy for this group of agents has been attributed to their ability to relax smooth muscle tone within the lower urinary tract via antagonism of α_{1A} AR subtype receptors. However, Kyprianou *et al.* first reported the proapoptotic effects of doxazosin as a potential mechanism for the long-term duration of efficacy for this agent in patients with LUTS suggestive of BPH [87]. The authors demonstrated that the apoptotic activity in the glandular and smooth muscle cells significantly increased after 3 months of therapy and remained elevated for up to 12 months. This increased in apoptosis correlated with degeneration of prostatic stroma and decreased smooth muscle actin expression as assessed by immunohistochemical staining.

Further studies from this group assessed the proapoptotic effect of terazosin and tamsulosin, demonstrating that terazosin therapy induced apoptosis in prostate epithelial and smooth muscle cells in patients with BPH [88]. In cell culture experiments, tamsulosin did not exhibit proapoptotic effects against prostate cancer cell growth [89]. The proapoptotic activity of doxazosin and terazosin may be due to their similarity in chemical structure as both agents possess a quinazoline nucleus whereas tamsulosin is structurally different as it is a methoxybenzene sulphonamide (see figure 1.8) [89].

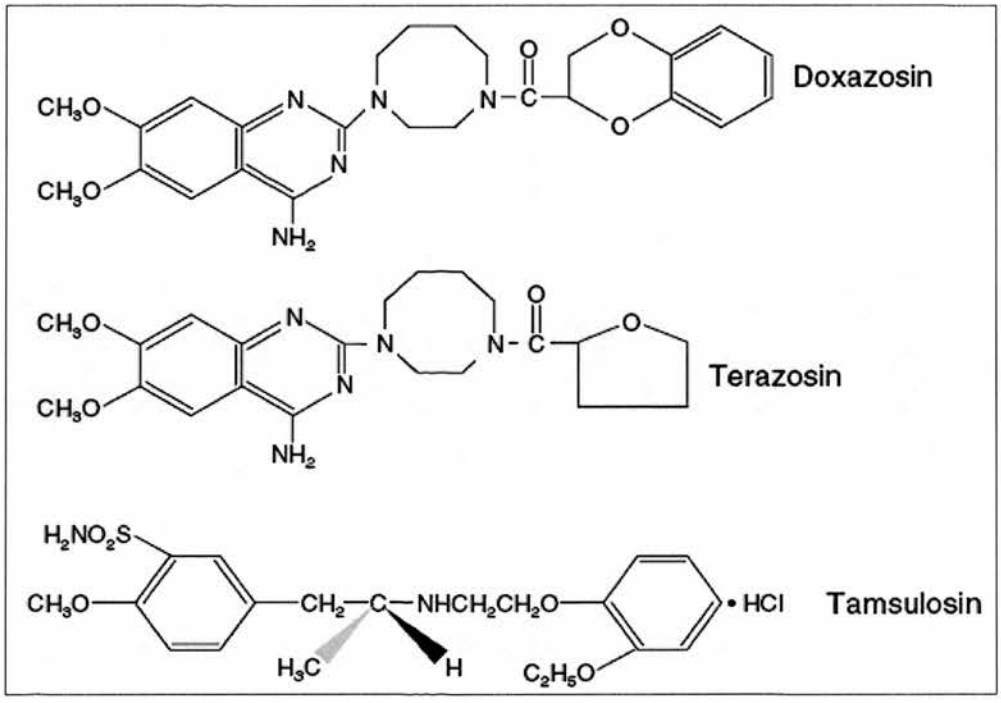

Figure 1.8: The chemical structure of alpha 1a antagonists. The quinazoline structure is shared by doxazosin and terazosin, but not by the methoxysulphonamide-derived alpha 1a antagonist, tamsulosin.

The pathways underlying the pro-apoptotic effect of quinazoline-based alpha blockers have been studied. Treatment with terazosin and finasteride caused an increase in the apoptotic index with increase expression of TGF - β_1 [90]. Molecular studies using prostate cancer cell lines demonstrated an induction of Caspase-3 and an induction of several TGF - β_1 signalling effectors in cells treated with doxazosin. This effect was not seen with treatment with tamsulosin [91]. Doxazosin was found to inhibit cell growth, adhesion and migration of human endothelial cells by interfering with VEGF and FGF-2 action [92]. These recent findings may suggest a

potential therapeutic use of quinazoline-derived alpha 1 antagonist in the management of malignant prostate disease [93].

5-α reductase inhibitors

The rationale for the use of these agents in the management of BPH is based on the observation that the embryonic development of the prostate depends upon the androgen, dihydrotestosterone (DHT). Conversely, suppression of DHT removes the stimulus for cell growth and induces apoptosis or prostate epithelial cells [94]. Testosterone physiology is discussed in section 1.1.4. The reduction in prostate volume is thought to decrease the static component of BOO. However, it is acknowledged that the pathophysiology of clinical BPH and LUTS are not directly correlated to prostate size.

Two isoenzymes of 5-α reductase have been identified: type 1 and type 2. Type 1 is found within the prostate but is the predominant enzyme in extra-prostatic tissue such as skin and liver whereas type 2 is the predominant prostatic 5-α reductase [95]. The 5-α reductase inhibitors licensed for use in the treatment of BPH are finasteride, which is a mono-inhibitor of type 2 isoenzyme, and dutasteride, a dual inhibitor of both isomers.

The Proscar Long-Term Efficacy and Safety Study (PLESS) reported the unique findings that the incidences of both AUR and BPH-related surgery were significantly reduced with long term 5ARI therapy [52]. Finasteride conferred a relative risk

reduction of 57% of AUR and 55% of BPH-related surgery at 4 years. However, the symptom score reduction of 2 points, and peak flow rate improvements 1.7ml/sec at the end of the study were modest and comparable to prior finasteride studies [96]. The detection of cancer was not significantly different between the treatment and placebo group implying that finasteride did not mask the diagnosis of prostate cancer [97].

Dutasteride is a dual inhibitor of 5-α reductase types 1 and 2 and is shown to have a greater impact on the suppression of serum DHT levels [98]. Results from early studies show similar results compared with finasteride. In a randomised controlled trial of 4325 men, the symptom score was improved by 4.5 points and the peak flow rate improved by 2.2ml/s at 24 months [99]. The relative risk reduction of AUR was 57% and the risk reduction of BPH-related surgery was 48% compared with placebo.

Combination therapy with alpha adrenergic blockers and 5-α reductase inhibitors

The Medical Therapy of Prostatic Symptoms (MTOPS) trial was established to determine whether medical therapy can influence the progression of BPH in the long term and what factors were associated with increased progression of the disease. Patients were randomised to doxazosin, finasteride, a combination of both and to placebo. The results of the trial show that the symptom score and peak flow rate improved significantly in the combination group compared with the monotherapy group. Patients on combination treatment experienced a relative risk reduction of BPH progression of 67% compared with 39% for doxazosin and 34% for finasteride

as monotherapy [53]. Interestingly, in the doxazosin monotherapy group, the total prostate volume increased from a baseline of 36.4 mls by 9.9mls by the end of the four year study. This suggests that doxazosin, despite its pro-apoptotic effects, does not interfere with the natural enlargement of the gland.

Combination versus Avodart or Tamsulosin (CombAT) trial recently reported the 4 year results. The results show that combination therapy with dutasteride and tamsulosin reduced the relative risk of AUR or BPH-related surgery compared with monotherapy with tamsulosin across all baseline subgroups by 43-77%. The reduction was not significant in patients with a baseline prostate volume of <40 ml [100].

Phosphodiesterase inhibitors

In 2002, the first clinical report was published documenting the improvement in LUTS in men given sildenafil for erectile dysfunction [101]. There has been significant interest in the role of phosphodiesterase inhibitors (PDEIs) as treatment options for LUTS. There is level 1 evidence confirming improvement in LUTS after treatment with PDEIs [102]. In these studies, there are no significant changes in the peak flow rate, which may suggest the mechanistic effects of PDEIs may be focused on detrusor function than on prostatic smooth muscle. The mechanisms by which PDEIs exert their effects on the lower urinary tract are the subject of ongoing intensive research.

Phytotherapy

Phytotherapy is the use of plant extracts for medicinal purposes. The extract of the American dwarf plant *Serenoa repens* is the most commonly used plant extract for the treatment of BPH. These agents are currently more used in the USA, Germany and France than in the UK. Permixon (Pierre Fabre Medicament, Boulogne, France), the *n*-hexane liposterolic extract of *Serenoa repens,* is the product most rigorously investigated of all the phytotherapeutic agents in use. However, the exact mechanism of action is yet to be determined as these extracts are a composite of several chemical molecules and display a wide range of pharmacological activity [103]. The postulated modes of action involve anti-androgenic action through inhibition of 5-α reductase isoenzymes 1 and 2; anti-inflammatory effects mediated via inhibition of cyclo-oxygenase and lipoxygenase enzymes and anti-proliferative action through inhibition of bFGF [104]. A recent systematic review by the Cochrane Database concluded that Serenoa repens was not more effective than placebo for the treatment of urinary symptoms consistent with BPH [105]. However, despite these studies, there is still a need for well designed, long term, randomised placebo/comparative controlled studies with defined BPH symptom score endpoints to determine the place of these agents in the medical treatment of BPH.

1.2.6. Surgical management of BPH

Surgical treatment for symptomatic BPH was the accepted treatment before the advent of medical therapies in the 1970s [39]. There are now many alternatives to surgical treatment with less associated morbidity. More recent modalities of treatment are compared to TURP as this is still considered the "gold standard" for the treatment of symptomatic BPH.

Open prostatectomy

An open prostatectomy is open abdominal procedure in which the prostate adenoma is enucleated through the bladder (transvescial prostatectomy) or through the prostate capsule (Millin's prostatectomy). The open approach is usually reserved for patients requiring the removal of very large prostates greater than 100g [106].

TURP

TURP is considered the gold standard to which other invasive procedures are compared. The efficacy of this procedure has been demonstrated in the many studies and is the treatment of choice in patients with significant symptoms [107, 108]. A recent review examining the changes in complication rates, indications and methods for managing complications following TURP conclude that the morbidity of TURP has improved with improvements in technology and surgical techniques [109].

Minimally invasive therapies

Minimally invasive therapies use high temperature to produce coagulation necrosis of the prostate. Transurethral microwave therapy (TUMT) uses a combination of heat delivered transurethrally and a water balloon to lower prostatic temperature to prevent urethral damage. This technique has been assessed in a number of trials but long term data is still lacking. It is however clear, that the TUMT offered less morbidity than TURP but was not as effective as TURP in improving LUTS or increasing peak flow rate as compared with TURP [110].

Transurethral needle ablation (TUNA) uses radiofrequency waves to deliver heat to the prostate. A meta-analysis in 2004 reported that the effect of TUNA was to halve the mean IPSS at 1 year. The peak flow rate increased by about 70% from baseline to one year but tended again to decline over time. The main criticism was the shortage of long term data [111].

Laser based therapies have been shown to achieve similar outcomes as TURP but the cost of the laser and operation times seem to be the main drawbacks of this procedure. Newer technologies have helped overcome some of the difficulties in treating large prostates and the minimal invasiveness of the various laser technologies has improved. A recent systematic literature review examining the evidence for photoselective laser vapourisation and holmium laser enucleation of the prostate has suggested that both these laser modalities are promising alternatives to TURP. However, the quality of the trials examined in this review were not completely robust and the follow up data was relatively short [112].

1.3. Mechanical characteristics of biological tissues

Clinical assessment such as digital examination has been used for centuries to qualitatively assess and diagnose the presence of tumours in accessible areas of the human body as these pathological processes can alter the mechanical properties of tissues. The mechanical properties of biological tissues are said to follow a viscoelastic model and contain varying elastic and viscous elements and are intrinsically related to their composition [113]. The understanding of the mechanical properties of soft tissues is important in the fields of biomechanics and bioengineering and its associated medical applications. There is significant interest in the application of biomechanics to the diagnosis, planning and treatment of various disease areas such as breast disease [114], vascular disease [115] and prostate disease [116].

Biological soft tissues consist mainly of cells and extracellular substances such as connective tissues such as collagen and myosin. These individual components have been isolated and found to possess different mechanical properties [113]. Indeed, there are significant variations in the proportion of cellular components at a given area of the organ or tissue studied. Biological soft tissues may not show a linear stress-strain relationship and therefore cannot be described or represented by a single elastic modulus. The elastic modulus is a measure of the stiffness of a material and this is gained from the application of stress to the material. Also, the mechanical properties of the tissue may not be the same in different directions and are therefore termed anisotropic materials. They often have a layered or very complex structure

and the perfusion of the tissue or organ often plays an important role with regard to the mechanical properties.

1.3.1. Mechanical measurements of the prostate

Despite the advancement of the field of biomechanics and bioengineering, there is not a standard method for quantifying the mechanical properties of biological tissues. Mechanical testing is usually conducted with tension or compression applied to the tissue at a range of controlled strain rates. These tests are termed quasi-static as they monotonically increase the displacement and measure the resulting load. There have been many reports of quasi-static mechanical testing of biological tissues, but this method of testing does not account for the viscous, or fluid, element of the tissue [117-119]. Krouskop *et a*l was the first to report quasi-static measurements of prostate tissue and demonstrated differences between malignant and benign tissue [120].

When ultrasound propagates through tissue, it causes a mechanical disturbance which is related to the elastic properties of the tissue. This disturbance or distortion can be detected in the pulse-echo (termed A-scan) ultrasonography to give a graphical representation of the reflected ultrasonic wave. This development of conventional ultrasound has been termed elastography, also called strain imaging, and is recognised as a new diagnostic imaging modality. Higher-density tissues allow less displacement with compression than soft tissue. Compression and decompression of the prostate is generated by freehand during ultrasound. A

comparison is made of the echo amplitudes through the tissue with and without compression applied to the tissue and elastograms are generated demonstrating areas of variation in stiffness. Several groups have utilised A-scan ultrasonography to produce images depicting areas of varying stiffness in tissues [121, 122]. This technique has matured over the last decade and there is recent evidence within the literature that this diagnostic tool may be useful in the detection of malignant lesions within the prostate [123, 124]. Sonoelastography utilises a device to introduce a vibration into the target tissue whilst real-time Doppler techniques are used to the image the resulting vibration pattern. A discrete hard inhomogeneity will cause a decrease in the vibration amplitude at its location [125]. Initial results seemed to suggest that elastography yielded images of more clarity over the images produced using sonoelastography. However, recent evidence suggests that sonoelastography is proving to be an accurate tool in the detection of prostate lesions [126]. However, despite these results, elasticity imaging does not provide information of the mechanical response of the tissue when subjected to a wide spectrum of strain frequencies. This knowledge is essential to the development of an effective *in vivo* measurement system.

To assess both the elastic and viscous components of a tissue, a dynamic mechanical test of applying a compressive strain to the tissue, will enable the modulus of the two components to be derived. The moduli commonly used to describe the two components are the amplitude ratio ($|E^*|$) and phase difference ($\tan \delta$) of the forces applied to the tissue. Previous work from the Prostate Research Group has been

focused on understanding the structure-property relationship of prostate tissue from TURP chippings. The research utilised a load-compression probe to perform point measurements of the mechanical properties of the target tissue. This technique acknowledges the elastic and viscous properties of biological tissues and measures the modulus dynamically (as the amplitude ratio and phase difference) between an oscillating strain (probe displacement) and the resulting force. The amplitude ratio and phase shift can therefore be used to determine the loss modulus and storage modulus of the tissue, which is a more complete measure of tissue elastic and viscous properties [127]. Furthermore, Phipps *et al* demonstrated that malignant prostate tissue can be differentiated from benign tissue on the basis of its mechanical characteristics [128].

The mechanical properties of prostate tissue have been shown to be a function of the underlying histological structure. Despite the number of tools available to the urologist to assess a patient with LUTS secondary to BPH, there is a poor correlation between the symptoms, clinical parameters and investigations. Also, these tests, when considered on their own, are not able to guide treatment nor can they predict the patient's response to a given treatment. From the results of the combination studies of MTOPS and CombAT, patients with a prostate size >30 ml and a PSA of 1.4ng/ml or greater should benefit from a 5 α-reductase inhibitor than an alpha blocker. However, studies have suggested that the severity of bladder outlet obstruction is dependent upon the density of smooth muscle within the prostate and the ratio of stroma to epithelium was the greatest in patients with clinical BPH [35, 42]. As the mechanical properties of the prostate may reflect the underlying

histology, this knowledge may be useful in guiding therapy and in predicting the response to a given treatment.

1.4. Hypothesis and objectives of this thesis

Previous work from the prostate research group has demonstrated that there is a relationship between the mechanical and histological properties of prostate tissue from TURP chippings and that there are measureable differences between malignant and benign prostate tissue. This work forms part of a project that has the ultimate aim of developing an effective *in vivo* measurement system to assess the mechanical properties of prostate tissue.

These samples were mainly stromal in composition than epithelial. We understand from the work by Franks and McNeal that the prostate, taken as a whole, is a heterogeneous organ with differing histological characteristics throughout its structure (see section 1.2.2). Different patterns of tissue composition of the prostate are seen when considering prostate size. In the smaller prostates the morphology of pathological features, such as nodules, are comprised mainly of stromal tissue. However, in the larger prostate, these nodules are comprised of mainly glandular tissue. To fully understand the relationships between morphology and mechanical characteristics in prostate tissue, the whole gland must be subject to assessment. The heterogeneous nature of the prostate cannot be assessed simply from TURP chippings. The aim of this thesis is to further explore the structure-property relationship of prostate tissue in sections of whole prostate.

In parallel to this work, studies will continue to utilise TURP chippings to understand the relationship between alpha blocker therapy and the effect upon prostate tissue. Studies have shown that quinazoline based alpha blockers, such as doxazosin and terazosin were found to cause apoptosis in prostate cells whereas tamsulosin, a sulphonamide based alpha blocker, did not have this effect (see section 1.2.5). The increase in prostate cellular apoptosis correlated with morphological stromal regression. Alfuzosin, a quinazoline based alpha blocker, has not been studied in relation to its effect upon prostate tissues. Therefore, this thesis also seeks to explore the relationship between alpha blocker therapy and the effect upon the morphological and mechanical properties of prostate tissue.

Chapter Two

Material and Methods

2. Introduction

The project has two main objectives: Firstly to examine the mechanical and morphological properties of prostate tissue harvested from radical cystoprostatectomy specimens.

Protocol for first objective as follows:

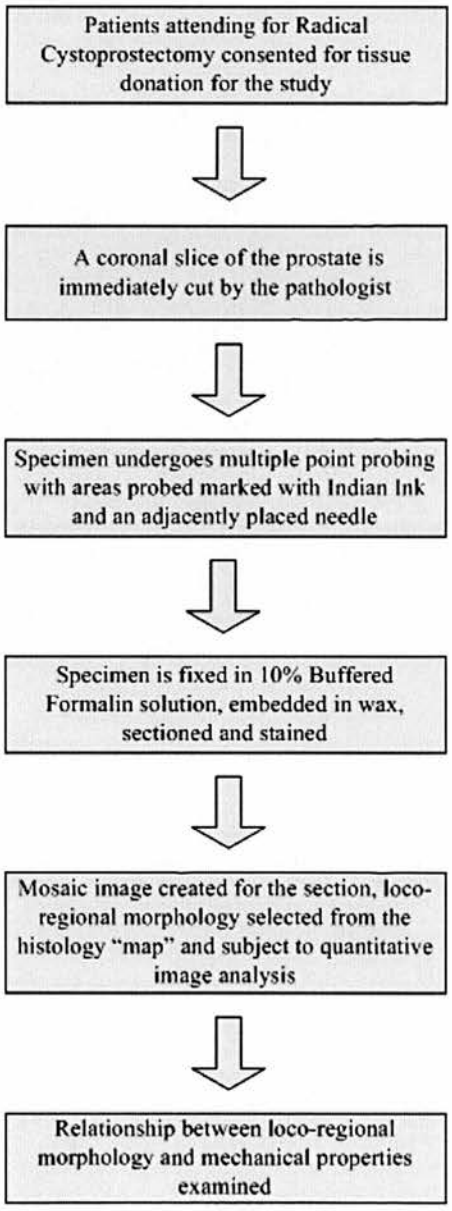

Secondly, to explore the relationship between alpha blocker therapy and the effects upon the mechanical and morphological characteristics of prostate tissue in TURP specimens.

Protocol for second objective:

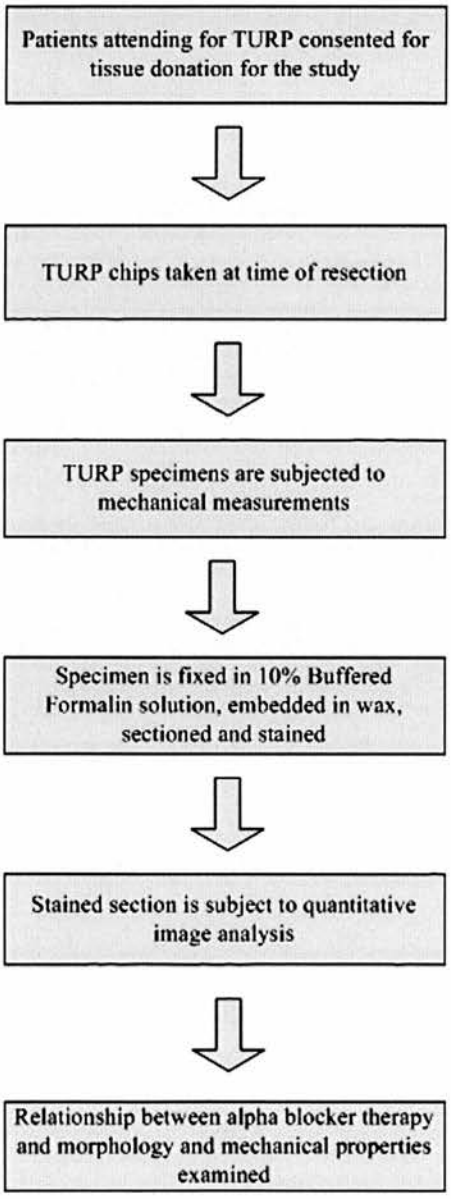

2.1 Materials, Chemicals and Equipment

The materials, chemicals and equipment used in this project are described in detail.

2.1.1 Chemicals used

Concentrated hydrochloric acid (HCl) (Scientific & Chemical Ltd, Bilston, UK)

Tris[hydoxymethyl]aminomethane Trizma Base (Tris) (Sigma, Poole, UK)

Citric acid (Sigma, Poole, UK)

Tri-sodium citrate (Fisher Scientific, Loughborough, UK)

Sodium chloride (NaCl) (BDH, Poole, UK)

Sodium Hydroxide (NaOH) (BDH, Poole, UK)

Phosphate buffered saline tablets (PBS) (Oxoid, Basingstoke, UK)

Xylene – Analytical Grade (Fisher Scientific, Loughborough, UK)

Absolute ethanol – Analytical Grade (Fisher Scientific, Loughborough, UK)

Hydrogen peroxide (J.T. Baker, Deventer, Holland)

Depex mounting medium (BDH, Poole, UK)

Ethylenediaminetetraacetic acid (EDTA) (Sigma, Poole, UK)

DAB peroxidase substrate tablet set (Sigma, Poole, UK)

2.1.2 Solutions prepared

Tris-Buffered Saline, 0.05M pH 7.6 (TBS)

Dissolve 30.25g Tris in 400ml de-ionised water. Add 16.5ml concentrated HCl.

Dissolve 40.5g NaCl in 4600ml de-ionised water.

Mix the two solutions to make up 5l.

Adjust pH to 7.6 using either 4M HCl or 1M NaOH.

Citrate Buffer 0.1M pH 6.0

Make up stock solution of 0.1M citric acid (21.01g / litre).

Make up stock solution of 0.1M sodium citrate (29.41g / litre).

Mix 18ml of the citric acid with 82ml of the sodium citrate and make up to 1000ml with de-ionised water.

Adjust to pH 6.0 using either 4M HCl or 1M NaOH.

Phosphate Buffered Saline (PBS)

Make up using Oxoid PBS tablets, at one tablet per 100ml de-ionised water.

Tris-EDTA buffer (50X stock solution)

Dissolve 37g of EDTA with 40g of Tris in 2L of distilled water to make stock solution.

To prepare a working solution, add 60mls of stock solution to 1.5L distilled water.

Adjust pH to 8.0 if necessary

Diaminobenzidine (DAB)

Make up with one diaminobenzidine (DAB) tablet and one urea hydrogen peroxide tablet (both tablets supplied in the DAB peroxidase substrate kit).

per 5 ml of de-ionised water.

Proteinase K buffer

Dissolve 12.14g of Tris in 1L of distilled water and adjust to pH 8.0 using concentrated HCl to give 100mM Tris-HCl pH 8.0

Add 1.861g of EDTA (50mM EDTA) to give a stock solution of Proteinase K buffer.

2.1.3 Immunohistochemical reagents

a) Primary Antibodies

Monoclonal mouse anti-human prostate specific antigen, clone ER-PR8 (Dako, Ely, UK)

Monoclonal mouse anti-human smooth muscle myosin heavy chain, clone SMMS-1 (Dako, Ely, UK)

Polyclonal rabbit anti-human anti-active caspase-3 (Promega, Southampton, UK)

DeadEnd Colorimetric TUNEL system (Promega, Southampton, UK)

b) Secondary Antibodies

Biotin conjugated goat anti-mouse secondary antibody (Autogen Bioclear, Calne, UK)

Biotin conjugated swine anti-rabbit secondary antibody (Dako, Ely, UK)

c) Blockers and visualisation agents

Goat Serum (Diagnostics Scotland, Carluke, UK)

Swine Serum (Dako, Ely, UK)

Avidin/ Biotin blocking kit (Vector Laboratories, Peterborough, UK)

StreptABComplex streptavidin, horseradish peroxidase (Dako, Ely, UK)

Diaminobenzidine Tablets (Sigma, Poole, UK)

2.1.4 Equipment used

a) Mechanical Testing

A description of equipment used in the mechanical testing of prostate tissue is in Section 2.3

b) Tissue processing

Tissue-Tek Vacuum Infiltration Processor (Model E150, Bayer Diagnostics, Basingstoke, UK)

Tissue-Tek Tissue Embedding Console System (Model 4715, Bayer Diagnostics, Basingstoke, UK)

Rotary Microtome (Model AS325, Shandon, Runcorn, UK)

Superfrost Plus 72x25x1mm Microscope Slides (BDH, Poole, UK)

Cover Glasses 18x18mm and 24x40mm, thickness no.1 (BDH, Poole, UK)

c) Image capture and analysis

Leica DMR light microscope with automated stage (Leica Microsystems, Cambridge, UK)

Leica DC digital camera (Leica Microsystems, Cambridge, UK)

QImaging QICAM digital camera (Mediacybernetics, Berkshire, UK)

Pro-series Turboscan and Surveyor specimen scanning software (Mediacybernetics, Berkshire, UK)

Leica Q550 imaging workstation personal computer with Leica Qwin image analysis software (Leica Microsystems, Cambridge, UK)

Image-Pro Plus 5.1 image analysis software (Mediacybernetics, Berkshire, UK)

Panavue ImageAssembler - Trial Version (Panavue, Quebec, Canada)

2.2 Patients and Tissues

This section describes the source of the prostate tissue used in this project.

2.2.1 Ethical approval and consent

Full ethical approval for this project was granted by the Lothian Research Ethics Committee (certificate reference LREC/2002/8/38). Written informed consent was obtained from patients who agreed to donate a small proportion of their prostatic tissue excised at radical cystoprostatectomy or at TURP for the purposes of this research.

2.2.2 Source and collection of tissue specimens

Radical cystoprostatectomy specimens

Prostate tissue was collected from attending for radical cystoprostatectomy for bladder cancer at the Urology Department, Western General Hospital, Edinburgh. Tissue was not collected from patients who had previous prostate surgery or prostate biopsies as this may alter the morphology of the prostate tissue harvested. Immediately following excision of the prostate and bladder, the specimen was transported to the pathology department where a transverse slice of the whole prostate was obtained. The specimen was taken close to the bladder neck to ensure inclusion of the transitional zone of the prostate. The prostate specimen was then subjected immediately to mechanical testing in the laboratory prior to fixation in formalin and subsequent routine histopathological processing. Prepared histological sections were studied to determine the morphology of the specimen and the protocols are described in section 2.6

TURP specimens

Prostate tissue was collected from patients attending for TURP at the department of Urology, Western General Hospital. Patients currently taking monotherapy of an alpha blocker, alfuzosin or tamsulosin were selected. Tissue was not collected from patients who were currently taking 5-alpha reductase inhibitor monotherapy or a combination therapy of both alpha blocker and 5-alpha reductase inhibitor. It was

felt that 5-alpha reductase inhibitors may alter the morphology or cellular properties of the tissue examined. Patients were excluded if they had a diagnosis of prostate cancer or had undergone previous prostate surgery. The TURP chippings were taken at random and subjected immediately to mechanical testing in the laboratory.

Radical Prostatectomy specimens

A retrospective cohort of patients was identified to provide a comparison group to the TURP group. This group comprised patients who were commenced on alpha blocker therapy (alfuzosin or tamsulosin) for LUTS and were subsequently found to have localised prostate cancer and radical prostatectomy was offered to these patients. Paraffin-embedded archival tissue was used in this study. In an attempt to ensure that the blocks represented a similar area of the prostate as represented by the TURP specimens, tissue blocks were carefully selected (with the assistance of an uro-pathologist) to reflect the transition zone of the prostate. Tissue blocks which contained foci of prostate cancer were not utilised.

2.2.3 Clinical data

In this study, prostate specimens were acquired from patients undergoing two different surgical procedures for urological disease. Specimens were obtained from 12 patients undergoing radical cystoprostatectomy, and from 16 patients undergoing TURP and from 16 patients undergoing radical prostatectomy for localised prostate cancer. Clinical data for the three groups are presented below.

12 transverse slices were obtained from 12 patients undergoing radical cystoprostatectomy for bladder cancer. In 5 patients, prostate cancer was subsequently diagnosed. Each specimen that underwent mechanical testing was subsequently examined by a histopathologist to ensure that there was no evidence of prostate cancer. The 12 patients had a mean age of 72 years (range 62-80).

32 TURP chippings were obtained from 16 patients undergoing TURP for BPH. The 16 patients were stratified into 3 groups on the basis of medical therapy. Of the 16 patients, 6 patients received tamsulosin only and 4 patients received alfuzosin only. 6 patients formed the control group as these did not receive any pharmacotherapy. The mean age for the tamsulosin group is 62 years (range 57-76), for the alfuzosin group is 73 years (range 68-80) and for the control group is 67 years (range 60-72). The mean PSA for the tamsulosin group is 5.3 (range 2.6-7.6), alfuzosin group is 4.7 (range 1.8-8.9) and for the control group is 5.3 (range 1.2-6.3).

16 patients who experienced LUTS related to BPH were identified retrospectively. These patients underwent radical prostatectomy for localised small volume prostate cancer. Of these 16 patients, 5 patients received tamsulosin only and 5 patients received alfuzosin only prior to radical prostatectomy. A control group for this cohort comprised 6 patients who did not receive alpha blocker therapy. The mean age for the tamsulosin group is 64 years (range 58-68), for the alfuzosin group is 60 years (range 50-67) and for the control group is 63 years (range 56-68). The mean PSA for the tamsulosin group is 6.4 (range 4.9-7.8), alfuzosin group is 5.9 (range 1.2-15) and for the control group is 9.1 (range 6.4-12.5).

Full clinical details of the patients from whom tissue taken for analysis are presented in Appendix I.

2.3 The measurement of mechanical properties of prostatic tissue

2.3.1 Equipment

The mechanical measurements were obtained from a test rig developed by a research associate from the School of Engineering and Physical Sciences (Mechanical Engineering) Heriot Watt University, Edinburgh. The development of this rig was the subject of a PhD thesis by the research associate. During this project, modifications to the test rig have been made to the probe size and motor control of the probe.

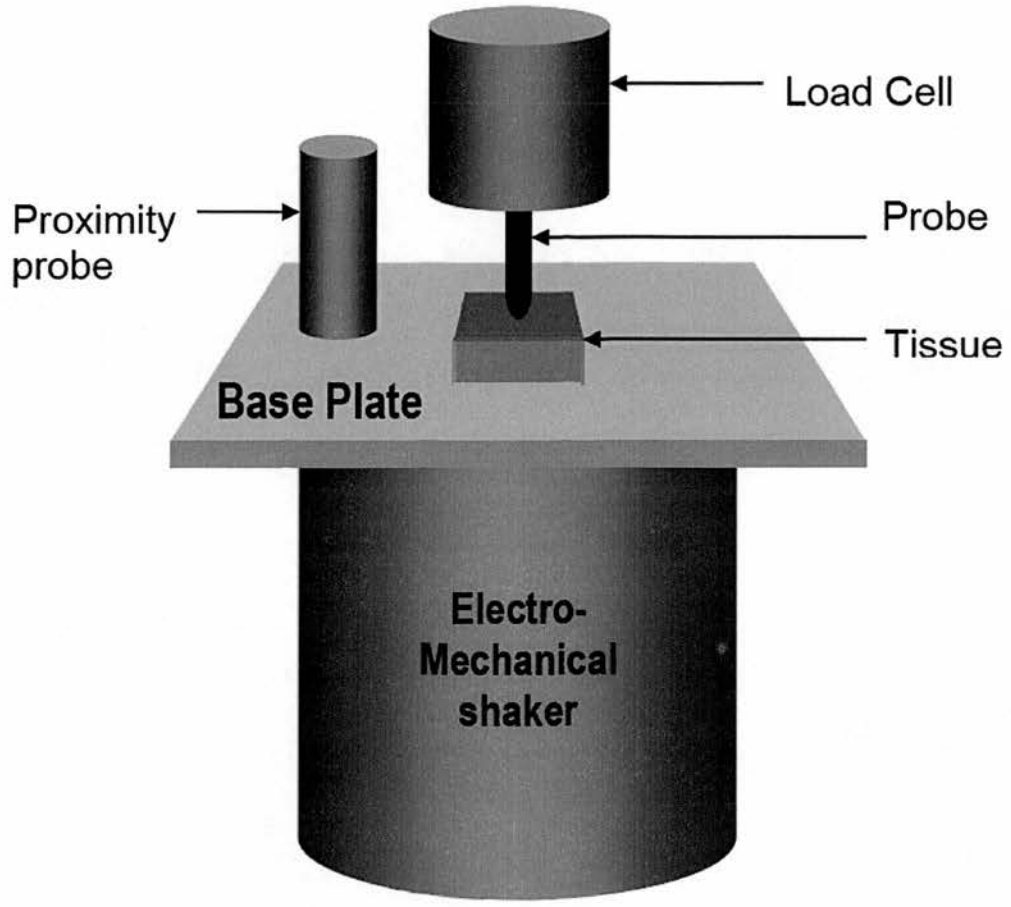

Figure 2.1 – Schematic diagram of the arrangement of the mechanical test rig.

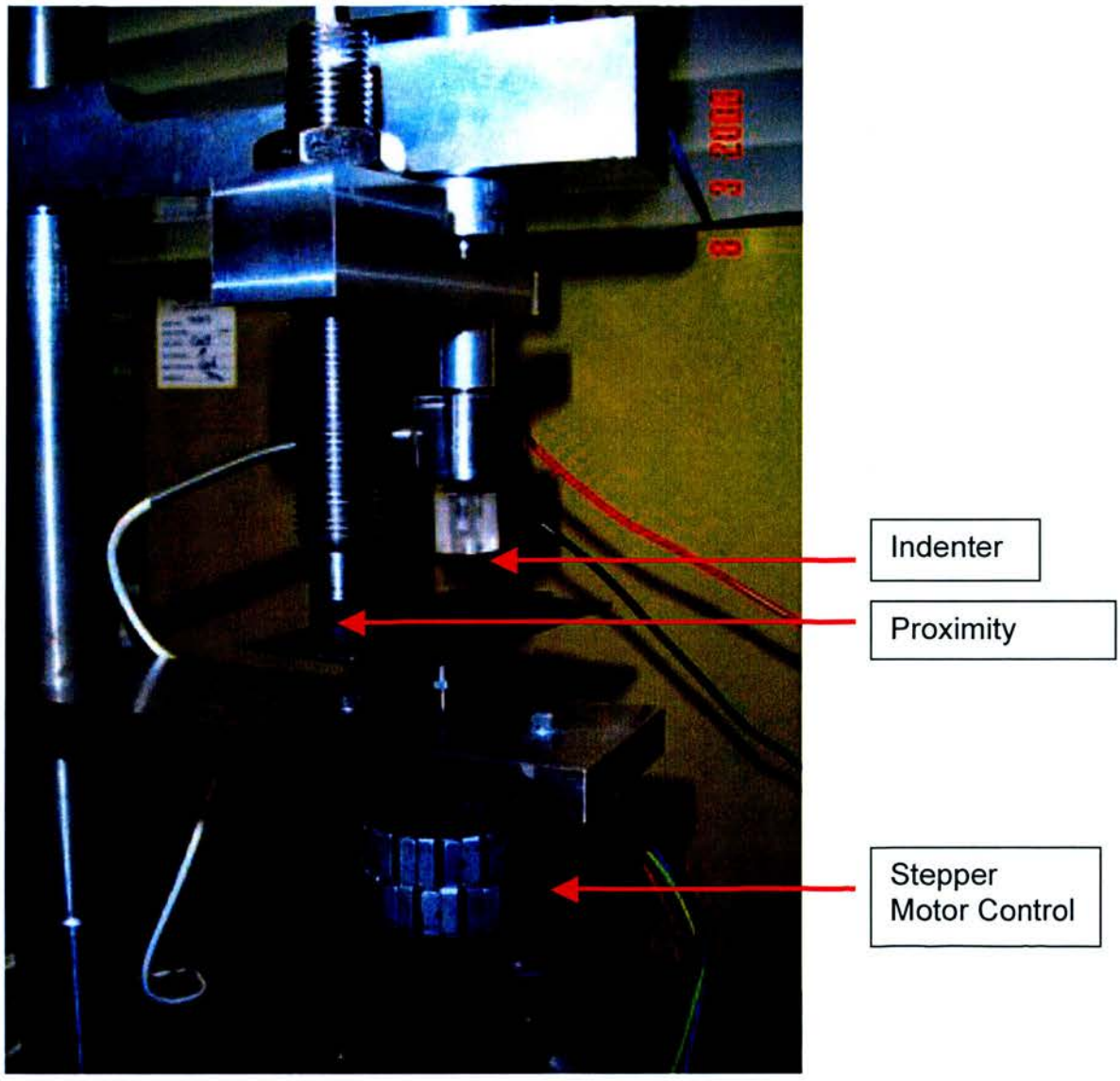

Figure 2.2 – Modified mechanical test rig for the dynamic measurement of prostate tissue. Electromechanical shaker has been replaced by a stepper motor controlled base plate.

The mechanical test rig originally consisted of an electro-mechanical shaker (LDS V201 with amplifier PA-25E) capable of inducing cyclic load between 1Hz and 50Hz at displacements between 0.5mm and 1mm. A load cell (Sensotec Model 31)

with signal conditioning unit (Measurements Group 2311) was used to measure the load resulting from the cyclic loading, and a proximity sensor (Bentley Nevada 3300XL) was used to measure the displacement of the induced cyclic strain at the shaker system. A schematic diagram of the arrangement of the test rig is shown in figure 2.1. The data acquisition system consisted of a National Instrument 6036E card, and Labview was used to generate the actuation frequencies at the shaker system and to acquire the analogue signals of cyclic displacement (ε) and cyclic load (σ) from the proximity sensor and load cell respectively. The dynamic testing system and its calibration using phantom tissues has been described in [129].

A number a modifications was made to the test rig prior to the testing of whole prostate slices. The electro-mechanical shaker was replaced with a stepper motor (shown in Fig 2.2) to allow finer control of the cyclic load to the tissue. The probe size measures 2mm in diameter. In order to understand the effect that probe size has on the mechanical measurements, the probe was exchanged for a micro-indenter measuring 400μm x 500μm. Experiments utilising the 2mm diameter probe were termed macro-probing experiments whereas the experiments utilising the 400μm x 500μm probe were termed micro-probing experiments. The overall aim of this work is to develop an *in vivo* measurement system to assess the mechanical properties of prostate tissue. In a collaborative project with a micro-engineering facility, the Rutherford Appleton Laboratory, the development and assembly of a micro-engineered palpation device for measuring mechanical properties of biological tissues was in progress. Understanding the structure-property relationship of biological tissue at the micro level is crucial in the development of this device.

2.3.2 Mechanical testing protocol

Following collection of the specimen at cystoprostatectomy, the bladder and prostate were transported to the pathology laboratory and a transverse slice of the whole prostate was obtained. The slice measured at least 5mm in thickness. The specimen underwent immediate mechanical cyclic probing. The area subjected to mechanical testing was marked with Indian ink and a needle was embedded into the tissue adjacent to the test point to aid localisation of the test point. Following collection of the TURP specimens, the individual TURP chippings were subjected to immediate mechanical testing.

A controlled compressive cyclic strain is applied to the tissue specimen through the movement of the base plate by the electro-mechanical shaker or stepper motor. The displacement of the plate is measured by the proximity sensor, and the force arising from the specimen is measured by the load cell via the probe which is in contact with the specimen surface. Each specimen was probed at actuation frequencies (ω) between 5Hz and 50Hz at an increment of 5Hz with the pre-strain to ensure that the probe did not lift off the specimen during cyclic loading. The dynamic modulus was determined by two components, the amplitude ratio ($|E^*|$) and phase difference ($\tan \delta$).

$|E^*|$ is the ratio of the amplitudes of the waveforms of these two forces. The phase difference between these two waveforms is $\tan \delta$. Previous work from the Prostate Research Group has demonstrated that the mechanical properties of prostate tissue

from TURP chippings follow a viscoelastic model, analogous to the suspension of a car. The stromal component is likened to the springs and the epithelial content is likened to the dampers of the vehicle, and these components are described mathematically by $|E^*|$ and $\tan \delta$, respectively [127, 128].

2.4 Tissue processing, embedding and sectioning

Once the prostate specimens obtained from TURP or radical cystoprostatectomy had been subjected to mechanical testing, the tissue was fixed in 10% formalin for 48 hours and processed and paraffin embedded. Both types of specimens were processed by infiltration with paraffin wax using a Tissue- Tek Vacuum Infiltration Processor (Model E150, Bayer Diagnostics, Basingstoke, UK) employing a protocol used in the Department of Histopathology at the Western General Hospital, Edinburgh, before being embedded in paraffin wax cassettes using a Tissue-Tek Tissue Embedding Console System (Model 4715, Bayer Diagnostics, Basingstoke, UK). As the whole prostate slices were too large to mount on a standard 75 × 25 mm glass slide, the specimen was divided into individual right and left lobes and then further divided again to yield four specimens that fit into standard embedding cassettes. The TURP specimens were mounted singly on each glass slide. The blocks were cooled on ice before histological sections were cut from the paraffin blocks. Consecutive 4μm-thick sections were cut from each paraffin block using a Rotary Microtome (Model AS325, Shandon, Runcorn, UK). Individual sections were mounted on 75 x 25 x 1mm Superfrost Plus microscope slides (BDH, UK)

which were allowed to stand until dry and then incubated overnight in an oven at 37°C.

2.5 Immunohistochemical Staining

2.5.1 Antibodies for morphological analysis

Primary antibodies to smooth muscle (clone SMMS-1, Dako, Ely UK) and PSA (clone ER-PR8, Dako, Ely, UK) were chosen as these have been demonstrated to represent the tissue components which have an effect upon the mechanical characteristics [130, 131]. The working dilutions of both antibodies were 1:100. Connective tissue proteins such as Collagen Type I and Type III have not been shown to affect the mechanical properties of the tissue [130]. Preliminary studies with anti-fibroblast antibodies did not yield encouraging results as the staining was sub-optimal. Additionally, it was difficult to choose an appropriate antibody which targeted the correct stage of fibroblast development.

The immunohistochemical staining protocol used has been proven by previous work within the group. Essentially, unwanted antibody sites were blocked with serum from the species in which the secondary antibody was raised. Endogenous peroxidase activity was quenched with hydrogen peroxide and endogenous biotin sites were blocked with avidin. The section was then incubated with the primary antibody overnight at 4°C and then incubated with the appropriate biotin conjugated

secondary antibody. Visualisation of staining employed a biotin-streptavidin-peroxidase technique in conjunction with a Diaminobenzidine (DAB) chromogen. The section was fixed with a xylene based fixative.

The full protocol is described below.

2.5.2 Protocol for Immunohistochemical staining of formalin-fixed, paraffin embedded sections

Immunohistochemical staining was carried out as follows:

1 Prepare 4μm-thick sections mounted on superfrost slides as described in section 2.4

2 Place sections in staining rack and incubate at 60°C for 15 minutes

3 Two washes in xylene for 10 minutes.

4 Two washes in absolute ethanol for 2 minutes.

5 Two washes in 90% ethanol for 2 minutes.

6 Two washes in 70% ethanol for 2 minutes.

7 Two washes in 30% ethanol for 2 minutes.

8 Two washes in TBS for 2 minutes.

9 Heat Induced Epitope Retrieval consists of:

a) In the microwave oven, bring 1000ml of citrate buffer or EDTA to the boil by heating for 15 minutes.

b) Add sections and boil for 5 min. Add de-ionised water after boiling to replace water lost as steam. Repeat this step 3 more times.

c) Allow to stand for 20min, then cool dish and sections in sink of cold water for 15-30min, wash once in de-ionised water for 3 min and twice in TBS for 3 min.

10 If blocking serum is frozen, defrost at this point.

11 Wash sections in 3% H2O2 for 10 min.

12 Make up solution of 20% serum in TBS.

13 Separate the 20% serum solution into two portions: to the 1st add 4 drops/ml of avidin. To the other add 4 drops/ ml biotin and then add primary antibody at recommended concentration.

14 Place sections in sequenza using distilled water, then run TBS over each slide.

15 When the TBS has run through, run 100µl serum/ avidin solution over each section. Leave for 30 min.

16 Prepare solution for –ve controls: biotin in 20% serum solution (ie no primary antibody).

17 Run 100µl control solution over the –ve controls.

18 Run 100µl serum/ primary antibody solution over remaining sections. Leave overnight at 4°C.

19 Run TBS over sections twice.

20 Make up a 1 in 200 solution of biotinylated secondary antibody of the appropriate species.

21 Make up streptavidin solution in 5ml of TBS by adding 1 drop of reagent A with 1 drop of reagent B from the supplied kit. Must made up at least 30 min before use.

22 Run 100µl secondary antibody solution over each section. Leave for 30min.

23 Run TBS over each section twice.

24 Run 100µl Streptavidin/TBS solution over each section. Leave 30 min.

25 Run TBS over sections twice.

26 Make up solution of DAB.

27 Treating 10 sections at a time, add 100µl DAB to each for 5 min.

28 Pour DAB back into tube and add DAB neutralising solution.

39 Rinse each slide with tap water.

30 Two washes in TBS for 2 min.

31 Two washes in 30% ethanol for 2 min.

32 Two washes in 70% ethanol for 2 min.

33 Two washes in 90% ethanol for 2 min.

34 Two washes in absolute ethanol for 2 min.

35 Two washes in xylene for 2 min.

36 Mount coverglasses using Depex mounting medium in fume cupboard.

2.5.3 The detection of apoptosis

There are a variety of methods used in the detection of apoptosis with the two most common approaches cited in the literature are observation of cell morphology and detection of DNA fragmentation [132]. Despite the usefulness of these techniques, both techniques have problems with interpretation and artefacts. The specific changes in the cell nucleus, such as segmentation of the nucleus, are cytological hallmarks of apoptosis but are difficult to interpret in paraffin embedded sections. The detection of fragmented DNA strands using TUNEL assays has been used to

detect apoptosis but this method is not specific to apoptosis *per se* as cell necrosis also generates fragmented DNA [133].

Recent understanding of the events in the apoptosis cascade have highlighted that caspase activation (the cleavage of procaspase to active caspase) is a specific indicator of cell suicide mechanism. Caspase 3 is a central effector of caspase and mediates the cleavage of itself and other caspases downstream. The development of antibodies to the neoepitopes of caspases has been shown to detect apoptotic events with high specificity and sensitivity [134]. Therefore the studies of apoptosis in BPH tissue are conducted using two methods of detection, namely, TUNEL assay (Promega, Southampton, UK) and Anti-active Caspase-3 (Promega, Southampton, UK).

2.5.4 Protocol for the detection of apoptosis using Colorimetric TUNEL kit in paraffin embedded sections

Supplied with the 40 reactions TUNEL assay kit from Promega, UK are:

9.6ml of Equilibration Buffer

40µl Biotinylated Nucleotide Mix (2 × 20 µl)

40µl Terminal Deoxynucleotidyl Transferase, Recombinant (2 × 20 µl)

70ml SSC Buffer (20× concentration)

10mg Proteinase K

40µl Streptavidin HRP (0.5mg/ml)

200µl DAB 20× Chromogen

200µl DAB Substrate 20× Buffer Solution

The following protocol describes the steps necessary for the detection of apoptosis using the Colorimetric TUNEL assay:

1 Prepare 4µm-thick sections mounted on superfrost slides as described in section 2.4.2.

2 Two washes in xylene for 5 minutes.

3 One wash in absolute ethanol for 5 minutes.

4 One wash in absolute ethanol for 3 minutes.

5 Two washes in 90% ethanol for 3 minutes.

6 Two washes in 70% ethanol for 3 minutes.

7 Two washes in 30% ethanol for 3 minutes.

8 Two washes in PBS for 3 minutes.

9 Remove the liquid from the tissue and place the slides on a flat surface. Prepare a 20µg/ml Proteinase K working solution from the 10mg/ml Proteinase K stock solution (10mg Proteinase K reconstituted with 1ml of Proteinase K buffer detailed in section 2.1.2.) by diluting 1:500 in PBS. Add 100µl of the 20µg/ml Proteinase K solution to each slide to cover the tissue section and incubate slides for 10 minutes at room temperature.

10 Two washes in PBS for 5 minutes.

11 Remove excess liquid by tapping the slides. Cover section with 100µl of Equilibration Buffer. Equilibrate at room temperature for 5-10 minutes.

12 While the sections are equilibrating, thaw the Biotinylated Nucleotide Mix on ice and prepare sufficient rTdT reaction mix. 100µl of reaction mix is used to cover each section. 100µl of Reaction mix is composed of 98µl of Equilibration Buffer and 1µl of Biotinylated Nucleotide Mix and 1µl of rTdT Enzyme. For negative controls, omit rTdT enzyme from the reaction mix.

13 Blot around the equilibrated areas and add 100µl of the reaction mix to the sections.

14 Cover with plastic coverslips to ensure even distribution of the reagent. Incubate slides at 37oC for 60 minutes inside a humidified chamber to allow end-labelling to occur.

15 Dilute the 20X SCC 1:10 with deionised water. Remove plastic coverslips and terminate reactions by immersing slides in 2X SCC for 15 minutes.

16 Two washes in PBS for 5 minutes.

17 Block endogenous peroxidases by immersing slides in 0.3% hydrogen peroxide in PBS for 3 minutes.

18 Two washes in PBS for 5 minutes.

19 Dilute the Streptavidin HRP solution 1:500 with PBS. Add 100µl to each slide and incubate for 30 minutes at room temperature.

20 Two washes in PBS for 5 minutes.

21 Combine the DAB components just prior to use. Add 50µl of the DAB Substrate 20X Buffer to 950µl deionized water. Then add 50µl of the DAB 20X Chromogen and 50µl of Hydrogen Peroxide 20X. Add 100µl of DAB solution to each slide and develop until there is a light brown background

22 Rinse several times in deionised water.

23 Counterstain with Haematoxylin and develop with ammonia water.

24 Two washes in 30% ethanol for 2 min.

25 Two washes in 70% ethanol for 2 min.

26 Two washes in 90% ethanol for 2 min.

27 Two washes in absolute ethanol for 2 min.

28 Two washes in xylene for 2 min.

29 Mount coverglasses using Depex mounting medium in fume cupboard.

2.6 Quantitative image analysis of a transverse section of prostate tissue

2.6.1 Introduction

Quantitative image analysis was performed using an upgraded Leica image analysis system (Leica Microsystems, Cambridge, UK). In addition to the Leica DMR light microscope with an automated stage, the original digital camera was upgraded to a QImaging QICAM digital camera (Mediacybernetics, Berkshire, UK) and the software upgraded to Image Pro Plus 5.1 with Pro-series Turboscan and Surveyor specimen scanning software ((Mediacybernetics, Berkshire, UK). The Turboscan and Surveyor software allows for accurate mosaics (stitched composite images) of the specimen to be captured and created.

The protocol for morphometric analysis of TURP specimens has been established by Phipps *et al* [135]. Briefly, at x200 magnification, the whole section, mounted on a motorised stage, was scanned by the microscope and the images written to the hard disk. Quantitative image analysis was performed on each image and a percentage area occupied by the target histological component was calculated and exported to an excel file (see section 2.6.3).

This protocol was adopted for the analysis of whole transverse sections of prostate. As described in section 2.4, the specimen was divided into four sections to allow for mounting of the specimens to standard glass microscope slides. This protocol generated a significant increase in the number of images captures per section. An

average of 60 to 100 images would represent one TURP specimen. Application of this protocol to sections of mounted whole prostate resulted in 800-1000 images per section. Lower magnifications (×50 and ×100) of image capture were considered but did not provide the image resolution needed for accurate morphometric analysis.

The following section describes the methodology used to analyse the morphology of transverse sections of prostate tissue.

2.6.2 Methods

Multiple mechanical test points were made on transverse sections of whole prostates. The areas tested were marked with Indian ink and a pin-hole was created by embedding a needle adjacent to the test point prior to the formalin fixation process. These measures were used to enable accurate localisation of the test points after the section was fixed, processed and stained. A transverse slice of prostate was fixed and processed as described in section 2.4. Each prostate lobe was halved to yield four blocks which were embedded in wax, cut and mounted on a standard microscope glass slide. The morphometric analysis protocol to analyse TURP specimens (see section 2.6.1) was used to capture images of the transverse slice of prostate. To locate the individual areas of tissue that were subjected to mechanical analysis, a composite histological "map" of the whole specimen was generated. Panavue Assembler (Panavue, Quebec, Canada) software was used to manually

stitch individual rows of images to then form a mosaic or composite image of the whole section (see figure 2.3).

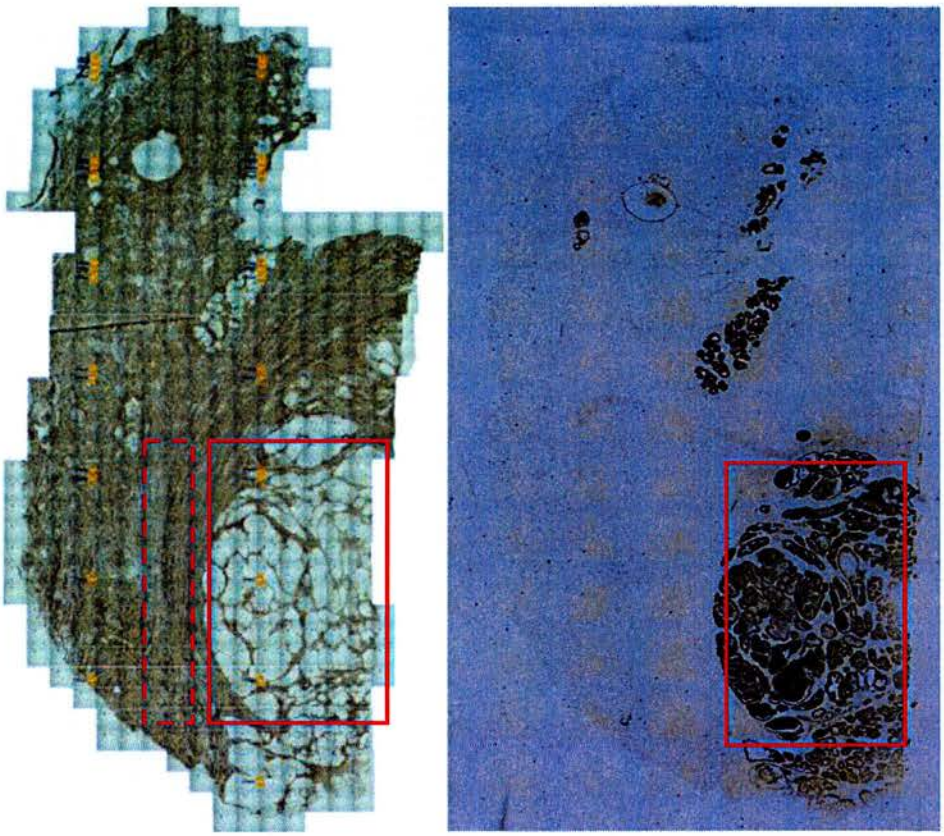

Figure 2.3 – Composite image or mosaic of a section stained with anti-smooth muscle antibody on the left and anti-PSA on the right. The image on the left is composed of 759 individual images taken at ×200 magnification. Solid lined red box corresponds to an area of interest corresponding to a glandular nodule, and dashed line box highlights a predominantly stromal area.

The individual images are numbered according to the sequence of capture. Therefore a numerical matrix corresponding to the individual images could be created for the whole section (see figure 2.4).

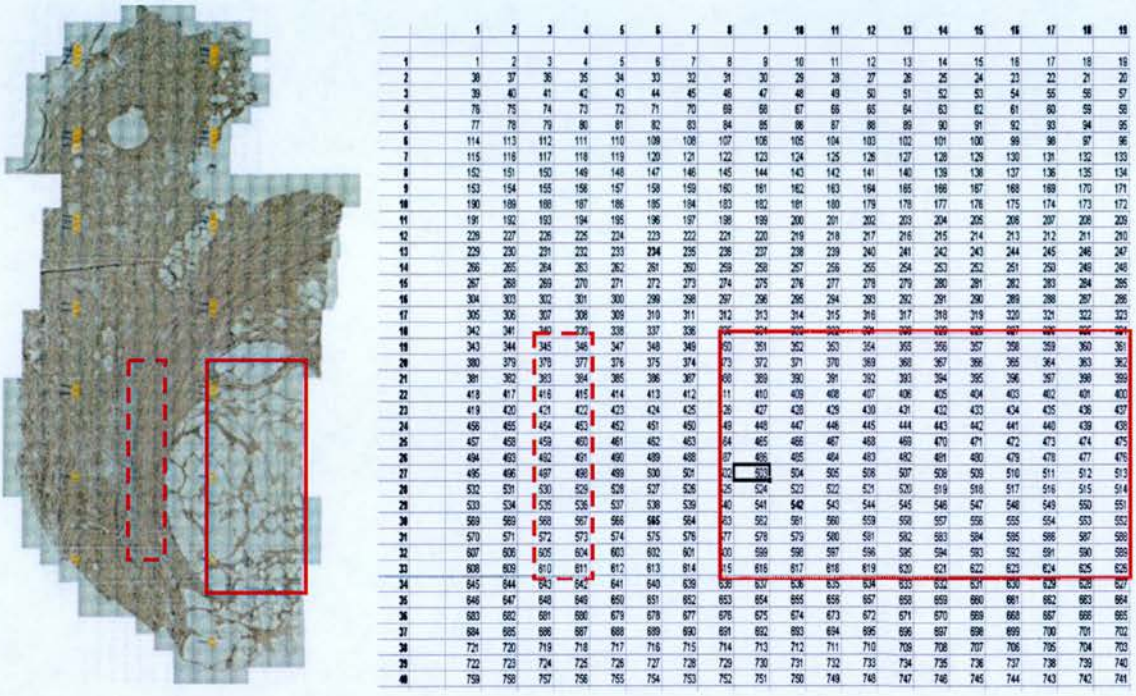

Figure 2.4 – The numerical "map" on the right corresponds to the group of individual images that comprise the whole section of prostate tissue (stained with anti-smooth muscle antibody). The dashed lined box corresponds to an area of stroma and solid lined box corresponds with a nodular area as seen in figure 2.3

Two main groups of tissue were of interest. Glandular nodules are defined as having an expansile border with glandular tissue branching into stroma. In nodules with high epithelial content, the stroma is usually reduced to a narrow band in between glands. Included in this definition were cystic glandular nodules which were

composed of distended, enlarged lumens with flattened epithelium (see figure 2.5). Stromal hyperplasia was defined as stroma with a predominant fibroblastic component with evenly dispersed smooth muscle cells [32]. Using these definitions, a group of images representing glandular nodules and stromal hyperplasia were selected and the morphology compared with each other.

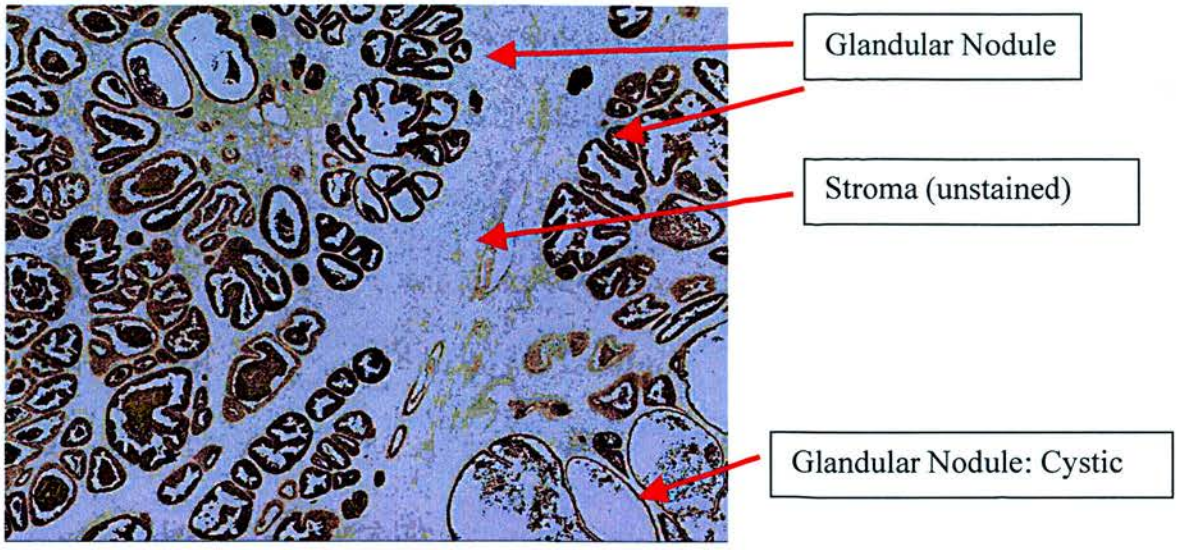

Figure 2.5 – Micrograph (× 200 magnification) showing hyperplastic nodules stained with anti-PSA antibody. The intervening stroma between the glands is not stained. However, it can be seem that the stroma is compressed between the glandular elements. Top left of the image shows a nodule with a normal branching glandular pattern and bottom right of the image shows a nodule with a cystic pattern.

As each image comprising the mosaic corresponded to a value on the numerical matrix, areas of interest were delineated, selected and subjected to quantitative image

analysis. The solid red box in figure 2.3 delineates an area of interest corresponding to a glandular nodule. Individual images that comprise this nodule are highlighted in a solid red box in the numerical matrix or map of the section. Once the groups of images are selected, the percentage area of smooth muscle and epithelial tissue within each individual image are measured using quantitative image analysis software using the protocols and methods described in section 2.6.3.

2.6.3 Quantitative morphometric analysis of nodular and stromal areas

Using Leica Qwin image analysis software (Leica Microsystems, Cambridge, UK), colour detection thresholds were used to identify the brown colour of the DAB chromogen within an image. An example of an image demonstrating the brown DAB chromogen and the subsequent software colour detection is seen in Figure. 2.6

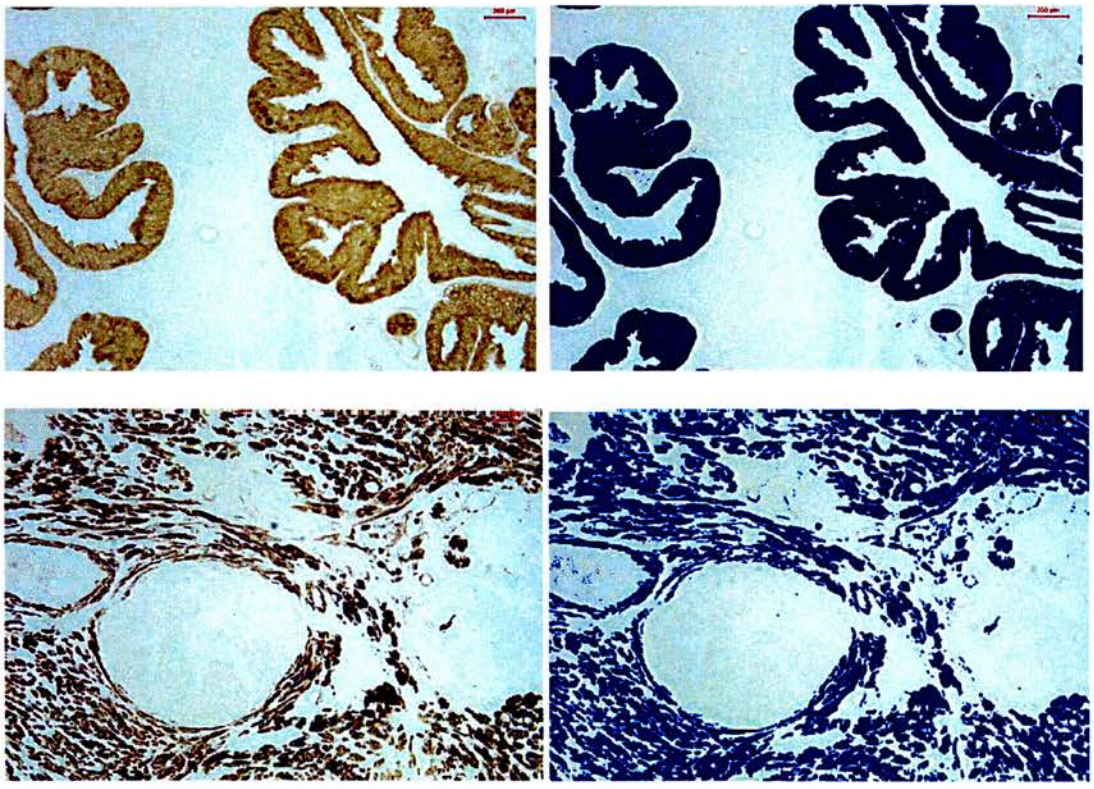

Figure 2.6 – Top left hand image demonstrates an image stained with anti-PSA (x200 magnification). Top right hand image demonstrates the same image with the brown colour detected by the software – signified by the blue colouring. Bottom left hand image is an image stained with anti-smooth muscle antibody. Bottom left demonstrates the brown chromogen detected by the software.

The simple detection and calculation of the percentage area of brown colour within an image was suitable for images stained with anti-smooth muscle antibody. Calculation of the area occupied by the epithelial gland, stained with anti-PSA antibody, requires the software to calculate the percentage area of the lumen. The "fill" parameter of the software is used to "fill in" the area bordered by brown colour. Figure. 2.7 demonstrates the software "filling-in" the luminal area of epithelial tissue. These measurements are performed for each image and data is exported into an excel spreadsheet. Calculation of the overall percentage of brown staining within a group of images, the mean values of the measurements of the individual images was used. Percentage of smooth muscle (%SM), percentage of epithelial tissue (%ET) and the mean acinar area were calculated.

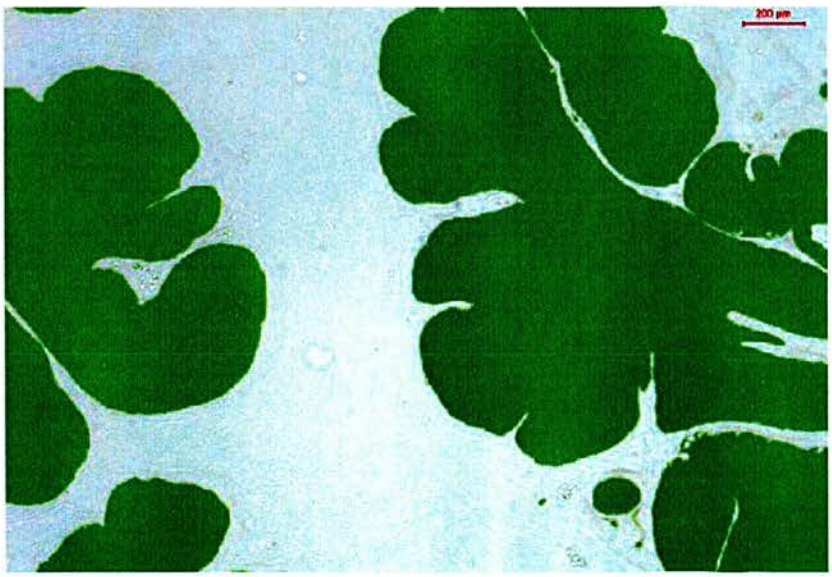

Figure 2.7 – The green colour shows the software "filling-in" the luminal area of the epithelial gland, thereby calculating the percentage area occupied by the glands in the image.

2.6.4 Results of the comparative studies of nodular and stromal areas

This study examines the relationships between histological areas classified as glandular nodules or stromal hyperplasia in a whole transverse section of a prostate. The methodology of morphometric analysis is described in section 2.6.2 and 2.6.3. The whole section of prostate is divided into four sections and subjected to immunohistochemical staining for anti-smooth muscle myosin and anti-PSA. From each section, an area representative of a nodule and of an area of stromal hyperplasia was selected for analysis. The %SM and %ET was calculated from the individual images representing this area of interest and the mean values are presented in tables 2.1 and 2.2. These values are presented with the mean %SM and %ET of the whole section.

%SM	Section 1 (Mean ±SD)	Section 2 (Mean ±SD)	Section 3 (Mean ±SD)	Section 4 (Mean ±SD)
Nodule	18 ± 11	15 ± 7	20 ± 11	23 ± 18
Stroma	42 ± 8	30 ± 5	37 ± 5	35 ± 4
Whole section	34 ± 16	19 ± 9	27 ± 11	30 ± 13
ANOVA	<0.005	<0.005	<0.005	<0.005

Table 2.1 – Morphology of areas classified as nodules, stroma and the whole section. %SM is presented as a mean of the group of images selected to represent these areas of interest. The results of the ANOVA analysis between the groups are presented.

%ET	Section 1 (Mean ±SD)	Section 2 (Mean ±SD)	Section 3 (Mean ±SD)	Section 4 (Mean ±SD)
Nodule	58 ± 23	51 ± 27	36 ± 22	49 ± 22
Stroma	24 ± 21	19 ± 16	24 ± 20	18 ± 15
ANOVA	<0.005	<0.005	<0.005	<0.005

Table 2.2 – Morphology of areas classified as nodules and stroma. %PSA is presented as a mean of the group of images selected to represent these areas of interest.

The results presented in tables 2.1 and 2.2 are a summary of the morphometric analysis of a whole prostate section at × 200 magnification. The mean number of images used to "describe" a whole section is 332 (range is 252 – 437). Comparisons of the %SM and %ET between areas classified as nodules and stroma were made using single factor analysis of variance (ANOVA). This statistical test provides an analysis of variance of the data for two or more samples. This tests the hypothesis that the mean for each sample considered are drawn from the same underlying probability distribution. The ANOVA demonstrates that there were significant differences between the morphology of nodules and stroma with respect to the morphology of the whole section.

2.6.5 Discussion

In this study, the complex architecture from a transverse slice of prostate is examined in great detail at × 200 magnification. The ability to create a histological map of the whole section allows areas of histological interest to be identified, and in association with the numerical map, quantified. The results presented in this section show that areas of histological interest such as glandular nodules or predominantly stromal areas can be represented in a quantitative manner and are found to be significantly different to each other and to the section area taken as a whole. The description of the histological hallmarks of BPH, nodular hyperplasia of both glandular and stromal elements, has been reported by Price *et al* [32]. Their work highlights the heterogeneity of tissue composition in BPH and with increasing gland size; the epithelial-rich nodules were the most rapidly evolving tissue component. The results presented here confirm that there are discrete areas in the prostate with different morphological characteristics. Within the four sections, that represent a transverse section of a whole prostate, there is significant heterogeneity in the morphology. There are easily recognisable histological hallmarks of BPH such as glandular nodules and stroma hyperplasia. The results from this work are in agreement with the studies of Price *et al*.

This methodology of morphometric analysis is a very labour intensive process and places great demands on both the computer hardware and software and also the researcher. The number of images used to represent just a quarter of a whole slice is between 600-800 images. These images require significant computation resources to

allow for the stitching of images together to form a mosaic. This process also demands a significant amount of time from the researcher to manually stitch the images together. Therefore, section 2.7 reports on the modification of the above methodology to decrease the time involved in quantitative image analysis. It was important not to compromise the unique opportunities that this methodology offers in the analysis of discrete histological areas of interest within a whole transverse section of prostate.

2.7 Quantitative image analysis of loco-regional morphology

This section describes the modifications to the methodology used in section 2.6 to allow for the rapid and accurate location of histological areas of interest to be subject to computerised morphometric analysis.

2.7.1 Introduction

In the methodology described above for the image capture of prepared sections of whole prostates, the manual creation of histological maps of the sections to allow analysis of regional areas of interest is very demanding of resources. The development of a less demanding methodology for generating a histological map of a section, without compromising the level of detail obtained, is the main aim of this study.

The addition of the Turboscan and Surveyor software (Mediacybernetics, Berkshire, UK) to the morphometric analysis workstation allows the user to capture the whole section at lower magnification (×5 magnification) to create a low-resolution mosaic. As the microscope is calibrated accurately to an automated motorised stage, the user can use the software to pinpoint an area of interest on the lower magnification mosaic. A new "origin" point (that is, a point on the mosaic from which the microscope will begin scanning at again) can be placed over an area of interest, and a user defined area can be captured at higher magnification to give images of higher resolution suitable for quantitative image analysis.

2.7.2 Methods

In order to localise the position of the area of prostate tissue subjected to mechanical testing, the probe tip was covered in Indian ink. The probe was applied to the tissue surface and subjected to cyclic compressive strain to obtain the mechanical measurements. Once the probe was removed, a small pin, measuring 0.7mm in diameter was inserted into the tissue adjacent to the marked point. Each prostate lobe is halved to enable mounting onto a standard 75 x 25 x 1mm Superfrost Plus microscope slide (BDH, UK) as described in section 2.4. The prostate specimen was processed and paraffin-embedded with the pin in situ and removed prior to sectioning the specimen. Once the section had undergone immunohistochemical staining, the area subjected to mechanical testing could be identified easily on the low power mosaic created by the software.

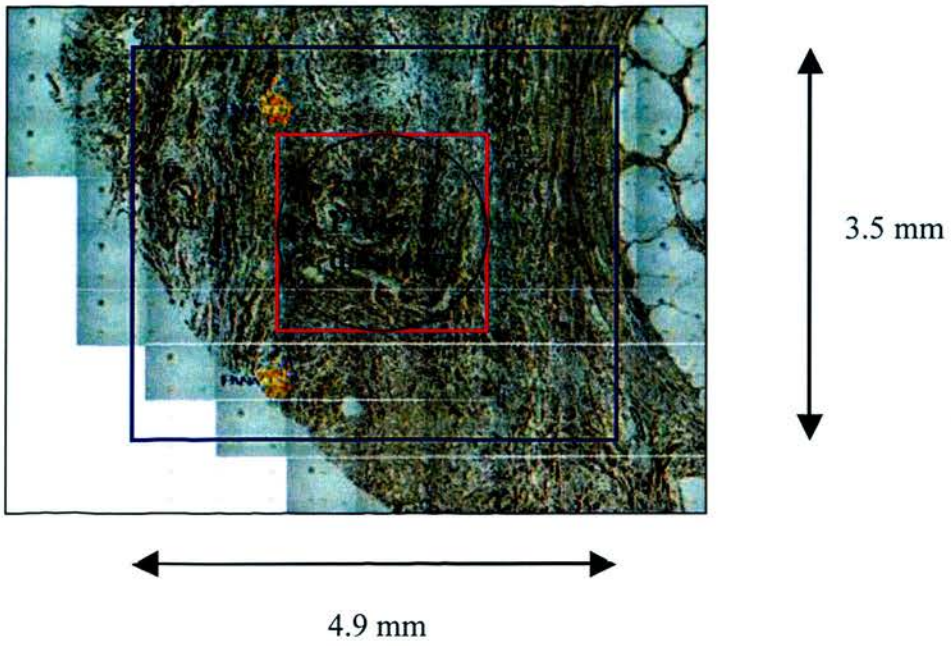

Figure 2.8 - Mosaic image demonstrates the relationship between the number of images corresponding to the macro probe size which is 2mm in diameter (red box) and the selected 7 x 7 matrix of images for morphometric studies of loco-regional morphology (blue box).

The mechanical measurements were conducted via a circular probe size of 2mm in diameter (see section 2.3.1), and the area under the probe was calculated using the mathematical formula of πr^2 (π equals 3.14 and r denotes the radius) to be 3.14mm^2. The equivalent number of frames at ×200 magnification is roughly 3 × 3 frames with one frame measuring 0.7mm × 0.5mm. However, there is the issue of uncertainty of the area of histology considered corresponding to the area subjected to mechanical point probing. A self-similarity exercise was performed to determine the optimum area to capture and use for loco-regional morphometric studies.

Self-similarity studies

The protocol used 49 images in a 7 × 7 matrix to analyse loco-regional areas of interest. An assessment was made as to the suitability of this arbitrarily chosen matrix size. Within this 7 × 7 matrix, the image could be divided into various smaller matrix of which, 3 × 3 matrix would correspond to the macro probe size (see figure 2.8). In mathematics, self-similarity describes an object that is exactly or approximately similar to a part of itself. In this "self-similarity" test, the aim is to assess which matrix pattern is most similar to itself. Using the framework of the 49 images, a "self-similarity" test was used to determine the pattern of results obtained from using a 3 × 3 matrix, a 4 × 4 matrix and then a 5 × 5 matrix of images to assess the morphology. This study quantifies the observed variability within the histological values when considering different sizes of matrix that represent the areas of interest studied.

Initially, a 3 × 3 matrix or "mask" was applied to the grid of 49 individual images that contains the area of interest. A matrix of 3 × 3 yields 9 images. Within the overall framework of the 7 × 7 matrix, it is possible to describe 25 unique groups of 9 images.

This represents the uncertainty of the actual position of the macro indenter probe on the tissue. Using single factor analysis of variance (ANOVA), the variability and difference *within* these 25 groups of 9 images was analysed. The p values from this analysis are tabulated in the columns labelled "3 × 3" in Table 2.3. The non-

significant analyses, i.e. $p>0.05$, are highlighted in bold in table. That is, there is no significant variability between the 25 groups of 9 images. In other words, the area of interest examined is very homogenous.

A larger matrix of 4×4 was applied to the 7×7 matrix frame which gave a possible 16 groups of 16 individual images. The variability and difference was analysed between these groups using ANOVA. The p values of these analyses are tabulated in the "4×4" columns. Non-significant variability between groups is highlighted in bold. Finally a 5×5 matrix was applied to the 49 images which gave a possible 9 groups of 25 images. Again the same ANOVA test was applied to these groups.

Point	3x3 (M)	4x4 (M)	5x5 (M)	3x3 (P)	4x4 (P)	5x5 (P)
P70 Q1 Pt1	0.001	**0.635**	**0.965**	**0.077**	**0.393**	**0.789**
P70 Q1 Pt2	0.016	**0.227**	**0.961**	0.000	0.001	**0.222**
P70 Q1 Pt3	**0.068**	**0.583**	**0.710**	**0.531**	**0.753**	**0.430**
P70 Q1 Pt4	0.002	0.017	**0.158**	0.013	**0.092**	**0.487**
P70 Q1 Pt5	**0.762**	**0.734**	**0.745**	0.009	**0.055**	**0.583**
P70 Q2 Pt1	0.002	0.033	**0.382**	0.000	**0.008**	**0.493**
P70 Q2 Pt2	**0.059**	**0.262**	**0.977**	0.004	**0.175**	**0.884**
P70 Q2 Ot3	**0.213**	**0.951**	**0.812**	0.000	0.000	0.002
P70 Q2 Pt4	0.012	**0.086**	**0.498**	**0.072**	**0.422**	**0.775**
P70 Q2Pt 5	**0.643**	**0.714**	**0.080**	0.001	0.025	**0.285**
P70 Q3 Pt1	0.000	**0.070**	**0.564**	0.000	0.016	**0.406**
P70 Q3 Pt2	0.000	0.000	0.002	**0.678**	**0.968**	**0.906**
P70 Q3 Pt3	0.004	**0.563**	**0.741**	0.000	0.000	0.043
P70 Q3 Pt4	**0.581**	**1.000**	**0.971**	0.000	0.000	0.000
P70 Q4 Pt1	0.000	0.000	0.000	0.000	0.006	**0.795**
P70 Q4 Pt2	0.000	0.002	0.009	0.001	0.002	**0.145**
P70 Q4 Pt3	**0.902**	**0.974**	**0.884**	0.010	**0.132**	**0.668**
P70 Q4 Pt4	0.000	0.012	**0.437**	**0.990**	**1.000**	**0.993**

Table 2.3 - Results of a self-similarity test of morphometric analysis in loco-regional areas of histological interest. (M) denotes sections stained for smooth muscle and (P) denotes sections stained for epithelial tissue. 3 × 3, 4 × 4 and 5 × 5 denote the different sizes of areas of interest composed of the respective number of image frames. The bold highlights non-significant ANOVA results *within* the groups.

2.7.3 Discussion and conclusions

The protocol described in Section 2.7.2 allows for a smaller area to be captured for morphometric analysis. This protocol enables resources to be saved and less time is required to process images. The use of a matrix of 49 individual images to analyse an area which is morphologically different to adjacent areas has been addressed in the "self-similarity" study summarised in Table 2.3. With respect to the column "3 × 3", a significant proportion of the ANOVA results confirm that there are significant variability between the images captured using the 3 × 3 matrix. Considering the "4 × 4" column, the number of non-significant ANOVA results increase but the majority of the results demonstrate significant variability between images captured. The 5 × 5 column shows the majority of results are non-significant in the variability within the groups of images represented with this matrix. This implies that the area considered by these varying matrices are not significantly different from each other and therefore, using a matrix this size will give an "average" of the histology considered in this small area – whilst still acknowledging the heterogeneity of the histology from each individual microscope frame to the next. The pattern that is demonstrated is that in the 3 × 3 matrix group, the variability within each of the 25 groups is significantly different from each other. In other words, if using a matrix of 3 × 3, the difference in histology considered in this matrix will be significantly different to the next group. However, if using a 5 × 5 matrix, the incidence of non-significant analysis increases in this group. This indicates that the histology considered within the 9 groups of 25 individual images is likely not to be significantly different to the adjacent 5 × 5 matrix. This observation holds true for sections stained with anti-PSA

and anti-smooth muscle. The conclusion to this study is that a matrix of 7 × 7 is the optimum size for the capture of an area of loco-regional morphology that will yield sufficient detail to demonstrate the difference between areas classified as nodules and stroma.

2.8 Quantitative image analysis of apoptotic index

This section describes the methodology used to quantitatively assess the apoptotic index within prostate tissue. As discussed in section 2.5.3, two methods of assessing apoptosis are required to adequately assess the apoptotic activity in tissue. The two methods utilised in this study produce different images which have to be analysed in a different manner.

2.8.1 Caspase-3 Immunostaining

For quantitative analysis of immunohistochemical staining, an overall score was calculated by multiplying the intensity of the staining by the percentage of positive cells which exhibited the staining (overall score=percentage of positive cells multiplied by intensity). The percentages of positive cells were counted using the automated programme within Image Pro Plus 5.1 (Mediacybernetics, Berkshire, UK).

The validity of the automated counting of cells was confirmed by comparing results obtained manually by counting cells showing staining and counting the overall number of cells within a ×400 magnification image. The intensity was recorded on an ordinal scale of 0-3. 0 indicating absent staining and 3 indicating intense staining. The sections were evaluated independently by 2 observers and during the evaluation, each observer had reference images indicating the different grades of intensity. Figure 2.9 shows the reference images indicating intensity of staining.

10 randomly selected images at ×400 magnification were used to quantify the immunoreactivity of caspase-3 within prostate epithelial tissue. A mean apoptotic score was used in the analysis. Due to the small sample size, two blocks of tissue was used from each patient to ensure that the level of apoptosis was comparable in the two samples.

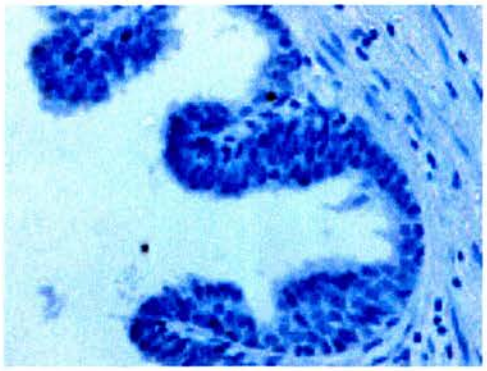

Control Image – Score 0

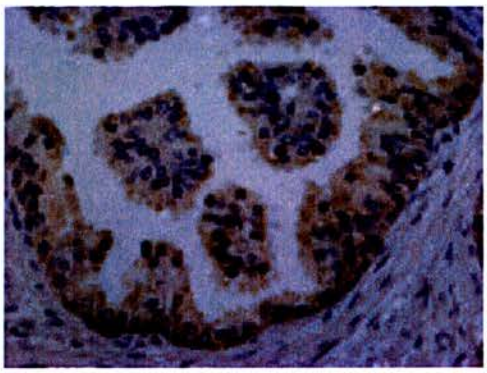

Mild staining – Score 1

Moderate staining - Score 2

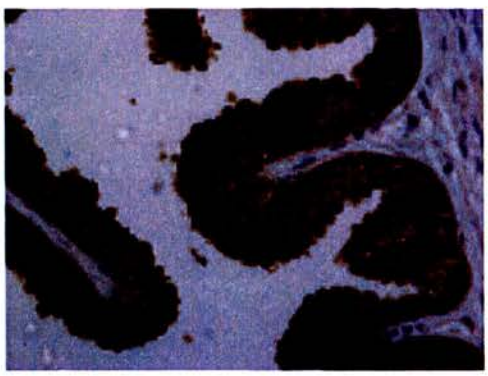

Strong staining – Score 3

Figure 2.9 – Reference images used in the analysis of Caspase-3 immunoreactivity in prostate epithelial cells.

2.8.2 TUNEL immunostaining

Deoxyribonucleic acid (DNA) fragmentation within prostate epithelial cell nuclei was evaluated using terminal deoxynucleotidyl transferase dUTP nick end labelling (TUNEL). The protocol for Immunostaining sections with the TUNEL kit (Promega, Southampton, UK) is described in section 2.5.4. A reference slide was used as a positive control which demonstrated positive staining of the nuclei. Using this slide, the automated image analysis system was programmed to count the total number of nuclei per microscope image captured (at ×400 magnification) and then counted only nuclei that was stained brown. The result was expressed as a percentage of positive cells stained over the total number of cells in the section. 10 random fields were selected per section and a mean score was calculated per section. As the sample size was small, two blocks of tissue per patient were evaluated.

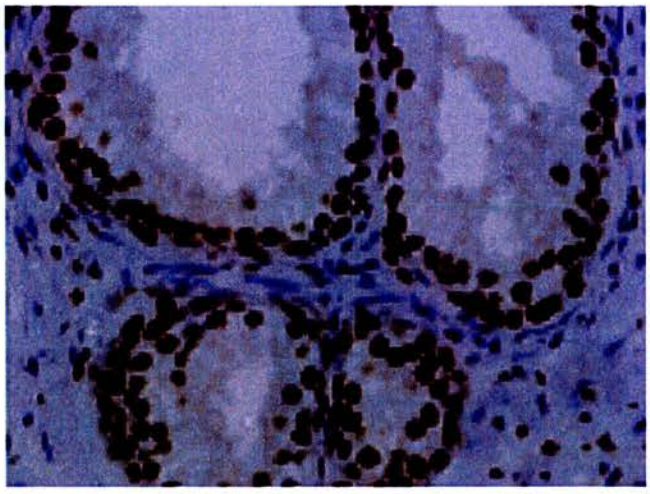

Figure 2.10 – Reference image demonstrating positive staining nuclei to the TUNEL assay.

2.9 Statistical Analysis

This section describes the statistical methods used in analysis of the data generated.

2.9.1 Introduction

There are two main aims of this project. Firstly, to explore the relationship between the morphology and mechanical properties of the prostate as analysed as a whole section. Secondly, to explore the relationship between alpha blocker therapy the effects upon apoptotic indices and the mechanical and morphological characteristics of prostate tissue. All statistical analysis of data was performed using Microsoft Excel (Microsoft, USA) with the Statplus Version 2.5 add-in. In all analysis, a p-value of 0.05 or less was considered to be statistically significant.

2.9.2 Single Factor Analysis of Variance

Single factor analysis of variance (ANOVA) was used to analyse the significance of the data when performing multiple comparisons between the morphological and mechanical measurements from different prostates. This test provides a simple analysis of variance on data for two or more samples. This tests the hypothesis that the mean for each sample considered are drawn from the same underlying probability distribution. This is used instead of the t-test when there are more than 2 samples to be considered.

2.9.3 Simple linear regression analysis

Simple linear regression analysis was used to assess the strengths of the correlations between the morphological and mechanical properties between prostates. When using this test, it is assumed that the relationship between the two variables is linear. The Pearson co-efficient is a measure of the strength of this relationship with a value ranging from +1 to -1. R^2 is the square of the Pearson co-efficient and describes the percentage of the variation in the dependent variable that is influenced by changes in the independent variable.

2.9.4 Multiple linear regression analysis

Multiple linear regression analysis was used to assess the strengths of the correlations between the morphological and mechanical properties between prostates. The relationships are assumed to be linear. Multiple linear regression analysis allows for the assessment of relationships between the "response" variable and multiple predictor or "independent" variables. The process generates a multiple R^2 which describes the percentage of variation in the dependent variable that is influenced by changes in the multiple independent variables.

2.9.5 Artificial Neural Networks

Artificial neural networks (ANN) are mathematical models based upon the physical low-level structure of the brain. The term "artificial" in ANN is used to differentiate the computer based system from the biological systems. ANNs have been used in widely diverse areas such as financial, industrial and medical applications. Within the realm of urology, Djavan *et al.* demonstrated the use of ANN in the diagnosis and prognosis of prostate cancer. [136]. There are different types of ANN that are used to assess various different types of problem areas. However, the "standard" type of ANN used in general practice is termed a "feed-forward" network which is the type used in this study.

The basic data structure in the human brain is the neuron which numbers approximately 10^{11}. The neuron has branching cell receivers called dendrites and a projection called an axon which propagates the nerve signal. At the end of the axon, the axon terminal transmits the electro-chemical signal across a synapse to the receiving cell. ANNs are computer programmes that mimic some of the features of this biological system. Neurons and synapses are modelled with various connection strengths, termed "weights", for each pair of connected neurons. Unlike the human brain, there are a specific set of input and output neurons, along with the synapses and weights of the system, which correspond to instructions from a computer program (See figure 2.11).

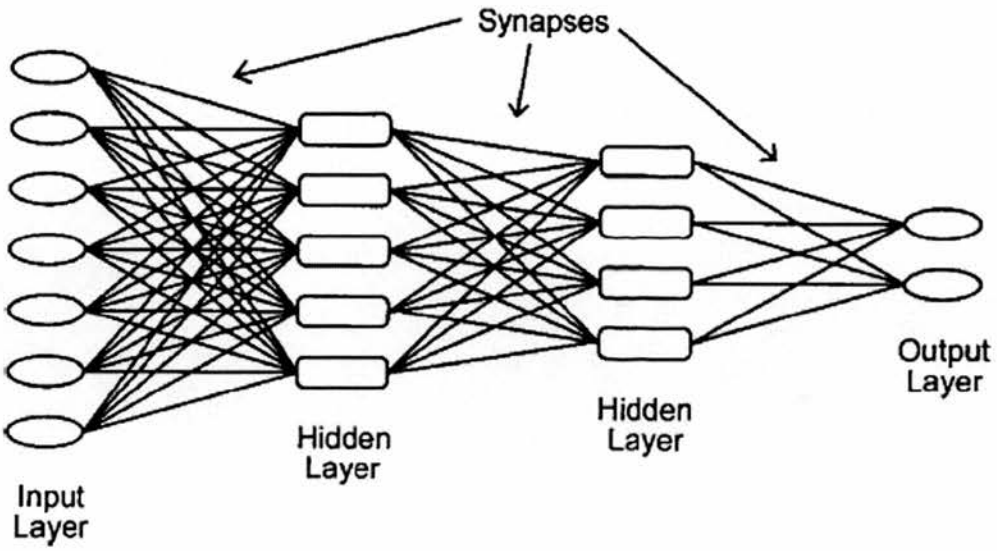

Figure 2.11. Schematic diagram depicting a multilayer feedforward neural network. This network has 7 input neurons, 2 hidden layers, 9 hidden neurons and 63 synapes/weights. These synaptic weights contain the "intelligence" of this system.

Neurons within a biological system are physically limited in the signal magnitude that can be passed onto the next neuron. Similarly, ANNs have a need to operate with signals restricted to a finite range usually between values of 1 and -1. Within ANN, there are a number of mathematical functions that take incoming signals with very large ranges and transform them into a smaller manageable range. This ensures an internal operating range consistency within the network.

A traditional computer program consists of a set of instructions which are explicitly carried out. ANNs are fundamentally different in that the program is told what to know rather than what to do. This is accomplished by training the ANN to recognise the behaviour or pattern of the desired system or dataset by repeatedly exposing the

network to historical data which characterise the effect of interest. The initial configuration of the network in terms of number of input neurons, hidden layers and output neurons are chosen by the ANN designer. There are no rules or standards to determine optimal parameter settings and trial and error based on experience seems to be the best method.

Initially, the network synaptic weights (the "intelligence" of the system) are randomised so that the system consists of "white noise". Training of the network consists of entering the training dataset through the network and calculating how many cases the system can process correctly. A correct case is defined as a result from the ANN which is sufficiently close to the established output from the training database. At first, the number of correct cases will be small. At the end of one training cycle, the network training module will examine the errors and adjusts the synaptic weights in attempt to increase the number of correct cases identified by the system. Once the adjustments have been made, the training data is inserted into the ANN again and this process repeats itself until the number of correct cases reaches a maximum.

Once the training phase of the system is complete, the system must be validated with more data from the original dataset. Usually 10-20% of the dataset is set aside to then be analysed by the trained system and therefore assess the system's ability to correctly process data that it has not seen before. If the validation data is assessed and deemed similar to the training data, then the network is ready for use in this particular application. However, if the validation data is not assessed to the same

accuracy, then the network must be adjusted by the programmer and the training and validation procedures repeated until the results are deemed acceptable. Once ANNs have been constructed, trained and then validated, they are usually encased in a user-friendly "shell" program so that data entry into the ANN is easier and the output from the system can be displayed in a form suitable for a specific application.

In Rodvold *et al.*, the output from an ANN is compared to the statistical model of linear regression [137]. This was shown to illustrate how ANN is comparable to commonly used statistical techniques in medical literature. The authors show that when ANNs are restricted in certain ways, they behave as linear regression models. Figure. 2.9 demonstrates the statistical equivalents of various configurations of ANN. However, when restrictions are not placed upon ANNs, a wider range of applications of the system can be used. ANNs are able to recognise more complex relationships within a given dataset in which regression analysis may not identify as ANNs can adapt to recognise non-linear relationships. Most linear regression models require some prior assumptions about the distribution of the dataset but in using ANN, predictive models can be created without specifying such information.

ANN model	Statistical Equivalent
Single linear perceptron	Linear regression
Simple linear perceptron	Multivariate multiple linear regression
Simple nonlinear perceptron	Logistic regression
Adaline network	Linear discriminant function
Functional link network	Polynomial regression
Multilayer perceptron	Simple nonlinear regression or multivariate multiple nonlinear regression

Figure 2.12 – Statistical equivalents of various configurations of ANN. The single linear perceptron is the equivalent of linear regression analysis but this is a very restricted ANN model. The multilayer perceptron ANN is the network demonstrated above in figure 2.11

However, even though ANNs are powerful analytical tools, there are criticisms from those who claim that scientific discipline is lacking in the application of ANNs. It can be true that the automated processes by which many ANNs operate can lull users into a sense of complacency when creating, training and validating a network. It can seem as if users input the data into the network and unquestioningly accept whatever output is given. The most difficult task when assessing an ANN is to know when the system is finished with its analysis. The architecture of the system is an important factor in the performance of the network. If the number of neurons and layers is too small, there is a risk that the network will be overwhelmed and performance will suffer. Also if the number of neurons and layers is too great, then there is a risk of the network simply memorising the data instead of identifying trends. Determining

this balance between under and over performance is a difficult task and usually involves repetitive runs of the system.

In some instances, the network can be "over-trained". During the training phase of optimising the network, the number of correct cases detected increases dramatically in the early stages but as the data is then recognised, the gains decrease. "Over-training" refers to the situation when the number of correct cases identified diminishes and the network is simply memorising the "noise" inherent in the data presented to it. One additional concern of ANN is that once it has been trained, the network will give an answer to any question posed even though it is not "qualified" or suitable to answer such a question. So if a completely dissimilar set of data from the training data is given to the ANN, it will output an answer. Therefore caution must be used in deploying ANN for situations clearly out with its area of expertise. The way to achieve this is to ensure that the prospective data to be analysed is not out with the ranges present in the training dataset.

In summary, ANNs are complex mathematical tools but not dissimilar to other commonly used statistical and analytical tools used in the medical and scientific literature. They can be easy to use and providing that safeguards and rigorous design and validation methodology is adhered to, ANNs offer a powerful and effective means to solve difficult problems.

ANN is used to assess the correlations between multiple morphological and mechanical variables between prostates.

Chapter Three

Loco-regional morphology and macro-probe point probing

3. Loco-regional morphology and macro-probe point probing

In this chapter, the results of the loco-regional morphometric studies are presented in context with corresponding mechanical measurements which were made using a 2mm diameter ball end probe (macro-sized probe). The methodology used to analyse loco-regional morphology is described in section 2.7.

3.1. Loco-regional morphometric studies

Sixty two morphological and mechanical measurements were obtained from random areas of transverse slices of whole prostate tissue from five radical cystoprostatectomy patients. The morphology was classified as predominantly glandular nodules or stromal hyperplasia. The percentage of smooth muscle, epithelial tissue and the mean acinar size of the glands for both histological groups are presented in table 3.1.

	Mean %ET ± SE	Mean %SM ± SE	Mean Acinar Area (μ^2) ± SE
Nodule (n=37)	47.63 ± 2.56	21.20 ± 1.38	189646 ± 26530
Stroma (n=25)	30.07 ± 3.91	25.62 ± 1.87	121349 ± 24440
p-value	<0.001	0.05	0.32

Table 3.1 – Summary of results of morphological characteristics of the glandular nodular group and stromal group.

The results show that there is a significant difference in the mean percentages of the epithelial tissue and of the smooth muscle content between glandular nodules compared to areas comprised mainly of stroma. The mean acinar areas between the two groups do not demonstrate any significant difference.

The relationship between the smooth muscle content and the epithelial content of glandular nodules were examined with simple linear regression analysis. The correlation between these histological components shows a strong negative correlation. This is shown in figure. 3.1

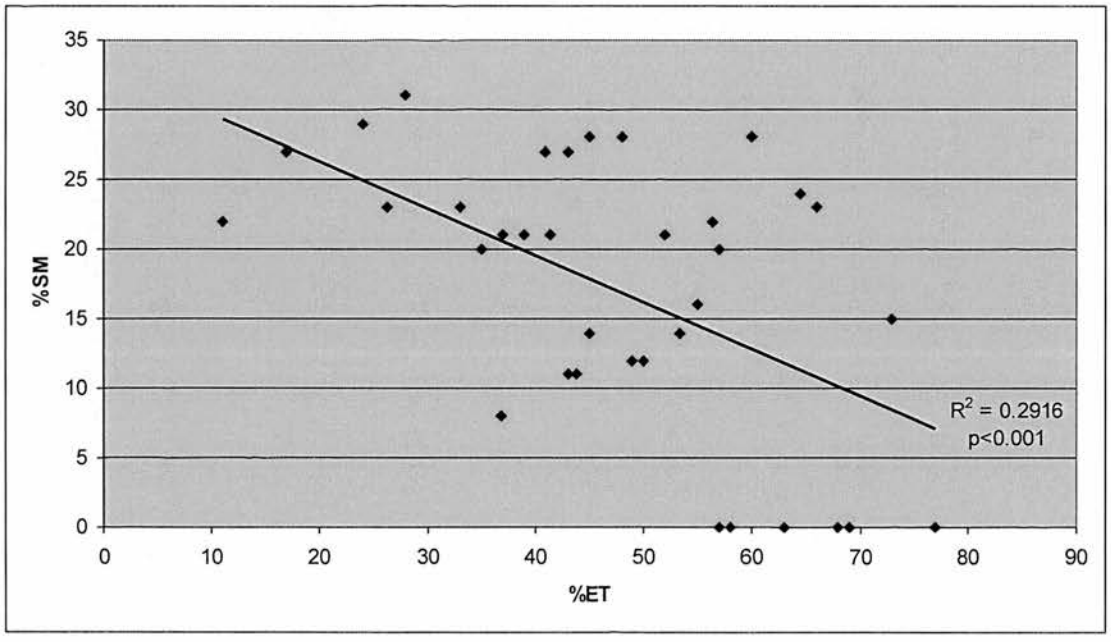

Figure 3.1 – The correlation between %ET and %SM within the nodule group (n=37).

The relationship between %SM and %ET within the stromal group were examined using simple linear regression analysis. See Figure 3.2 This demonstrates a strong negative correlation compared with the relationship seen within the nodular group.

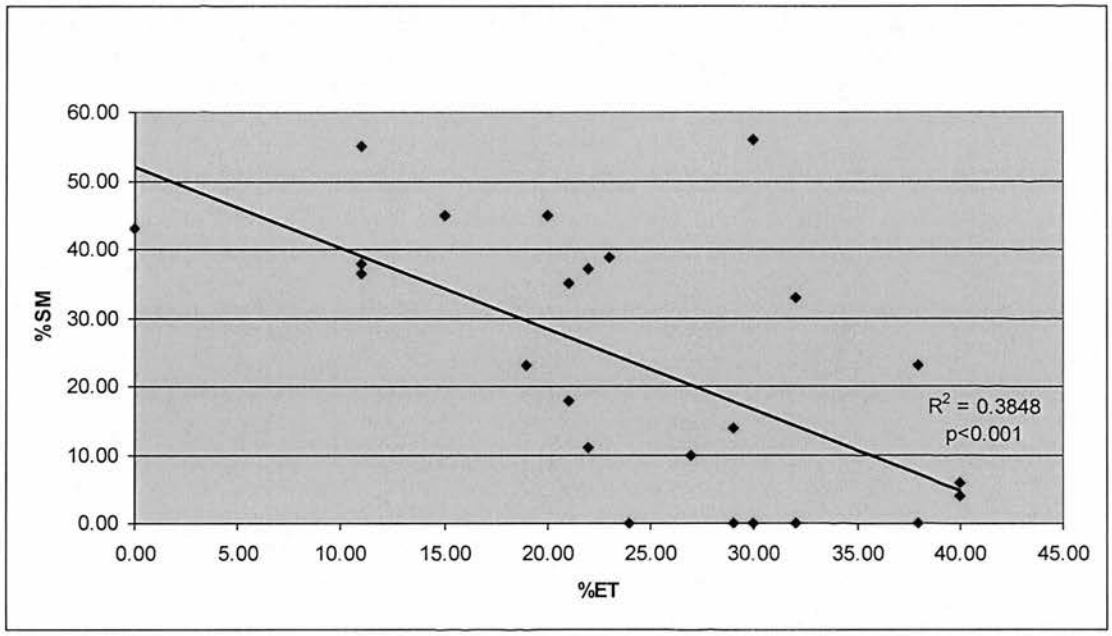

Figure 3.2 – The correlation between %ET and %SM within the stromal group (n=25).

The distribution of areas classified as glandular nodules and stroma, according to the calculated epithelial to stroma ratio, is presented in the histogram shown in figure 3.3. Stromal areas predominate in areas with an epithelial to stroma ratio <1. However, there are areas classified as stroma that have a higher epithelial content than expected. Upon review of the morphology, these points represent areas adjacent to glandular nodules and therefore, the epithelial to stroma ratio is higher.

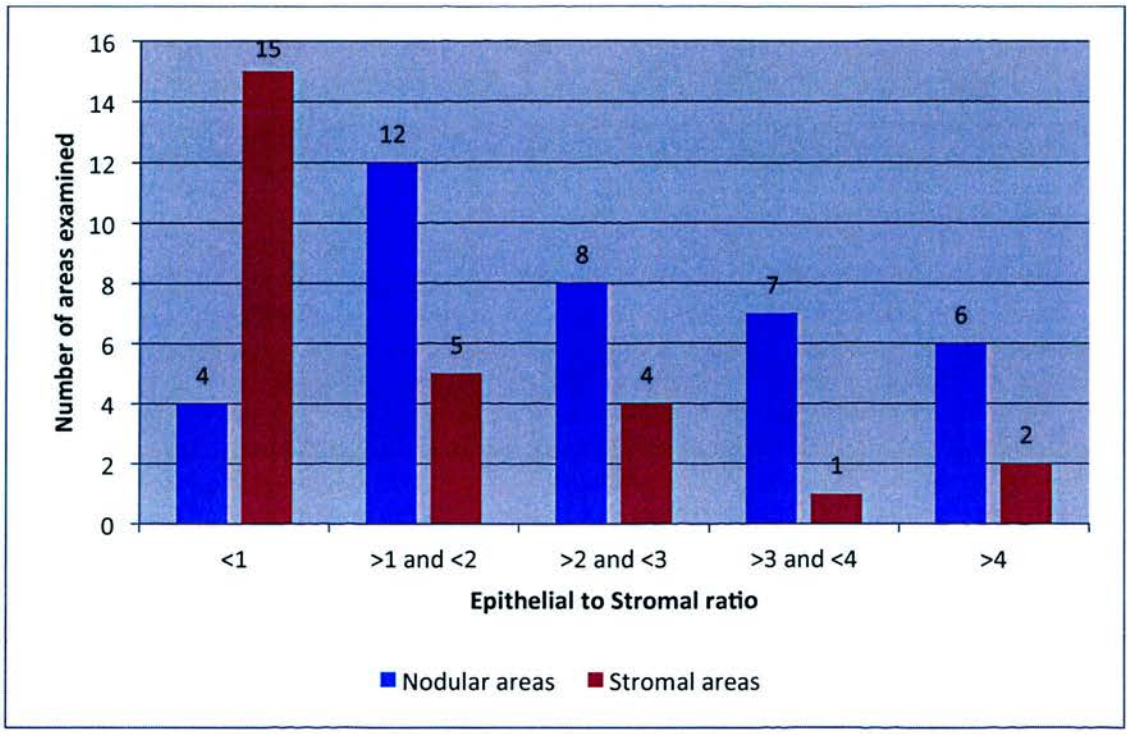

Figure 3.3 – The distribution of epithelial to stroma ratios within nodular and stromal areas.

The mean acinar areas of the epithelial glands in both the stromal and glandular nodular areas are presented in figure 3.4. The mean acinar area in the glandular nodule group is numerically greater than that of the stromal group. However, this observation is not statistically significant. This can be attributed to a small number of areas that contain a higher amount of epithelial tissue than expected (see figure 3.3).

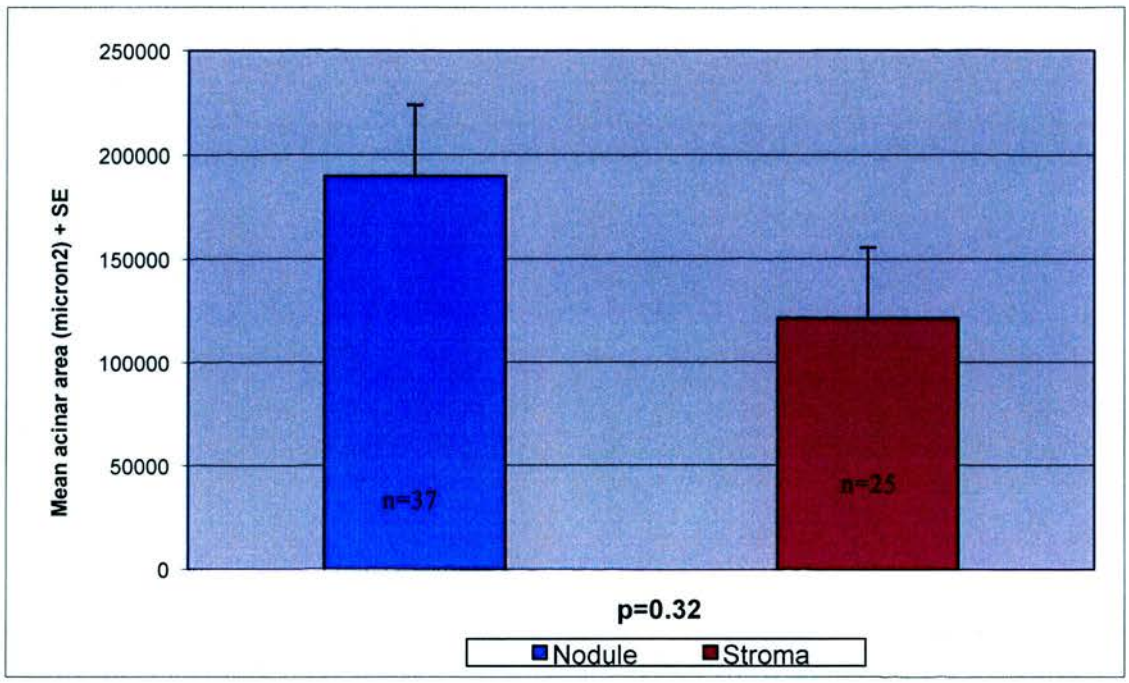

Figure 3.4 – Mean acinar area of glands within nodules and stroma.

3.2. Mechanical studies

For each test point classified as nodules or stroma, there are corresponding mechanical measurements. The mean |E*| (a measure of tissue stiffness) and tan δ (a measure of tissue viscosity) are measured. The results of the mechanical studies are presented in this section. In figure 3.5, the nodular areas are shown to be significantly stiffer than stromal areas. In figure 3.6, the stromal areas are significantly more viscous than the nodular areas.

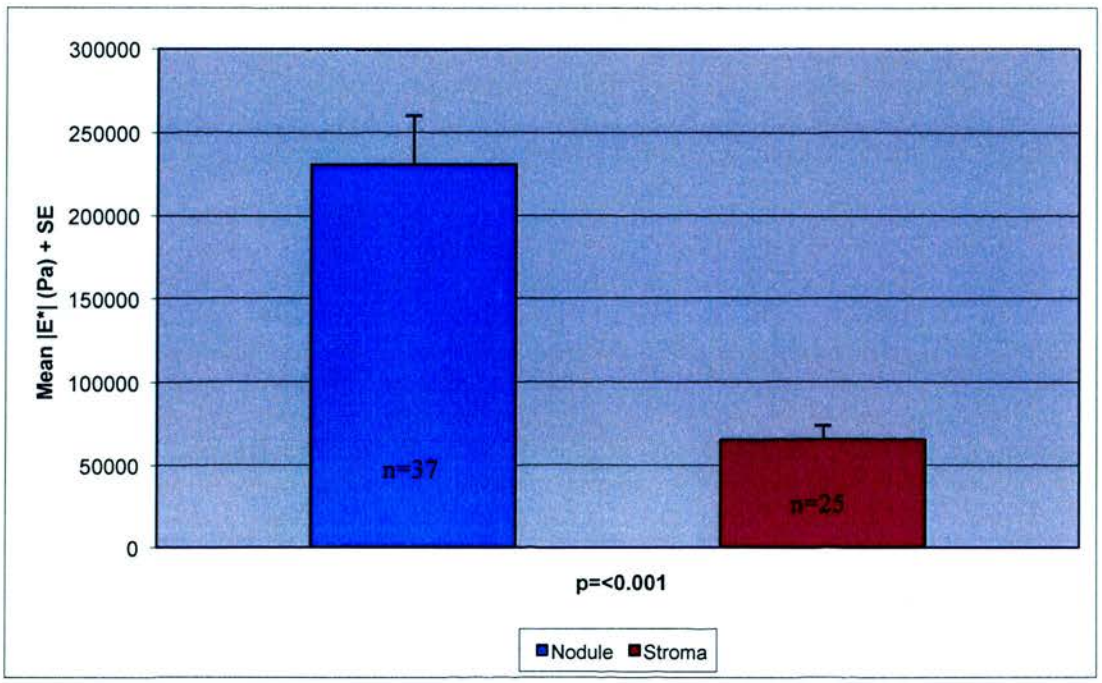

Figure 3.5 – Mean |E*| in areas classified as nodules and stroma.

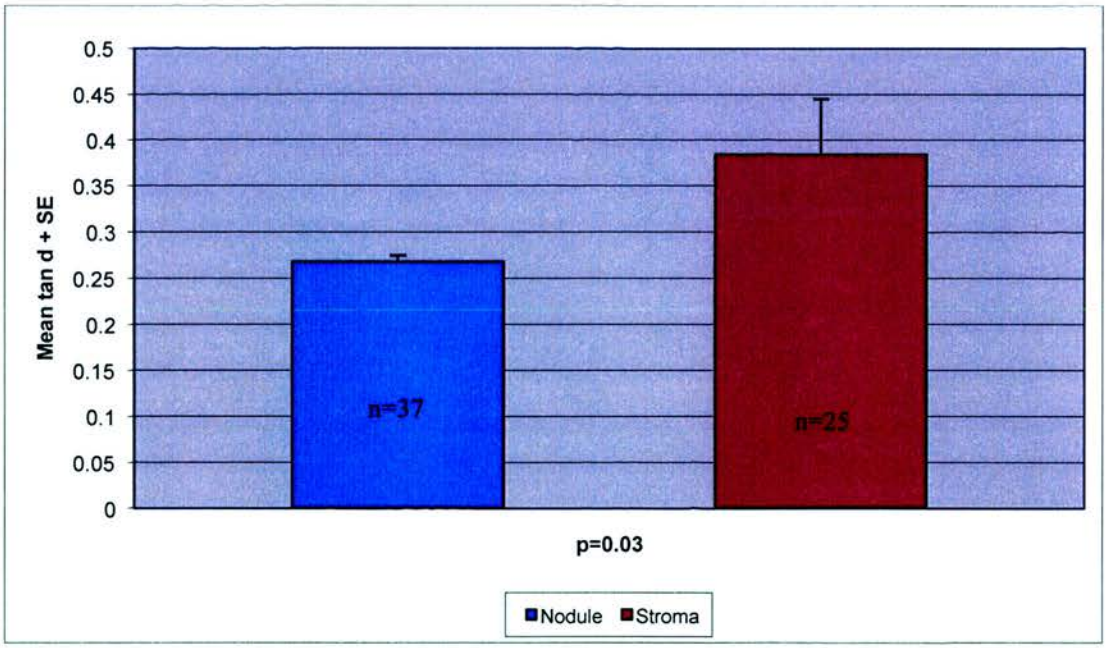

Figure 3.6 – Mean tan δ in areas classified as nodules and stroma.

3.3. Correlations between the morphometric studies and the mechanical measurements in the nodular group

The morphometric studies demonstrate significant differences in smooth muscle and epithelial tissue content between areas classified as glandular nodules and stromal areas. The mechanical studies confirm that nodules exhibit significantly different mechanical characteristics to stromal areas. Linear and multiple regression analysis were used to examine the relationships between the morphometric and mechanical parameters. The results of these studies, in the nodular group, are presented in this section.

Correlations between smooth muscle content and mechanical measurements

The relationships between %SM and the mechanical measurements, $|E^*|$ and tan δ are presented in tables 3.2 and 3.3. The results of linear regression analysis of %SM vs. $|E^*|$ and tan δ are presented as R^2 values. R^2 is the square of the Pearson co-efficient and describes the percentage of the variation in the dependent variable that is influenced by changes in the independent variable. The p value of the analysis is given if the R^2 is greater than 0.5. The morphological parameters, %SM and %ET, are stratified according to varying % content. All test points are considered initially, and then the data is stratified into tests points containing an increasing amount of smooth muscle or epithelial tissue. The corresponding number of test points associated with that grouping is noted in the table.

SM content	Number of points	R^2 **%SM vs |E*|**	R^2 **%SM vs tan δ**
All	37	0.063	0.004
>10%	29	0.088	0.002
>20%	20	0.116	0.020

Table 3.2 - Correlations between %SM and |E*| and tan δ within the nodular group. %SM is stratified according to increasing SM content.

SM content	Number of points	Multiple R^2 **%SM, Mean acinar area vs |E*|**	Multiple R^2 **%SM, Mean acinar area vs tan δ**
All	37	0.250	0.097
>10%	29	0.300	0.085
>20%	20	0.340	0.149

Table 3.3 - Multiple linear regression analysis with predictor variables of %SM and mean acinar area, and response variables of either |E*| or tan δ in the nodular group.

The results in table 3.2 shows that there are no strong correlations between %SM and |E*| and tan δ using linear regression analysis. Multiple regression analysis was used to assess the impact of including mean acinar area into the analysis. No strong correlations were seen in Table 3.3.

Correlations between epithelial tissue content and mechanical measurements

ET content	Number of points	R^2 **%ET vs |E*|**	R^2 **%ET vs tan δ**
All	37	0.016	0.097
>20%	35	0.011	0.095
>30%	32	0.024	0.152
>40%	27	0.020	0.182
>50%	17	0.004	0.168
>60%	8	0.338	0.325

Table 3.4 - Correlations between %ET and |E*| and tan δ within the nodular group. %ET is stratified according to increasing ET content.

ET content	Number of points	Multiple R^2 **%ET, Mean acinar area vs |E*|**	Multiple R^2 **%ET, Mean acinar area vs tan δ**
All	37	0.130	0.332
>20%	35	0.117	0.335
>30%	32	0.170	0.404
>40%	27	0.152	0.435
>50%	17	0.181	0.417
>60%	8	**0.753 (p=0.12)**	**0.897 (p=0.017)**

Table 3.5 - Multiple linear regression analysis with predictor variables of %ET and Mean acinar area, and response variables of either |E*| or tan δ in the nodular group.

In Table 3.4, there are weak correlations between %ET and |E*| and tan δ. Using multiple linear regression analysis, the additional variable of mean acinar area was considered in the analysis. The correlations strengthen when areas containing a higher amount of ET (>60%) were considered (see table 3.5). In the analysis with |E*|, there is a strong correlation seen (R^2 = 0.753) but the result does not reach significance. However, in the analysis with tan δ, there is a strong and significant relationship with %ET >60 and mean acinar area (R^2 = 0.897 p=0.017).

3.4. Correlations between the morphometric studies and the mechanical measurements in the stromal group

In this section, the results of the correlation analyses in the stromal group are presented. Linear and multiple regression analysis were used to examine the relationships between the morphometric and mechanical parameters.

Correlations between smooth muscle content and mechanical measurements

SM content	Number of points	R^2 **%SM vs |E*|**	R^2 **%SM vs tan δ**
All	25	0.038	0.118
>10%	24	0.020	0.127
>20%	19	0.036	0.135
>30%	9	0.002	0.075

Table 3.6 - Correlations between %SM and |E*| and tan δ within the stromal group. %SM is stratified according to increasing SM content.

SM content	Number of points	Multiple R^2 **%SM, Mean acinar area vs |E*|**	Multiple R^2 **%SM, Mean acinar area vs tan δ**
All	25	0.083	0.422
>10%	24	0.080	0.377
>20%	19	0.164	0.387
>30%	9	0.187	**0.673 (p=0.06)**

Table 3.7 - Multiple linear regression analysis with predictor variables of %SM and Mean acinar area, and response variables of either |E*| or tan δ in the stromal group.

Table 3.6 shows the correlation between %SM and |E*| and tan δ in stromal areas containing an increasing SM content. There are no significant correlations shown. In Table 3.7, multiple linear regression analysis was used to assess the relationship between the predictor variables of %SM and mean acinar area with the response variables of |E*| and tan δ. There are weak correlations with %SM, mean acinar area and |E*|. There are stronger correlations between stromal areas with >20% smooth muscle, mean acinar area and tan δ. However, this relationship does not reach statistical significance (p=0.06).

Correlations between epithelial tissue content and mechanical measurements

ET content	Number of points	R^2 **%ET vs |E*|**	R^2 **%ET vs tan δ**
All	25	0.003	0.068
>10%	19	0.007	0.081
>20%	14	0.138	0.019
>30%	27	0.294	0.013
>40%	5	0.024	0.013

Table 3.8 - Correlations between %ET and |E*| and tan δ within the stromal group. %ET is stratified according to increasing ET content.

ET content	Number of points	Multiple R^2 **%ET, Mean acinar area vs |E*|**	Multiple R^2 **%ET, Mean acinar area vs tan δ**
All	25	0.218	0.128
>10%	19	0.415	0.449
>20%	14	0.376	0.210
>30%	11	0.422	0.397
>40%	5	**0.985 (p=0.172)**	**0.993 (p=0.116)**

Table 3.9 - Multiple linear regression analysis with predictor variables of %ET and Mean acinar area, and response variables of either |E*| or tan δ in the stromal group.

Table 3.8 shows weak correlations between %ET and |E*| and tan δ. In Table 3.9, multiple regression analysis, demonstrates a strong correlation with %ET, mean acinar area and the mechanical measurements |E*| and tan δ in stromal areas with >40% epithelial content. However these relationships do not achieve statistical significance as a result of the diminished numbers in this group (n=5).

The results presented in sections 3.3 to 3.4 demonstrate that linear regression analysis is unable to discern meaningful relationships between morphometric parameters, %SM and %ET, and the associated mechanical measurements. It would appear that there are other factors unaccounted for. The morphometric parameter of acinar size of the glandular epithelium may have an impact upon the mechanical measurements. Multiple regression analysis was used to assess the impact of this additional morphometric parameter upon the relationships with the mechanical studies. There were stronger correlations seen in the epithelial studies in both the nodular and stromal groups when considering tissues with an increasing epithelial content (see tables 3.5 and 3.9). In the smooth muscle studies, a stronger correlation was seen in the analysis of %SM, mean acinar area vs. tan δ in the stromal group (see table 3.7). However, a significant number of test points are composed of a varying amount of smooth muscle and epithelial tissue and do not have a strong relationship with the mechanical parameters. Artificial neural networks are able to recognise more complex relationships within a given dataset in which regression analysis may not identify as ANNs can adapt to recognise non-linear relationships. The results of the analysis of morphometric and mechanical properties using ANN is presented in section 3.5.

3.5. The assessment of the impact of the morphology upon the mechanical properties using Artificial Neural Networks

A brief overview of artificial neural networks is presented in section 2.9.5. One of the many important applications of neural networks is pattern recognition. The analysis of any dataset by ANNs can be considered in three stages. The initial stage is the training phase or cycle of the network whereby a proportion of the raw data (input data), about 70%, is analysed in a cyclical manner until the maximum number of correct cases (output data) is reached. A correct case is defined as a result from the ANN which is close to the established output from the training database or input data. In effect, the network is trained to associate its outputs with input patterns. The dataset is organised differently from the previous studies. In this study, each parameter, whether it is morphometric or mechanical data, is represented by a column of raw numerical data. No attempt is made to stratify or classify the data. Once the training phase of the system is complete, the system must be validated with more unseen data from the original dataset. Usually 10-20% of the dataset is set aside to be analysed to assess the system's ability to correctly process the original data. Validation is when the network identifies the input pattern (the unseen data) and tries to output the associated target pattern. Once the system is validated, the network can be used to identify groups or patterns of data within any given dataset. In this case, the network gives the output that corresponds to the learned input pattern from the training phase (the target output). This is the final "test" phase of the ANN.

The relationships between the morphometric, %ET and %SM, and the mechanical parameters, |E*| and tan δ were assessed using an ANN. The ANN generates an output plot comprising three graphs representing the three stages of analysis. This output plot is a regression plot which shows the relationship between the outputs of the network and the targets. The ANN assigns a calculated value to both output and target values during the analysis. The dashed line in each axis represents the perfect result: output = targets. The solid coloured lines represent the best fit linear regression line between outputs and targets. The R value is an indication of the relationship between output and target.

Figure 3.7 shows the ANN analysis between %ET and |E*|. The training plot shows that the ANN is identifying a strong positive correlation between the two variables. The plot of the validation phase confirms that there is still a strong correlation between %ET and |E*| dataset. The reduction in data points reflect the process that 10-20% of the overall dataset is used in this phase (n=8). The final plot shows the output from the test phase. There remains a strong positive relationship between these two parameters despite a reduced dataset (n=8). In figure 3.8, there are similar conclusions drawn from the regression plots of the ANN analysis of %ET and tan δ.

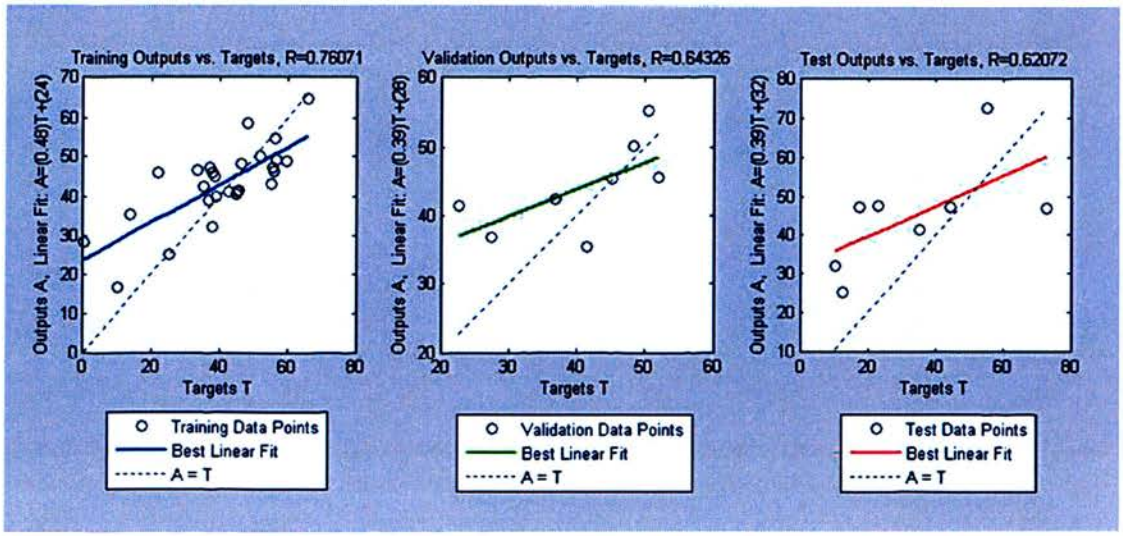

Figure 3.7 – Regression plot of the ANN analysis of the parameters %ET and |E*|. A strong and positive relationship is observed between these two variables.

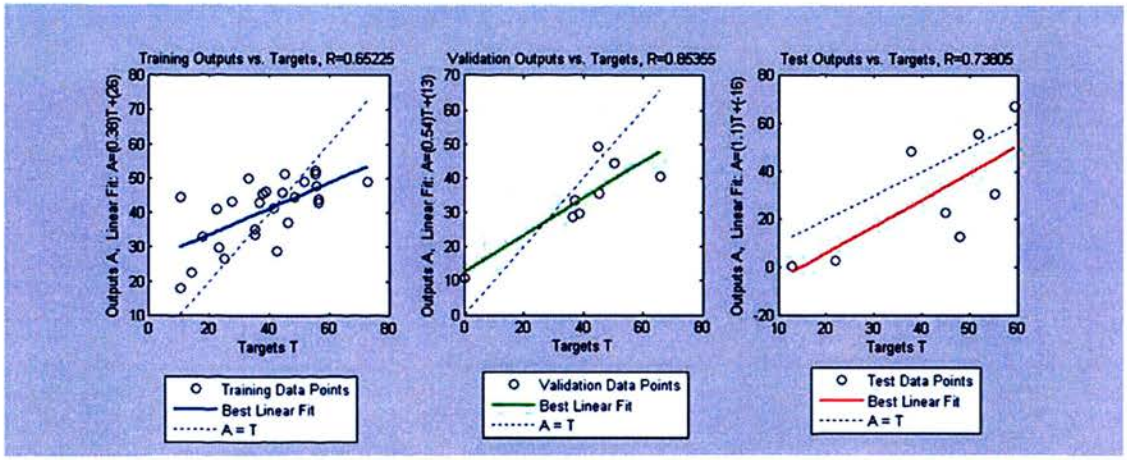

Figure 3.8 – Regression plot of the ANN analysis of the parameters tan δ and %ET. A strong and positive relationship is seen between these two variables.

The ANN was used to examine the relationship between all four parameters, %ET and %SM and |E*| and tan δ. Figure 3.9 shows the regression plot from this analysis. Examining the regression analysis of the training data plot, the ANN has found strong and significant relationships between the datasets of all four variables (R=0.806). The regression analysis of the validation and test plots show that the output (the testing of unseen data) corresponds strongly to the targets (the relationships learned during the training phase). This suggests that there are meaningful relationships between the morphometric and mechanical parameters which have not been identified using linear regression tools.

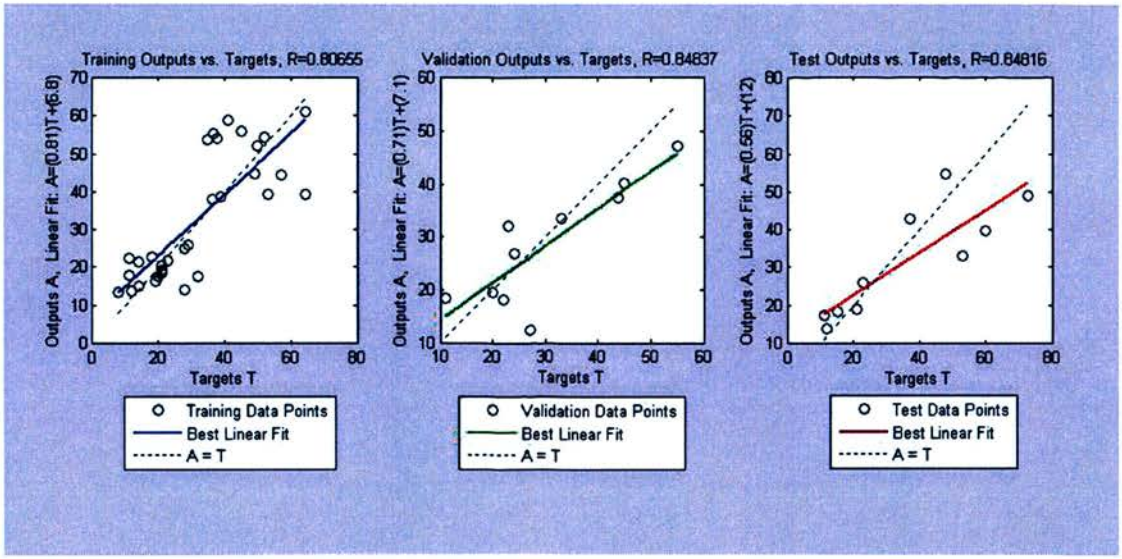

Figure 3.9 – Regression plot of the ANN analysis of the parameters %SM, %ET, |E*| and tan δ. There is a strong relationship between the datasets of both morphometric and mechanical measurements.

3.6. Loco-regional morphology and macro-probe point: summary of findings

The main findings from the study of loco-regional morphology and the mechanical measurements are summarised below:

1. There are significant histological differences between areas of loco-regional morphology classified as nodules and as stroma. The epithelial to stroma ratio is greater in the nodular areas compared with stromal areas.

2. The mean acinar area of glandular epithelium is greater in nodules than in stroma.

3. Areas classified as glandular nodules have a significantly higher mean $|E^*|$ than areas classified as stromal areas.

4. Areas classified as stromal areas have a significantly higher tan δ than areas classified as nodules.

5. Weak correlations were found between the morphological and mechanical measurements as assessed using linear and multiple linear regression analysis.

6. Within the nodular group, there are strong correlations between %ET, mean acinar area and the mechanical parameters of $|E^*|$ and tan δ in areas composed predominantly of epithelial tissue.

7. Artificial neural network analysis demonstrated strong relationships between the morphological and mechanical measurements.

3.7. Discussion

The results from Table 3.1 demonstrate that discrete areas of histological interest that have been classified as either nodular or stromal areas are significantly different in their composition with respect to %SM and %ET. This forms the basis of the concept that loco-regional morphology can be qualitatively classified and quantitatively assessed. In figure 3.4, the mean acinar area of the glandular epithelium in areas classified as nodules is greater than that of stromal areas. However, this is observation does not reach statistical significance and can be explained with reference to figure 3.3. The composition of each nodule stromal area can be represented by the epithelial to smooth muscle ratio (ET:SM). The histogram in figure 3.3 shows the distribution of nodular and stromal areas as a ratio of epithelial and smooth muscle. A significant proportion of stromal areas (n=15) have a ET:SM of less than one. However several areas classified as stroma are shown to contain a greater epithelial composition than expected. The morphology was reviewed and these areas were found to be adjacent to areas containing glandular nodules. The protocol for image capture and analysis dictates that an area of interest is represented by 49 images (arranged in a 7 x 7 matrix). The histological measurements can therefore partly represent areas that do not reflect the type of tissue tested. In areas adjacent to glands that may contain predominantly epithelial tissue, the morphometric measurements may be incorrectly skewed towards a tissue type. These pitfalls area acknowledged in the methodology presented in section 2.7, where the issue of the size of image capture and the rationale for using a larger matrix size is discussed.

Macroscopic examination of the slice of a whole prostate clearly reveals areas of nodular formation (see figure 1.6) which were found only in the transition zone of the prostate. Morphometric analysis of these nodules revealed that they were mainly composed of glandular epithelium with corresponding lower amounts of smooth muscle. Table 3.1 summaries the histological differences between nodules and stroma. The mean %ET composition of nodules is significantly greater than in stroma. However, the %SM content in stromal areas is significantly greater than that in nodules. The histogram in figure 3.3 demonstrates the distribution of the histological composition of nodules. There are a greater proportion of nodules that have an epithelial to smooth muscle ratio greater than two. In McNeal's original work, he demonstrated that there is diffuse enlargement of the transition zone with increasing age. Initially there is an increase in small nodules, mainly stromal, in the transition zone. However, subsequently there is an increase in nodule size which is associated with an increase in the epithelium to stroma ratio [25]. These nodules are considered a morphologic hallmark of BPH. Subsequent work from Price *et al* showed that small volume TURP resections were comprised mainly of smooth muscle with glandular tissue only comprising approximately 5% of the resected tissue. However in larger TURP resections and in whole prostate specimens from enucleations, nodules with an epithelial to smooth muscle ratio greater than one, predominated in the transition zone [32]. Schuster *et al* examined the tissue composition of TURP chippings according to the resection weight and found that as resection weight increased, there was a four-fold increase in the amount of the epithelial component [33]. The morphometric characteristics of these nodules are in agreement with the work noted above.

Nodule exhibit significantly different morphology compared with stromal areas. The mechanical studies demonstrate that nodules exhibit significantly different characteristics to stromal areas. In figure 3.5 and 3.6, nodules are shown to be stiffer and less viscous that stromal areas respectively. Using linear and multivariate regression analysis, relationships were sought between the mechanical and morphological characteristics of nodules. No correlation was seen between %SM and the mechanical properties (see tables 3.2 and 3.3). Figure 3.1 demonstrates the spread of histological composition of ET and SM within the nodule group. Within the nodular group, the mean %SM was only 21.2% which may explain the lack of correlation seen. The relationship between %ET and the mechanical properties was found to be weak. The impact of mean acinar area was assessed using multivariate regression analysis and strong relationship was seen only in nodules containing greater than 60% ET. These results are non-significant due to the very small sample size of the group. These findings suggest that in nodules mainly composed of epithelial glands with large acini, there is a significant impact upon the mechanical measurements. In nodules composed of less than 60% ET, weak correlations are seen and this may represent the heterogeneity of the morphology dataset as illustrated in figure 3.1. There is wide variation in the composition of nodules.

Artificial neural networks are used in situations whereby linear statistical tools are unable to recognise a relationship or patterns within a dataset. In section 3.5 the results of the ANN analysis show that there are significant relationships between the morphometric and mechanical parameters. The ANN can recognise non-linear patterns that linear statistical tools may fail to understand. However, the ANN is

unable to define precisely the relationship between the parameters. Instead, the ANN will train itself to look for patterns within a given dataset, apply the learnt pattern to an unseen set of data, and output a correlation between the new data and the previously learnt relationship. Adding further parameters may strengthen or weaken the output of the network. In figure 3.9, the impact of adding both the mechanical and morphometric parameters results in a stronger correlation between the variables. These findings suggest that the structure-property relationship in nodules may be dependent upon more than one variable or factor. A significant proportion of the composition is unaccounted for and it may be that other morphological components may exert an effect on the mechanical properties. The prostate stroma is composed of smooth muscle and associated connective tissue such as collagen, elastic fibres, fibroblasts, vessels and nerves. It is possible that these components may be a significant determinant of the mechanical properties of the tissue. However, based on work by Phipps *et al*, smooth muscle and epithelial tissue were the main determinants of the mechanical properties of prostate tissue from TURP chippings [127, 128]. Collagen III did not demonstrate any significant relationship to the mechanical characteristics of TURP tissue. Several immunohistochemical stains were evaluated for identifying fibroblasts but the results were weak. At present, the influence that collagen types and other components of the stroma have upon the mechanical properties of prostate tissue is currently unknown.

It appears that nodules display a mechanical property that does not correspond to the structure-property relationship identified in TURP tissues. Phipps *et al* demonstrated that prostate tissues from TURP containing a greater proportion of SM are stiffer

irrespective of their epithelial tissue content [127]. In this relationship the histology from TURP chippings is considered homogenous based upon morphometric studies of several TURP chippings [138]. It was also assumed that the TURP chippings were isotropic, that is their mechanical characteristics were the same irrespective of the direction of mechanical testing. In the study of transverse sections of whole prostates one must acknowledge the heterogeneity of the tissue composition found in such a specimen. Even within specific and discrete histological structures such as glandular nodules, there remains a significant degree of variability of tissue composition. One must also consider such a specimen to be anisotropic. Differing mechanical measurements were obtained from testing of a single nodule in two separate but adjacent locations. This may simply be a function of the underlying heterogeneous morphology of the nodule (the morphology was slightly different at the individual test points). However, it may also be a reflection of the 3-dimensional configuration of the structure, which may not be uniform in shape. Further studies will be required to explore these issues.

The mechanical properties of nodules clearly demonstrate that these structures are significantly stiffer than stromal areas (see figure 3.5) and are significantly less viscous than stromal areas (see figure 3.6). The observations and descriptions of glandular nodules given by McNeal may explain these findings [25]. The glandular proliferative process leads to tight packing of epithelial glands within a given area (see figure 1.5). The nodule is usually surrounded by a thin band of smooth muscle or stroma. One may postulate that fluid filled glands that are constricted by surrounding connective tissue bands may exhibit increased pressure within the

glands. This may explain the almost exponential rise in |E*| of nodules compared to surrounding stroma. A further explanation may relate to work performed by Watanabe *et al.* His group developed the concept of prostatic pressure coefficient (PPC). This is a measure of the pressure within the prostatic urethra using a balloon and a pressure transducer to measure the change in pressure from the balloon. The basis of this concept is that when a nodule develops, this exerts an outwards pressure on the surgical capsule of the prostate. The capsule also pushes back on the nodule. The elastic qualities of the surgical capsule may play a role in whether a nodule causes bladder outflow obstruction. If the capsule is sufficiently elastic, then the outward push from the nodule is accommodated. However, if the capsule is inelastic, then very little pressure within a nodule could cause clinical symptoms of obstruction. The raised |E*| values associated with nodules may be a function of the constrictive force of the prostatic surgical capsule. Further studies to assess the elasticity of the surgical capsule are required to understand these issues.

The results presented in this chapter demonstrate that there are significant differences with respect to the morphological and mechanical properties of loco-regional areas within a transverse slice of whole prostates. The inherent heterogeneity of the morphology and non-linear distribution of the data has posed a significant challenge to understanding the structure –property relationship of glandular nodules and stromal areas. However, the use of ANN has confirmed that there are strong correlations between the morphology and the mechanical properties. Further morphological studies to characterise the remaining components of the stroma may reveal significant relationships with the mechanical characteristics of the prostate.

Chapter Four

Loco-regional morphology and micro-probe point probing

4. Loco-regional morphology and micro-point probing

In collaboration with a micro-engineering facility, a parallel aim of this overall project is to develop a micro-engineered palpation device for the measurement of mechanical properties of prostate tissue. The rationale for the reduction in size of the device is that it should be able to be deployed via the working channel of a flexible cystoscope. In the design brief of the engineering department, the micro-engineered probe is designed around a hydraulic system with a piston at the operating end to apply the compressive strain to the tissue. The dynamic compressive force applied to the tissue will then allow for the measurement of the mechanical properties to be made. The compressive force is transmitted via a silicone diaphragm measuring 200μm × 500μm. This diaphragm is significantly smaller in cross-sectional area than the macro probe. The aim of this study presented in this section, is to investigate the mechanical measurements that are made with a micro-indenter measuring 400μm × 500μm. The area covered by the macro probe is 9.86mm^2 compared with 0.2mm^2 of the micro probe. The reduction in size of the indenter allows for the study of mechanical properties at a scale that approaches microscopic feature size.

Figure 4.2 illustrates the significant reduction in size of the indenter in relation to the morphology as represented by a mosaic image. The area occupied by the macro indenter is represented by 3 × 3 microscope frames at ×200 magnification and the micro indenter occupies an area measuring 40% of a single image.

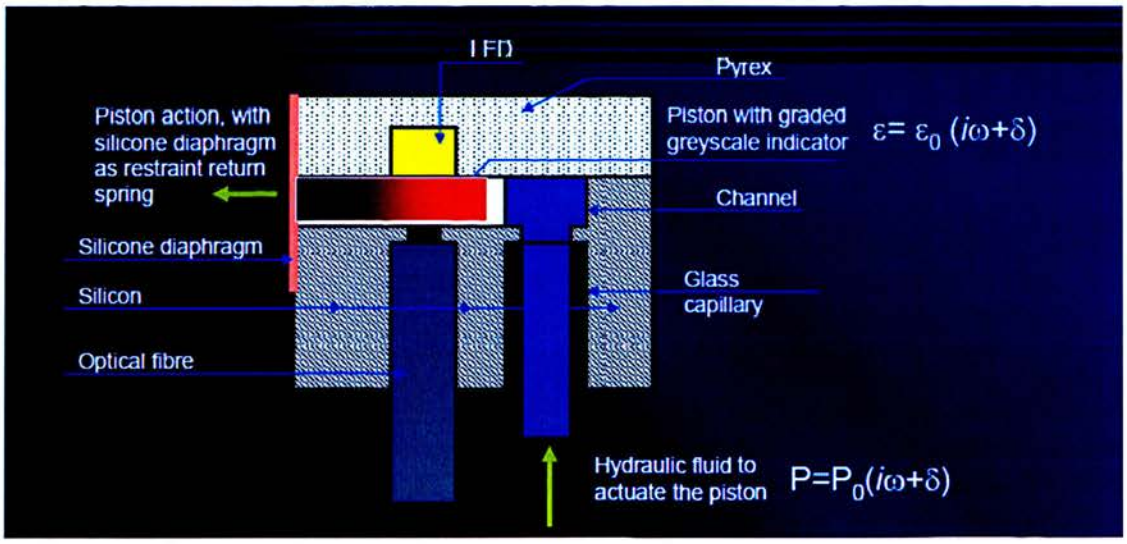

Figure 4.1 – Schematic diagram of the design of the micro-engineered probe. The piston (coloured red) acts upon a silicone diaphragm which measures 200μm × 500μm in size. This diaphragm will be in contact with the prostate tissue.

This presents the challenge of capturing loco-regional areas of interest that have been subjected to mechanical testing using the micro probe. The protocol outlined in section 2.7.3 captures an area represented by 49 images (a matrix of 7 × 7 frames) of histological data. Using this method of selecting points of interest, there is confidence that this area will include the point of mechanical measurement. However, the trade off is increasing the uncertainty that the histological measurement calculated from a large area will truly represent the underlying morphology that was subjected to mechanical testing. It is acknowledged that improvement is required to increase the precision of localising the test point subjected to mechanical testing. However, the current protocol for the analysis of loco-regional morphology is a balance of the workload burden of analysis of multiple

images with the goal of as accurate as possible , localisation of the histology subjected to testing.

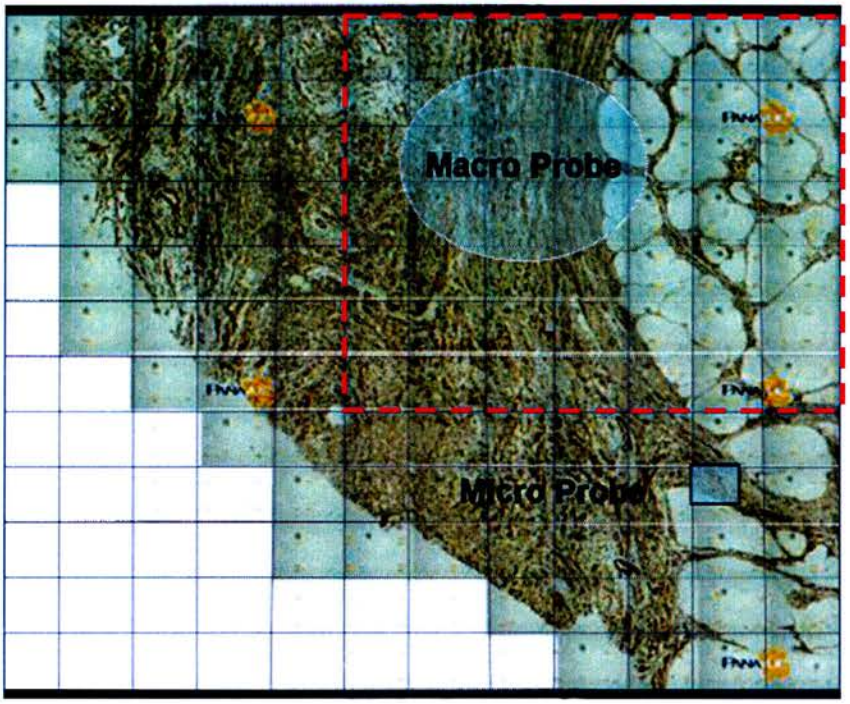

Figure 4.2 – Mosaic image showing the relative difference in sizes of the macro and micro probe indenters. The area outlined by the dashed line is the area of morphology captured using a matrix of 7 × 7 frames.

4.1. Loco-regional morphometric studies

7 radical prostatectomy specimens were used for this study and 71 individual point probing measurements were obtained from the fresh tissue specimens. Morphological studies were performed on the tissue after preparation as described in sections 2.4 to 2.7.

Morphological areas of interest corresponding to the tissue area subjected to mechanical testing were classified into two groups in accordance with their histological appearance. The area of morphological interest is represented by 49 individual images (taken at × 200 magnification) configured in a 7 × 7 matrix as described in section 2.7. The %ET and %SM for each individual image were determined by computerised morphometric analysis. The mean values of %SM and %ET of each individual 7 × 7 matrix were used. The mean acinar area of epithelial glands was measured. The methodology is described in depth in section 2.7.

The results described in table 4.1 show that there are significant morphological differences between areas classified as stroma and nodular areas. Nodules are shown to compose of predominately epithelial glands whereas stromal areas are shown to have a significantly increased smooth muscle composition. The mean acinar areas of the glands are significantly larger in nodules than in stromal areas.

	Mean %ET ± SE	Mean %SM ± SE	Mean Acinar Area (μ^2) ± SE
Nodule (n=38)	50.08 ± 2.23	21.26 ± 1.23	137953 ± 10986
Stroma (n=33)	29.37 ±2.14	26.27 ± 1.16	82063 ± 6378
p-value	<0.001	<0.01	<0.005

Table 4.1 – Summary of results from morphological characteristics of the nodular and stromal groups.

Figure 4.3 demonstrate the relationship between %ET and %SM within the nodule group. There is a significant negative relationship between the %ET and %SM. This is a reflection of greater ET content within areas classified as nodules than in stromal areas.

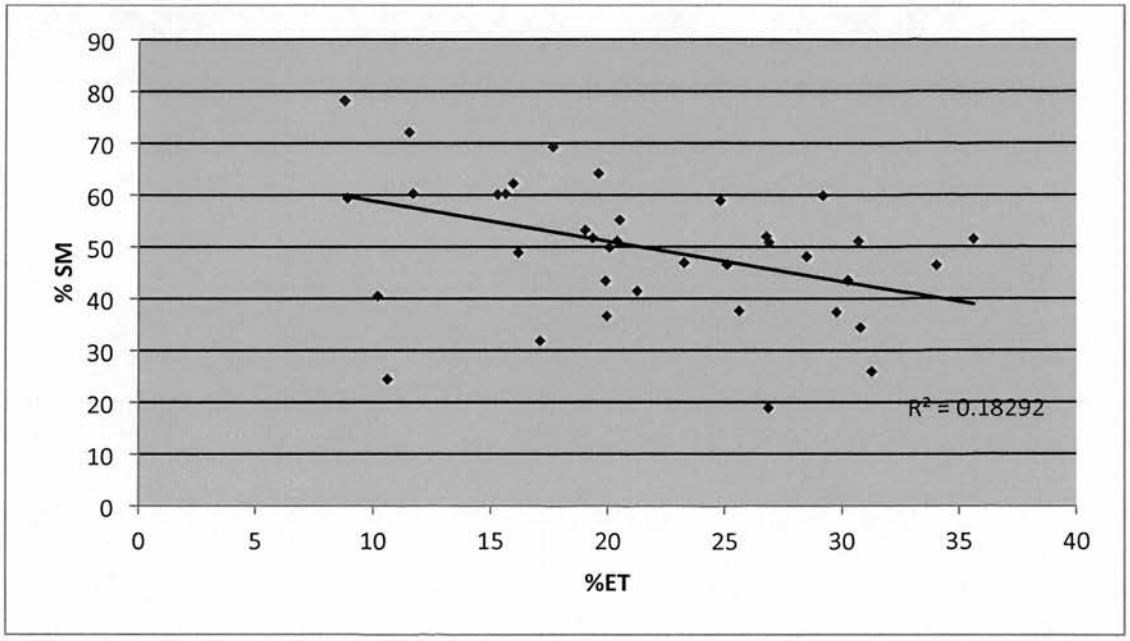

Figure 4.3 – Correlation between %ET and %SM in the nodule group (n=38)

The relationship between %ET and %SM within the stroma group is shown in figure 4.4. There is a significant negative relationship between %ET and %SM within the stroma group and this is a reflection of the greater smooth muscle content in areas classified as stroma.

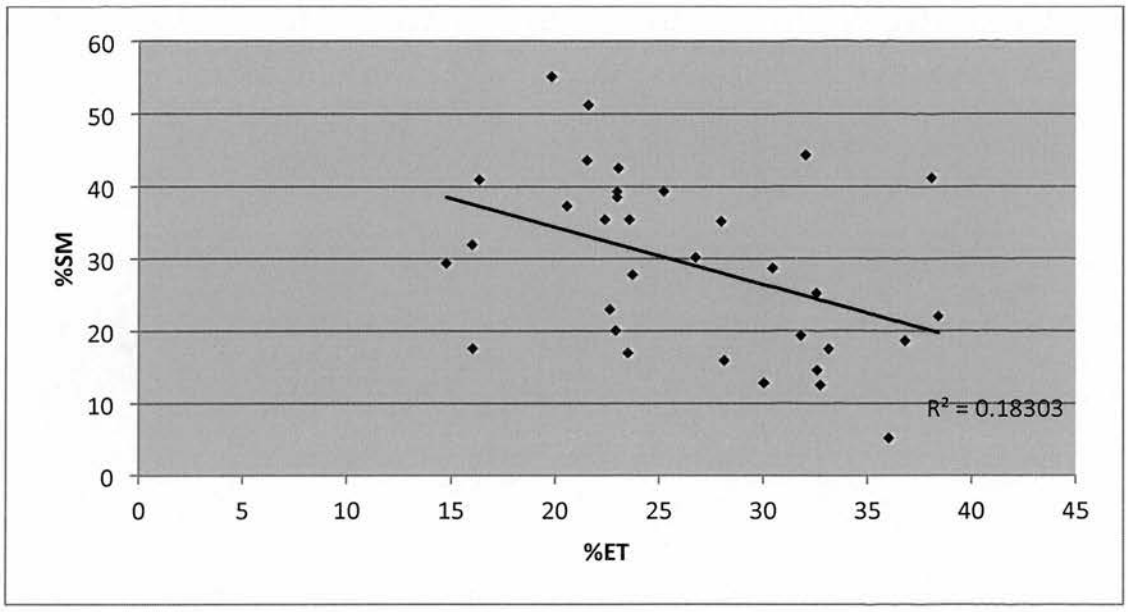

Figure 4.4 – Correlation between %ET and %SM in the stroma group (n=33)

Figures 4.3 and 4.4 demonstrate that there are significant relationships between these variables; however the correlations are weak within both the nodular ($R^2 = 0.183$) and stromal groups ($R^2 = 0.183$). This may reflect the heterogeneity and variability seen within both groups. A study of the distribution of morphology represented as a ratio of epithelial to smooth muscle components highlight the significant overlap in describing areas of interest using values of %ET and %SM. The calculated ratio of %ET to %SM for each area of interest is shown in the distribution histogram in figure 4.5. Moving from left to right, the greater the epithelial to smooth muscle ratio, the greater the epithelial content within the area of interest.

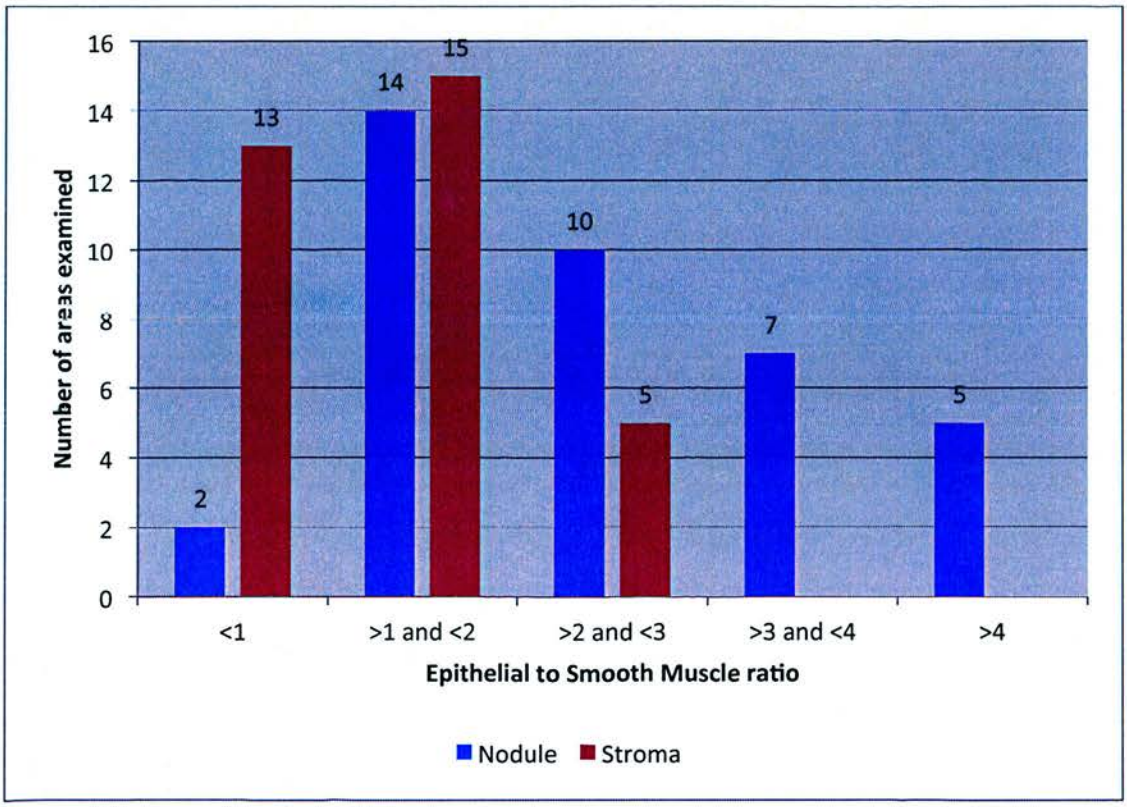

Figure 4.5 – Histogram of the distribution of areas of interest represented as a ratio of epithelial to stromal tissue. The number above the columns corresponds to the number of points within the stratified group.

In the nodule group, 12 areas have an epithelial to stromal ratio greater than 3. Stromal areas have an epithelial to smooth muscle (ET:SM) ratio less than 3. Between an ET:SM ratio of greater than 1 and less than 3, there is a significant overlap of both nodular (24 areas) and stromal (20 areas) areas represented. The dataset for both the nodule and stroma groups were reorganised to with respect to ET:SM ratio. The relationships between %ET and %SM were re-examined using linear regression analysis, but the correlations were found to be weak. The use of

epithelial to smooth muscle ratio did not sufficiently differentiate between stroma and nodular areas.

The mean acinar area of the epithelial glands in the stroma and nodular groups are shown in figure 4.6. There is a significant difference between the mean acinar area of the epithelial glands in areas designated as nodules (137953 μ^2) compared with stroma (82063 μ^2). The architecture of epithelial glands themselves within the nodules demonstrates large acini.

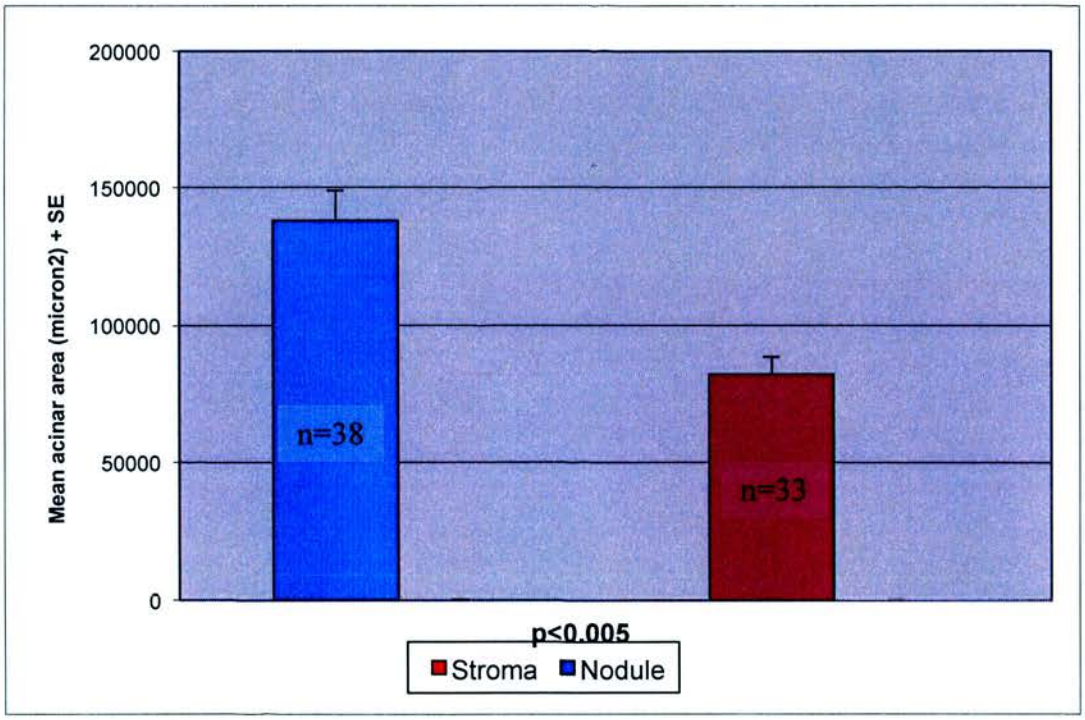

Figure 4.6 - Mean acinar area of epithelial glands within nodule and stroma areas

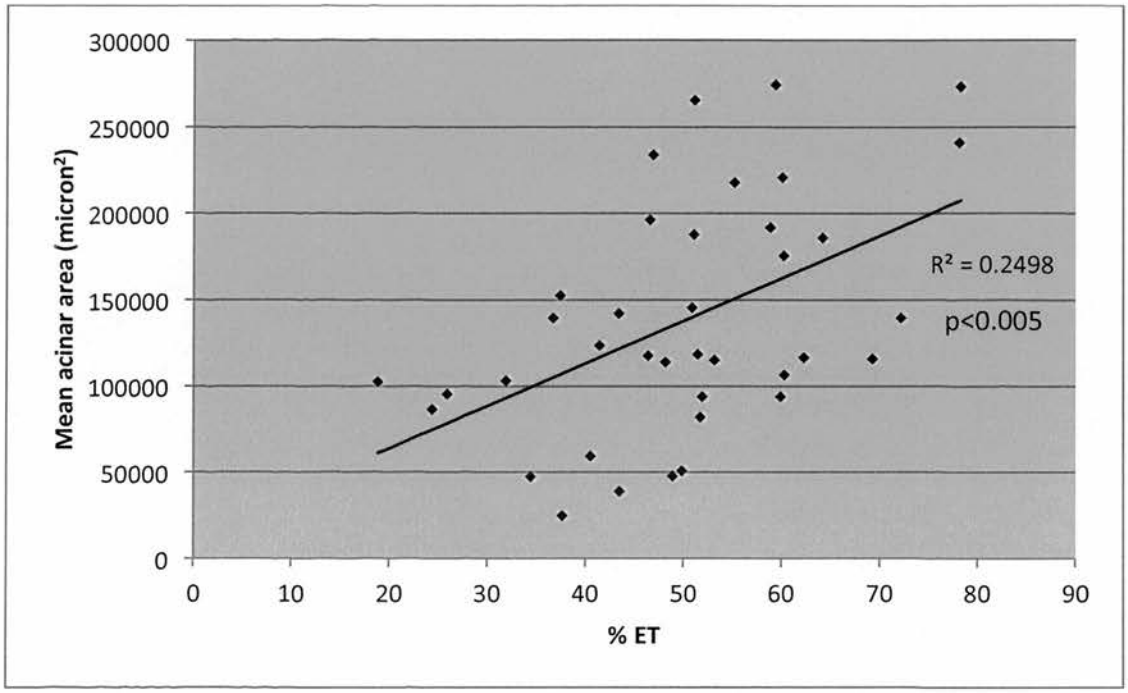

Figure 4.7 – Correlation between mean acinar area and %ET of epithelial glands within nodules (n=38).

Figure 4.7 shows the strong and significant relationship between %ET and the mean acinar area of epithelial glands within nodular areas (R^2=0.25 $p<0.005$). In nodules with increasing %ET, the size of the acini increases. However, the correlations between %SM and mean acinar area were weak in the nodule group.

The morphological data for the nodule group was again represented as epithelial to smooth muscle ratio (see figure 4.5) to explore whether stratification of the data would improve the correlations with the parameter, mean acinar area. The %ET data was sorted according to the ratio of epithelium to smooth muscle. Table 4.2 demonstrate no significant relationships between %ET and mean acinar are when the dataset is represented in this way.

The relationship between mean acinar area and the %ET and %SM in the stroma group were examined using linear regression analysis. The correlations between the morphological parameters %ET, %SM and mean acinar area were weak.

ET:SM ratio	Number of points	R^2 **mean acinar area vs %ET**
All (0-9)	38	**0.25 (p<0.005)**
< 2	16	0.11
>2 and <3	10	0.05
>3 and 4<	7	0.34 (p=0.13)
>4	5	0.10

Table 4.2 – Correlation between mean acinar area and %ET in the nodule group according to increasing ET:SM ratio

4.2. Summary of loco-regional morphometric studies

1. There are significant differences in the composition of nodules and stromal areas with respect to %ET, %SM and mean acinar area.

2. There is a significant overlap of tissue composition represented by ET:SM ratio in both nodules and stromal groups.

3. There is a strong relationship between mean acinar area and %ET within the nodule group.

4. These studies show that the measured individual morphometric parameters, %ET and %SM may not be sensitive enough to characterise an area to be stroma or a nodule.

4.3. Mechanical studies

71 individual point probing measurements were obtained from the fresh tissue specimens *ex vivo*. For each test point classified as nodules or stroma, there are corresponding mechanical measurements. The probe used in the application of a compressive cyclic strain to the tissue is micro-engineered to a size measuring 400μm × 500μm as described in section 2.3. The mean |E*| (a measure of tissue stiffness) and tan δ (a measure of tissue viscosity) are measured. The results of the mechanical studies are presented in this section.

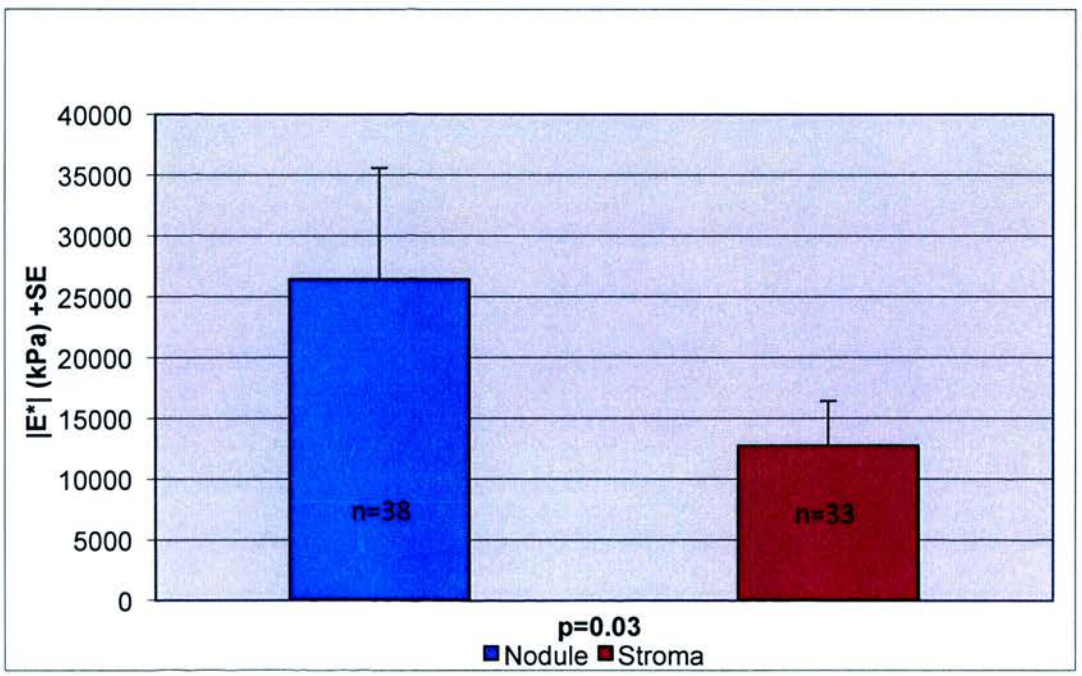

Figure 4.8 – Mean |E*| in areas classified as nodules and stroma. There is a significant difference between groups.

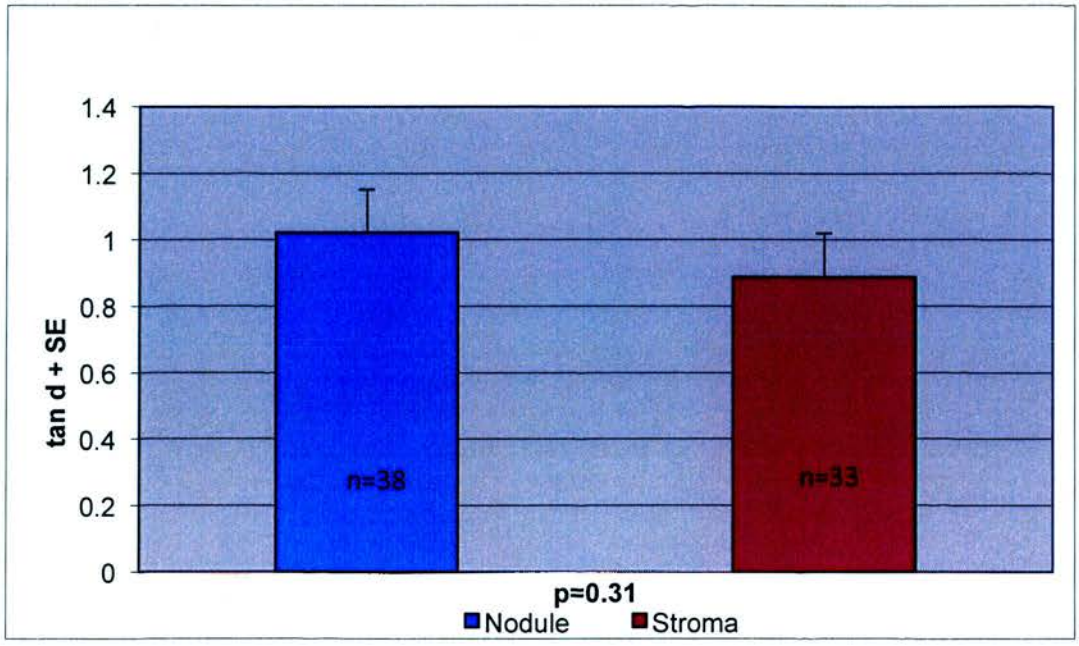

Figure 4.9 - Mean tan δ in areas classified as nodules and stroma. No difference was found between groups.

In figure 4.8, there is a significant difference between |E*| within nodules compared with stromal areas. Nodules were found to be significantly stiffer than stromal areas. However, tan δ was not found to be significantly different between the two groups as shown in figure 4.9.

4.4. Correlations between the morphometric studies and the mechanical measurement in the nodule group

The morphometric studies demonstrate that there are significant differences in smooth muscle content, epithelial content and mean acinar area between areas classified as glandular nodules and stromal areas. The mechanical studies show that there is a significant difference in |E*| between nodules and stroma. However, there is no difference found in tan δ between the groups. Linear and multiple regression analysis were used to examine the relationships between the morphology and mechanical measurements. The results are presented as R^2 values and the values highlighted in bold are significant correlations with the corresponding p value noted. In addition to the analysis of multiple variables, the data is stratified into different groups defined by percentage of epithelial or smooth muscle content to understand the impact this may have on the analysis. The results of these studies, in the nodular group, are presented in this section.

Correlations between smooth muscle and mechanical measurements

SM content (%)	Number of points	R^2 **%SM vs |E*|**	R^2 **%SM vs tan δ**
All	38	0.02	0.02
>10%	35	0.007	0.007
>20%	20	0.15	0.01
>30%	6	0.11	0.10

Table 4.3 - Correlations between %SM and |E*| and tan δ within the nodular group. %SM is stratified according to increasing SM content.

SM content (%)	Number of points	Multiple R^2 **%ET, Mean acinar area vs |E*|**	Multiple R^2 **%ET, Mean acinar area vs tan δ**
All	38	0.306	0.166
>10 and <20	18	0.245	0.128
>20 and <30	14	0.301	0.618
>30%	6	**0.945 (p=0.035)**	0.869

Table 4.4 - Multiple linear regression analysis with predictor variables of %SM and mean acinar area, and response variables of |E*| and tan δ in the nodule group.

The results in table 4.3 do not show significant relationships between %SM and |E*| and tan δ using linear regression analysis. Multiple regression analysis was used to assess the impact of including mean acinar area into the analysis. The results shown in table 4.4 demonstrate a significant positive relationship between %SM, mean acinar area and the |E*| in tissues containing >30% SM. This observation perhaps

reflects the finding that in tissues with a greater amount of SM content, the higher the |E*|. There is a positive relationship between %SM content of >30% with %ET, mean acinar area and tan δ, but this does not reach statistical significance. In stratifying the data according to %SM, there are fewer points within each group and therefore, this correlation is based only on a small number of data points. Despite incorporating additional measurements of morphology, the correlations between morphological and mechanical measurements are still weak.

Correlations between epithelial tissue and mechanical measurements

ET content (%)	Number of points	R^2 **%ET vs |E*|**	R^2 **%ET vs tan δ**
All	38	0.06	0.04
>20%	37	0.02	0.03
>30%	35	0.04	0.002
>40%	30	0.06	0.001
>50%	19	0.12	0.01
>60%	9	0.13	0.07

Table 4.5 - Correlations between %ET and |E*| and tan δ within the nodular group. %ET is stratified according to increasing ET content.

ET content (%)	Number of points	Multiple R^2 **%SM, Mean acinar area vs |E*|**	Multiple R^2 **%SM, Mean acinar area vs tan δ**
All	38	0.276	0.231
>18 and <40	8	0.545	**0.947 (p=0.003)**
>40 and <50	10	0.479	0.681
>50 and 60	11	0.650	0.543
>60 and <80	9	0.672	0.316

Table 4.6 - Multiple linear regression analysis with predictor variables of %SM and mean acinar area, and response variables of |E*| and tan δ in the nodule group

The results shown in table 4.5, there are no significant relationships between %ET and |E*| and tan δ using linear regression analysis. In table 4.6, there is a significant relationship between %SM, mean acinar area and tan δ within the group of points with low ET content (>18% and <40%). However, there are no significant correlations seen in the analysis between %ET with %SM, mean acinar area and |E*|.

Correlations between mean acinar size and mechanical measurements

Using simple linear regression analysis, the morphological measurements of %SM, %ET, mean acinar area and ET:SM ratio were compared with |E*| and tan δ within the nodule group. A significant positive correlation was seen in the relationship between mean acinar area and tan δ as shown in figure 4.10. As mean acinar size

increases, the phase lag, measured by tan δ increases. Tan δ, in the viscoelastic model, is considered the damping force of the model. This correlation suggests that tan δ is sensitive to gland size and the greater the gland acini size, the higher the measured viscosity.

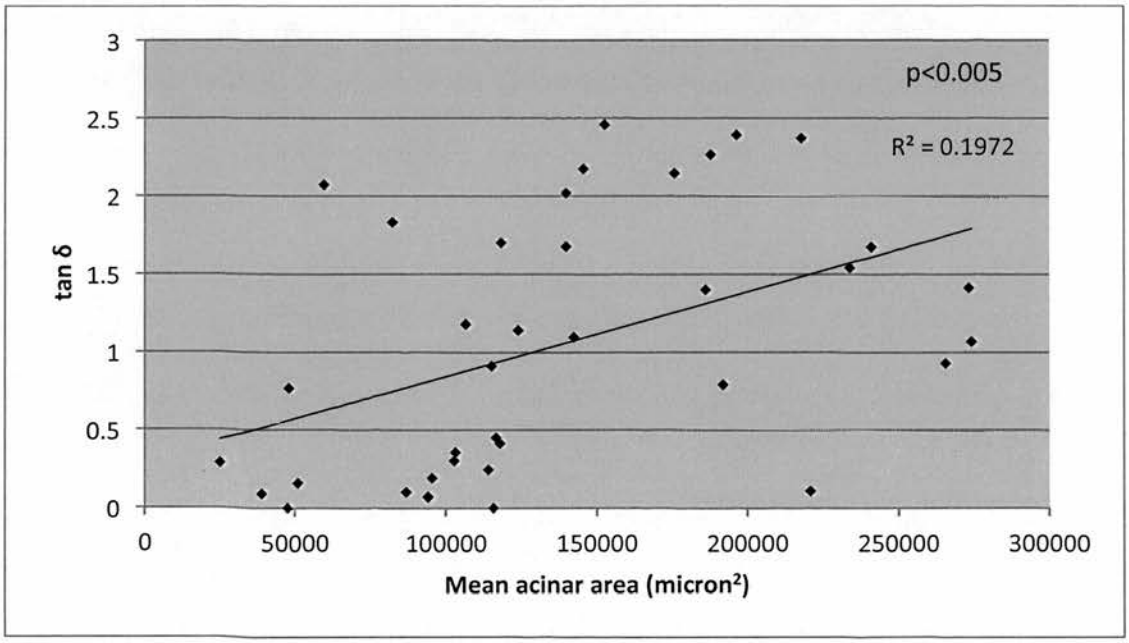

Figure 4.10 – Correlation between mean acinar area and tan δ (n=38) in the nodule group.

The correlation between mean acinar area and tan δ shown in figure 4.10 is strengthened when the data is stratified by ET:SM ratio. In nodular areas with an ET:SM ratio of <2, the relationship between mean acinar area and tan δ is significantly improved. This is shown in figure 4.11.

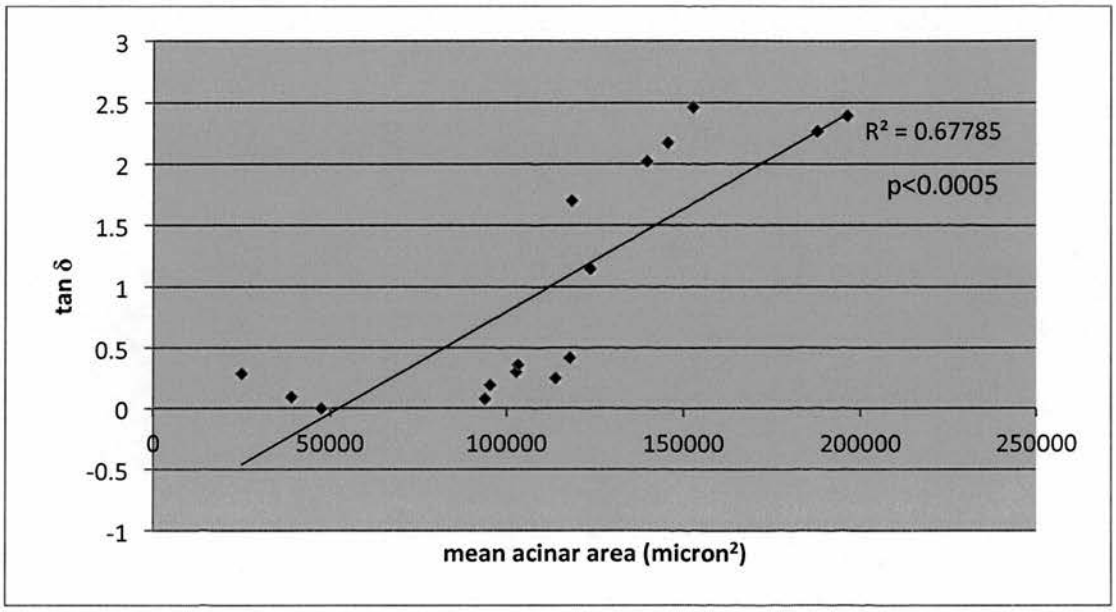

Figure 4.11 – Correlation between mean acinar area and tan δ (n=16) within the nodule group in areas where the ET:SM ratio is <2.

There is a significant positive relationship between mean acinar area and tan δ. From these results, it appears that mean acinar area is an important morphometric measurement that is shown to have strong relationships with the mechanical measurements within the nodule group.

4.5. Correlations between the morphometric studies and the mechanical measurement in the stroma group

Correlations between smooth muscle and mechanical measurements

SM content	Number of points	R^2 **%SM vs |E*|**	R^2 **%SM vs tan δ**
All	33	0.03	**0.20 (p=0.01)**
>20%	28	0.02	0.01
>30%	12	0.001	0.01

Table 4.7 - Correlations between %SM and |E*| and tan δ within the stroma group. %SM is stratified according to increasing SM content (n=33). There is a significant correlation between %SM and tan δ (see figure 4.12)

SM content (%)	Number of points	Multiple R^2 **%SM, Mean Acinar Area vs |E*|**	Multiple R^2 **%SM, Mean Acinar Area vs tan δ**
All	33	0221	0.406
>20%	18	0.195	0.165
>30%	9	0.514	0.131

Table 4.8 - Multiple linear regression analysis with predictor variables of %ET and Mean acinar area, and response variables of either |E*| or tan δ in the stroma group.

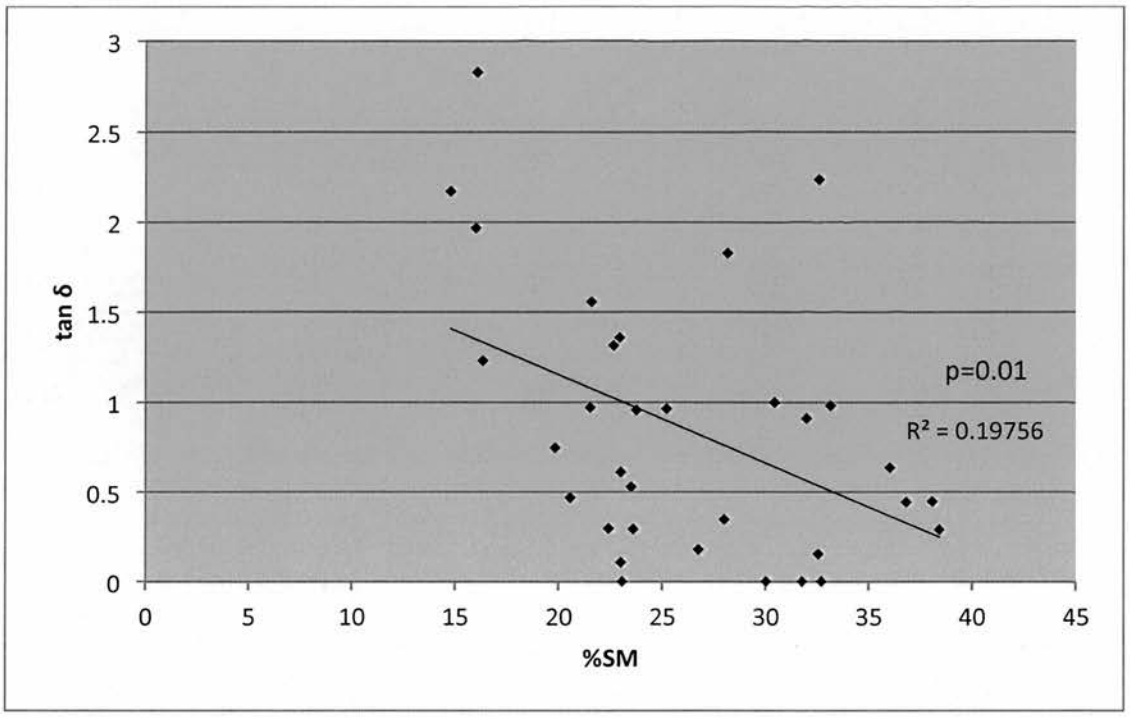

Figure 4.12 - Correlation between %SM and tan δ (n=33) within the stroma group.

Table 4.7 demonstrate a significant correlations between %SM and tan δ (R^2 =0.2; p=0.01). In figure 4.12, the correlation graph shows a negative relationship between increasing %SM and tan δ. Stromal areas are shown in table 4.1 to comprise of significantly greater %SM compared with nodular areas. The correlation between %SM and tan δ suggest that as %SM increases, the glandular composition of the tissue decreases, and this is reflected in the lower viscosity of the tissue.

Table 4.8 show the correlation results using multiple regression analysis. No significant correlations are seen within %SM, mean acinar area and E*| or tan δ.

Correlations between epithelial tissue and mechanical measurements

ET content	Number of points	R^2 **%ET vs |E*|**	R^2 **%ET vs tan δ**
All	33	0.002	0.007
>20%	23	0.014	0.005
>30%	16	0.050	0.054
>40%	7	0.174	0.102

Table 4.9 - Correlations between %ET and |E*| and tan δ within the stroma group. %ET is stratified according to increasing ET content.

ET content (%)	Number of points	Multiple R^2 **%SM, Mean acinar area vs |E*|**	Multiple R^2 **%SM, Mean acinar area vs tan δ**
All	33	0.065	0.133
>20	21	0.105	0.227
>30	15	0.258	0.341
>40	7	**0.898 (p=0.037)**	0.645

Table 4.10 - Multiple linear regression analysis with predictor variables of %SM and mean acinar area, and response variables of |E*| and tan δ in the stroma group

Table 4.9 shows the correlations between %ET and |E*| and tan δ in the stroma group. No significant correlations are seen. Table 4.10 shows the results using multiple regression analysis with %ET and Mean acinar area, and the response

variables of either |E*| or tan δ. There is a significant correlation between %ET, %SM, mean acinar area vs |E*| in stromal areas containing >40% of ET. The relationship between %ET, %SM, mean acinar area vs tan δ do not reach statistical significance.

4.6. The assessment of the impact of the morphology upon the mechanical properties using Artificial Neural Networks

In section 4.4 and 4.5, it has been shown that there are very few significant correlations between the morphometric and mechanical parameters. Linear regression and multiple regression analysis has failed to identify strong relationships between the groups. The significant correlations observed within sub-group data-sets however, cannot completely explain the complex interactions and relationships between the morphology and mechanical properties seen in a whole section of prostate tissue. Artificial neural networks are able to recognise complex relationships that regression analysis may not be able to identify.

As in the work presented in section 3.5, the use and the results of ANN are reported in this section. The organisation of the dataset is similar to the method explained in section 3.5. Briefly, in this study, each parameter whether it related to morphometric or mechanical data, is represented by a column of raw numerical data. The ANN analyses the data in three stages; the training, validation and finally the output phase.

ANN analysis of %ET and %SM with |E|*

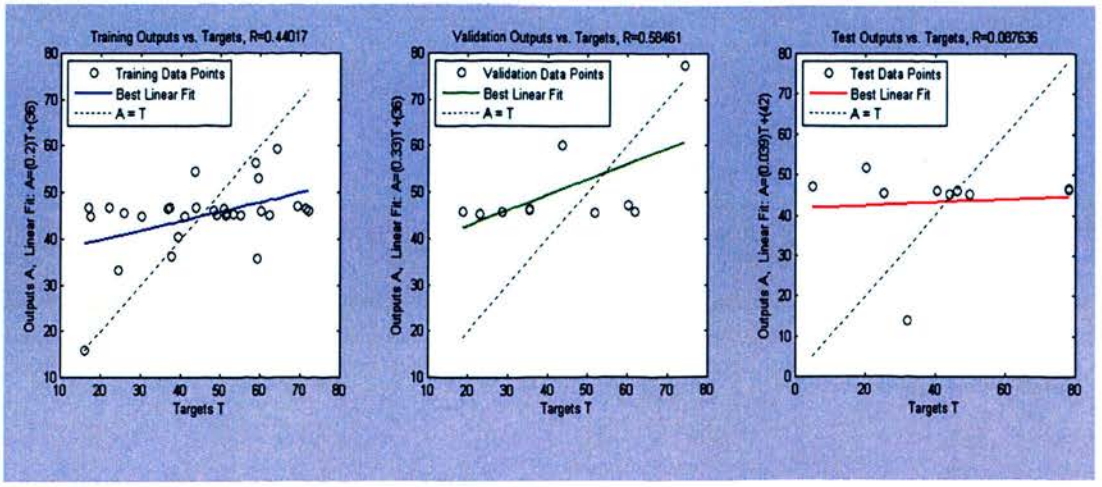

Figure 4.13 – Regression plot of ANN analysis of the parameters %ET and |E*|.

There is no relationship between |E*| and %ET (R^2=0.088).

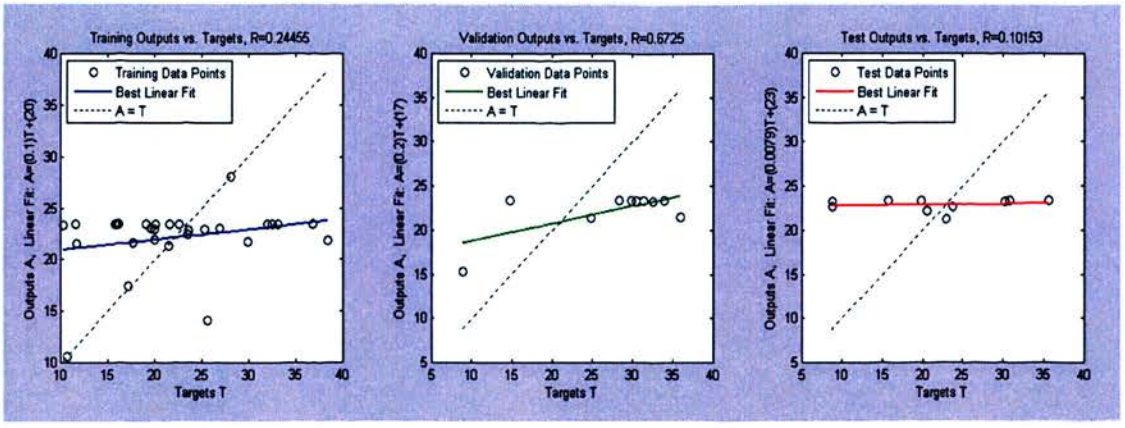

Figure 4.14 - Regression plot of ANN analysis of the parameters %SM and |E*|.

There is no relationship seen between |E*| and %SM (R^2=0.101).

From this analysis shown in figures 4.13 and 4.14, the morphometric variables, %SM and %ET do not show a strong relationship with the mechanical variable, |E*|.

ANN analysis of %ET and %SM with tan δ

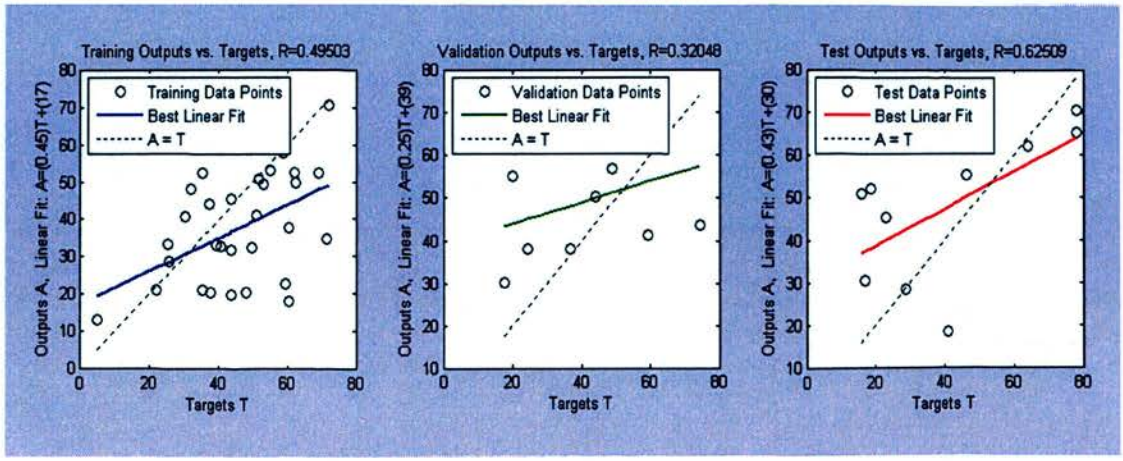

Figure 4.15 - Regression plot of ANN analysis of the parameters %ET and tan δ.

There is a significant relationship between these variables ($\mathbf{R^2=0.625}$)

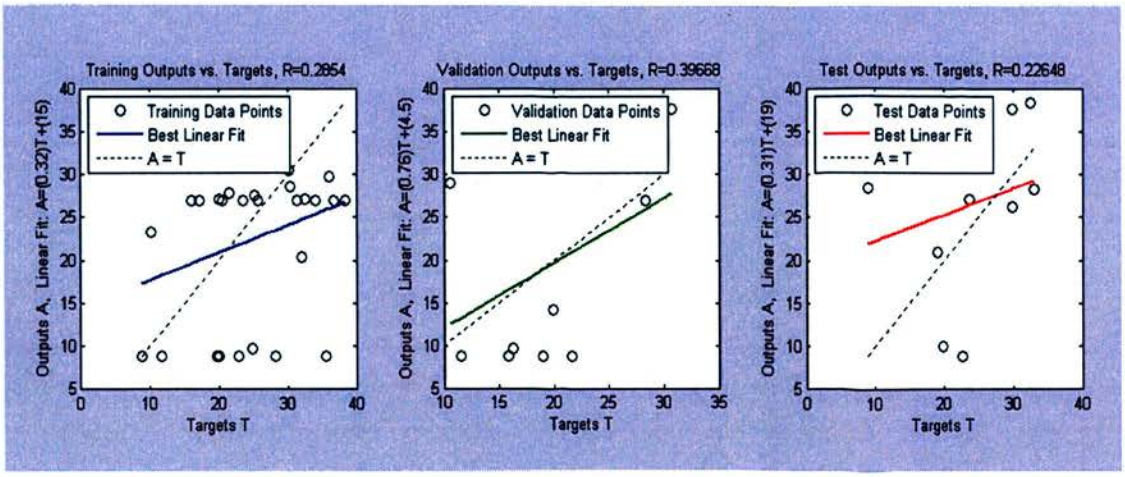

Figure 4.16 - Regression plot of ANN analysis of the parameters %SM and tan δ.

There is no significant relationship between these two variables (R^2=0.226).

In figures 4.15, there is a significant positive relationship between tan and %ET. No relationships were seen between %SM and tan δ. However, in table 4.7 and in figure 4.12, there is a weak but significant negative relationship between %SM and tan δ. The observations calculated using linear regression analysis is based upon classification of the dataset into stroma and nodular groups. In the ANN analysis, the dataset is not classified, and the ANN performs the analysis on the dataset as a whole. These results are not directly comparable, but the findings highlight difficulty in identifying strong relationships within a heterogeneous dataset.

ANN analysis of %ET and %SM with |E| and tan δ*

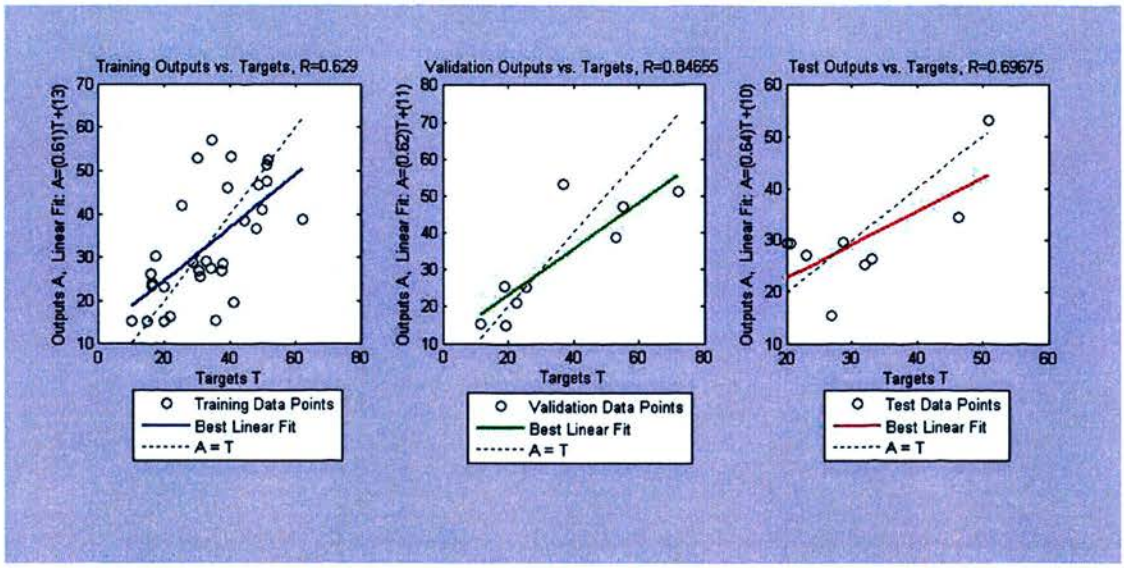

Figure 4.17 – Regression plot of ANN analysis of the parameters %SM, %ET and |E*| and tan δ. There is a strong relationship between the morphometric parameters and the mechanical properties when considering both all variables within the analysis (**R^2=0.697**).

The ANN analysis of both the morphometric and mechanical parameters in figure 4.17 demonstrate that there are significant positive relationships between all four parameters. It can be inferred that the neural network is seeing patterns and variations that are not possible when assessed in a linear fashion. The drawback of the ANN analysis is that the system does not declare the path it took to arrive at these conclusions. The raw data that is entered into the Neural Network is not shown in any original form at the end of the analysis. The graphical points do not indicate numerical values of morphological or mechanical data. Instead they are markers of how close the output points are to the validation data points or training data points.

4.7. Loco-regional morphology and micro-probe point: summary of findings

The main findings from the study of loco-regional morphology and the mechanical measurements are summarised below:

1. There are significant histological differences between areas of loco-regional morphology classified as nodules and as stroma.

2. Mean |E*| in nodular areas are significantly higher than in stromal areas.

3. Mean acinar area is an important morphological parameter. There are significant correlations between mean acinar area and the mechanical measurements.

4. Multiple linear regression analysis yielded mixed results in analysis of the impact of multiple morphometric variables upon the mechanical measurements.

5. Artificial neural networks analysis demonstrate that there are significant correlations between all the morphological parameters (%ET and %SM) and mechanical measurement (|E*| and tan δ)

4.8. Discussion

The results in Table 4.1 demonstrate that there are measurable differences between loco-regional areas classified as nodules and stroma. The mean acinar area of nodules is significantly greater than that of stroma. Figure 4.5 demonstrate the distribution of the epithelial to stroma ratio within all examined areas of histology. The majority of nodules have an epithelial to stroma ratio >1. These morphometric results are in accordance with the results from the previous work in Chapter 3.

The morphometric and mechanical measurements show that $|E^*|$ is significantly greater in nodules than in stroma. Mean acinar size is significantly greater in nodules than in stromal areas. However, it appears that tan δ, used alone, is a poor discriminator between stromal and nodular areas regardless of acinar size (figure 4.9).

The results presented in section 4.4 and 4.5 examine the relationships between the morphology and the mechanical properties of nodule and stroma groups. Within the nodule group, there are poor correlations between %SM content with the mechanical measurements. The addition of mean acinar area to the analysis, seen in table 4.4, shows a strengthening of the relationship but only in areas containing >30% smooth muscle. These areas area predominantly smooth muscle in composition and appears to exhibit different mechanical properties to areas composed of less smooth muscle. As the tissue studied comprised of mainly smooth muscle, it may be that the tissue behaves according to the viscoelastic model shown in TURP chippings. In this

model, there is a direct relationship between %SM and |E*|. However, these conclusions cannot be made with certainty as the number of points tested in this sub-selected group is 6 compared with 38 for the whole nodule group.

Examining the relationships between %ET and the mechanical properties, there are no significant correlations seen despite stratifying the dataset in increasing % content of ET (see table 4.5). In the multiple regression analysis, the addition of mean acinar area to the analysis strengthens the relationships between the morphology and mechanical properties. The positive effect of mean acinar area is seen in the relationships between both |E*| and tan δ, but do not reach statistical significant due to reduced numbers of data points (see table 4.6).

In the linear regression studies of morphological and mechanical properties of the prostate, mean acinar area appeared to be highly discriminative of nodular and stroma classification. There were significant correlations between mean acinar area and tan δ within the nodular group (figure 4.10). The relationship improves further in areas of the nodule with an ET to SM ratio is less than 2 (fig 4.11). It appears that mean acinar area is shown to have an important relationship with tan δ within nodular areas. As the gland size increases, there is a linear increase in the viscosity of the tissues. This relationship maintains this strong relationship in areas that area have a low ET:SM ratio. This suggests that the mechanical properties of nodules with increased ET:SM content (i.e. nodules comprised of mainly epithelial tissue) exhibit different mechanical properties. There may be other histological parameters

that are not considered in this study, that may be influencing the mechanical properties of nodules with varying ET content.

The results of the ANN analysis in figures 4.13 and 4.14, demonstrates that there are poor relationships between %ET and %SM with |E*|. It appears that taken individually, these parameters do not influence |E*|. In figure 4.15 demonstrate a significant relationship between %ET and tan δ. However, this relationship is not seen between %SM and tan δ (figure 4.16). As an individual morphometric parameter, %ET has most influence on tan δ. Considering all morphometric parameters, the analysis presented in figure 4.17 show a strong and positive relationship between |E*| and tan δ. The advantage of the ANN is that analysis of the data in a non-linear fashion can identify correlations that are difficult to elucidate. ANN confirms that there are measureable relationships between morphology and mechanical properties of the prostate. It does not suggest that there are simple, linear and strong relationships between the morphometric variables and mechanical measurements employed in this study.

The results shown from these studies of prostate morphology and mechanical properties using a micro-probe indenter suggest that the structure property relationship of the prostate does not appear to follow the simple viscoelastic model described in previous work by *Phipps et al* [127]. Briefly, Phipps *et al* have shown that in tissues taken at time of TURP, there was a strong correlation between the SM content of the tissue and |E*|. However, in this study, the tissue studied comprised mainly SM and very little epithelial tissue. In this study of whole prostates, the main

tissue composition for most of the specimens have high epithelial to stroma ratio. Therefore our studies cannot be closely compared. The studies suggest that the amplitude ratio, |E*|, maybe a more sensitive discriminator between hyperplastic nodules or stroma with an increasing SM or ET content. Relationships strengthen when mean acinar area and %ET content is considered in multiple regression analysis. As %ET and mean acinar area increases, the most likely structure to be described is a glandular nodule with tightly bound acini (see figure 4.18).

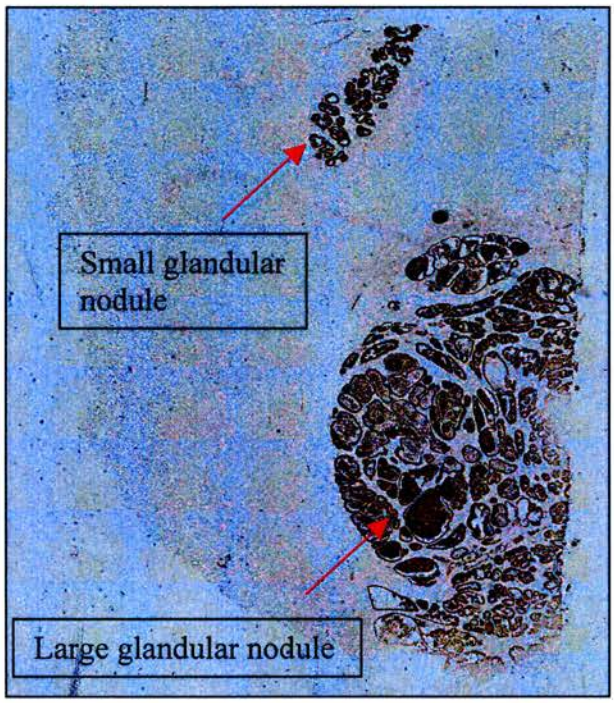

Figure 4.18 – Mosaic photomicrograph depicting a large glandular nodule within a transverse slice of whole prostate stained with anti-PSA

The morphometric analysis of this nodule show a fairly homogenous dataset. A cyclic compressive forced is applied to the tissue with a micro indenter measuring

400μm × 500μm ($0.2mm^2$) yet the histology area captured as the area of interest measures $42mm^2$. Therefore, if a large glandular nodule is the area of interest, the histology represented by each 49 image could be relatively homogenous. In contrast, figure 4.19 shows an area of interest (represented by 7 x 7 matrix of images) and the heterogeneity of % smooth muscle content per image captured is significant. Several frames lie on predominately stromal areas and others on glandular areas.

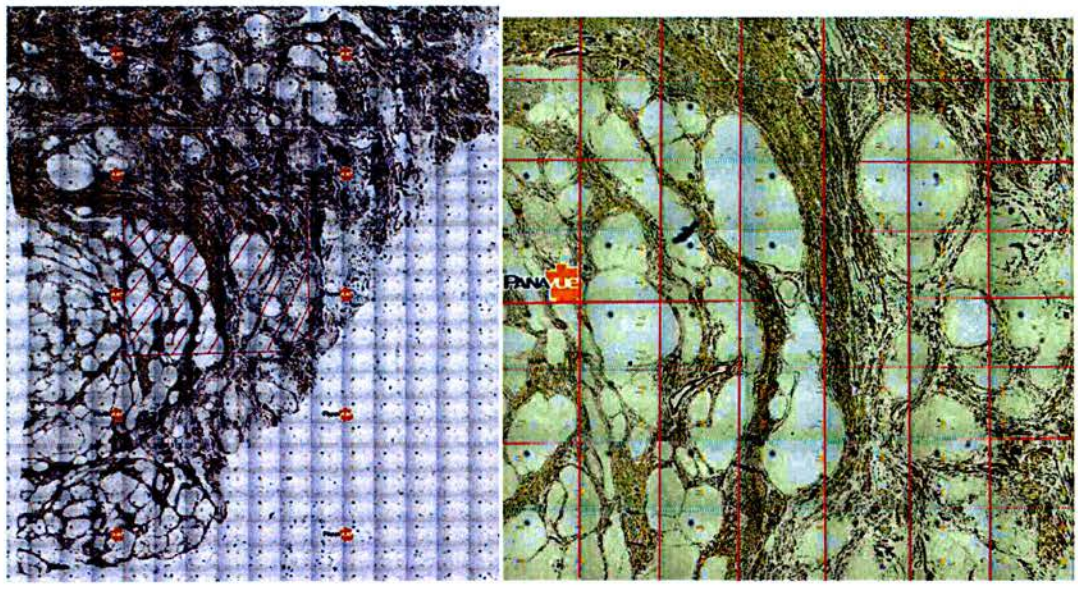

Figure 4.19 – Mosaic photomicrograph. On the left is a whole section of prostate stained with anti-SM myosin. A large glandular nodule can be seen within the stromal framework seen. On the right is the area of histological interest represented by 7 x 7 images. In several frames, the amount of SM can clearly be seen to be very different between adjacent frames.

This study demonstrates the difficulties in comparing the histological features with the mechanical data generated from a micro-sized indenter. The initial approach to assessing loco-regional morphology was to use the protocol described in section 2.7.3. A "self-similarity" exercise was performed and results are seen in Table 2.5 and the discussion is in section 2.7.4. Using a smaller matrix of captured images, such as 3 x 3 size, has possible advantages. However, due to the small size of the indenter, it was no longer possible to mark accurately the area of tissue subjected to point probing. Therefore using a smaller area of interest would increase the uncertainty of using histological data that was not subjected to mechanical testing. Therefore the aim was to use a 7 x 7 matrix as the assumption is that the area examined should contain the test point. Several attempts were made to analyse data with respect to individual histological values from each single microscopic frame taken at x200 magnification. However, these analyses yielded very poor result with no correlations found. Despite the use of multiple linear regression analysis and using ANN, no significant relationships were found between the core variables such as %ET, %SM, $|E^*|$ and tan δ. The heterogeneity of the histological results hampered analysis. A mean value of the histological results per point probed was used in all calculations within this chapter. In using the mean of all 49 images describing one point, there were measurable differences with significant correlations between tan δ, mean acinar area and %SM.

The lack of correlations may be as a result of other histological structures contributing to the mechanical properties of the prostate which are measured in this study. Collagen III (CIII) was studied along with smooth muscle and glandular

tissue by Schuster *et al*. This group showed that CIII composition remained roughly at 30-35% in all sizes of prostates examined [33]. Phipps *et al* demonstrated that CIII estimation did not affect mechanical properties within TURP chippings despite comprising 15-44% of the composition [127, 128]. It was based upon this finding that, in this study, Collagen III was not studied as a histological parameter. Fibroblasts are thought to comprise a significant proportion of the stroma but identification of fibroblasts is often difficult due to the lack of suitable markers [139]. However, recent availability of a suitable antibody, TE-7, has been shown to positively identify human fibroblasts within formalin fixed tissue [140].

The prostate is considered as a heterogonous organ, and based upon the studies of McNeal, different zones of the prostate exhibit different pathological processes and tissue composition [9]. In this study, the use of transverse sections of whole prostates allow for the examination and appreciation of the heterogeneous architecture of the prostate. TURP chippings are composed of mainly stromal tissue as the resection is from the transitional and anterior fibromuscular zone of the prostate.

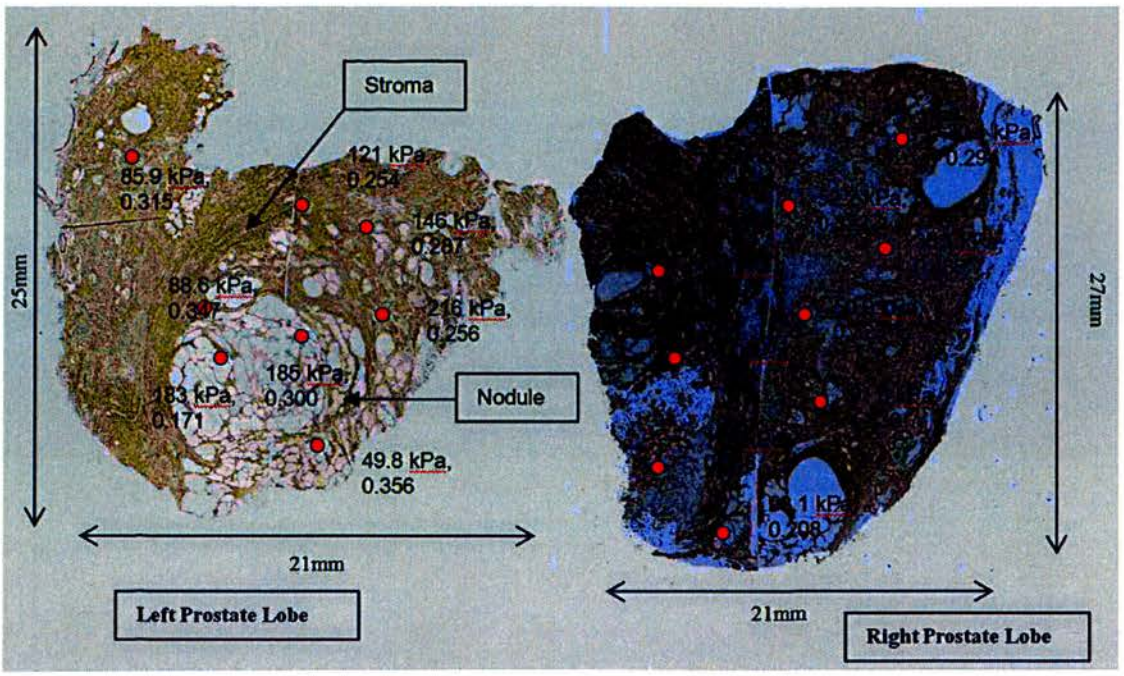

Figure 4.20 – A composite "map" showing histological and mechanical variation across a whole transverse slice of prostate.

In figure 4.20, a composite image of a whole section of prostate, stained with anti-smooth muscle antibody, demonstrates the variability of histology as well as mechanical measurements across this specimen. It may be too simplistic to describe or quantify loco-regional areas of morphology that are so distinct from each other with just two components of prostate tissue, namely smooth muscle and epithelial tissue. As the mechanical properties are functions of the morphology of the gland, further characterisation of the components of the stromal area within the prostate may lead to further development and understanding of the relationship between morphology and the mechanical properties of the gland.

The limitations of the present study

1. Morphological examination does not take into account of the various components that are in addition to the smooth muscle and glandular components of the gland.

2. The mechanical measurements are a function of the morphology and if the morphology is incomplete, the mechanical measurements cannot reflect the morphological map.

3. Micro-probe may give better discrimination on histological components but placement precision is needed to be improved to accurately assess the loco-regional morphology subjected to testing.

4. Artificial neural network is a useful tool to understand the possible relationships between various, seemingly unconnected variables. There is a requirement for more test points to be studied so that the ANN can function to its best potential.

Chapter Five

The relationship between alpha blocker therapy and the mechanical properties of prostate tissue

5. Introduction

Studies have shown the pro-apoptotic effects of quinazoline-based alpha blockers, terazosin and doxazosin, upon BPH tissues [43, 87, 88]. An increase in the apoptotic index (AI) correlated with a decrease in smooth muscle content of the tissue. However, no study to date has examined the apoptotic effects of alfuzosin, a quinazoline-based alpha blocker, upon prostate tissues and whether there is a relationship with morphology.

Previous work from Phipps *et al* have shown that the mechanical properties of TURP tissue are a function of smooth muscle content when measurements are made using a macro-probe [127]. Therefore, this study was conducted on patients undergoing TURP and were selected based upon the type of alpha blocker therapy used in the initial stages of treatment of LUTS secondary to BOO. The TURP patients were classified into treatment groups based upon quinazoline (alfuzosin) or non-quinazoline-based (tamsulosin) alpha blocker therapy and a control group of patients with no medical therapy. The clinical characteristics of this group are presented in Table 5.1.

The prostate tissue was subjected to mechanical testing using the 2mm diameter ball end macro-probe. The tissue is subsequently processed, fixed and morphometric studies are carried out to determine the %SM and %ET composition. The assessment of the AI of the tissues was performed using TUNEL specific staining

and immunostaining using anti-Caspase-3 antibodies (see Section 2.8 for methodology).

Recruitment into this prospective group of patients resulted in a small number of patients within the alfuzosin and tamsulosin groups. Excluded were patients on combination therapy of an alpha blocker and a 5ARI as the latter is shown to decrease ET content of prostate tissue and may affect the mechanical characteristics of the tissue. Obtaining tissue from men undergoing TURP who were currently taking a single alpha blocking agent was challenging due to small number of patients fitting this criteria.

Therefore a second cohort of patients were sought to allow further studies on the effects of alfuzosin and tamsulosin upon the morphology and AI of prostate tissue. This cohort of patients was retrospectively chosen from the database of patients who have undergone radical retropubic prostatectomy (RRP) for localised prostate cancer. These patients had initially presented to the clinic with LUTS and several were commenced on alpha blocker therapy. All patients in this group responded to medical therapy but underwent RRP upon the diagnosis of localised prostate cancer. The patients were stratified into treatment groups based upon their alpha blocker therapy with a control group of patients in whom no medication was taken.

Particular attention was given to the selection of tissue blocks from these patients. The histo-pathologist ensured that the blocks selected reflect the transitional zone of the prostate so that meaningful comparisons can be made with the morphometric

studies from the TURP group. Unfortunately, due to the retrospective nature of this cohort, no mechanical measurements could be taken from the tissue as it was processed and fixed. Therefore this group of patients, who have shown response to alpha blocker therapy, will provide information regarding the effect of alpha blocker therapy upon the morphology and how this relates to the apoptotic indices of the tissue. The clinical characteristics of this group are presented in Table 5.2.

The aim, therefore, of this study is to examine the inter-relationship between apoptotic effects of alpha blocker therapy with the mechanical and morphological characteristics of the BPH tissue.

5.1. Clinical materials employed

Prostate tissue was obtained from 16 patients who underwent TURP. Morphometric and mechanical measurements were performed as previously described. In this group, 6 patients were on Tamsulosin, 4 patients were on Alfuzosin and 6 patients did not take any medications. Clinical characteristics of this group are provided in Table 5.1

Patient No	Age	PSA	Duration of medication (months)
Tamsulosin Group			
25	61	3.4	6
28	57	6.5	8
31	59	2.6	12
54	58	5.5	3
55	76	7.6	6
67	61	6	12
Alfuzosin Group			
3	71	3	6
30	75	5	12
74	80	1.8	36
76	68	8.9	3
Control Group			
24	68	2.3	No medication
51	71	6.3	No medication
53	71	5.6	No medication
56	60	1.2	No medication
63	62	6.2	No medication
75	72	10	No medication

Table 5.1 – Clinical characteristics of the TURP group.

Prostate tissue from patients who underwent RRP was used as a comparison group in the apoptotic experiments with TURP tissues. In this group, 5 patients were treated with tamsulosin, 5 with alfuzosin and 6 without medication. The patients on treatment continued their treatment until they underwent RRP for localised prostate cancer. The tissue blocks were examined by a pathologist to ensure that the transitional zone of the prostate was studied. Clinical characteristics of this group are provided in Table 5.2

Patient No	Age	PSA	Duration of medication (months)
Tamsulosin Group			
12907	76	4.9	12
3800	76	n/a	10
799	68	7	8
1070	69	7.8	6
8324	77	6	14
Alfuzosin Group			
524	76	4.7	10
105719	72	1.2	7
17962	65	5	15
13566	69	15	9
3574	56	3.5	18
Control Group			
8489	64	n/a	No medication
5359	74	8.9	No medication
4559	64	12.3	No medication
2153	78	n/a	No medication
16921	71	n/a	No medication
11442	74	6.4	No medication

Table 5.2 – Clinical characteristics of the RRP control group

5.2. The measurement of apoptotic indices in the TURP group

The study of apoptotic events with in the TURP tissues are conducted using two methods of detection as outlined in Section 2.5.3. Briefly, immunohistochemistry is used to assess Caspase-3 activity within the tissue. The overall apoptotic score was calculated by multiplying the intensity of the staining by the percentage of positive cells which exhibited the staining as outlined in section 2.8.1

TUNEL is a specific stain to detect DNA fragmentation by labelling the terminal end of nucleic acids. The apoptotic score was calculated as the percentage of positive stained cells over the total number of cells per high powered field as outlined in section 2.8.2.

5.2.1. Measurement of apoptosis employing the Caspase-3 assay

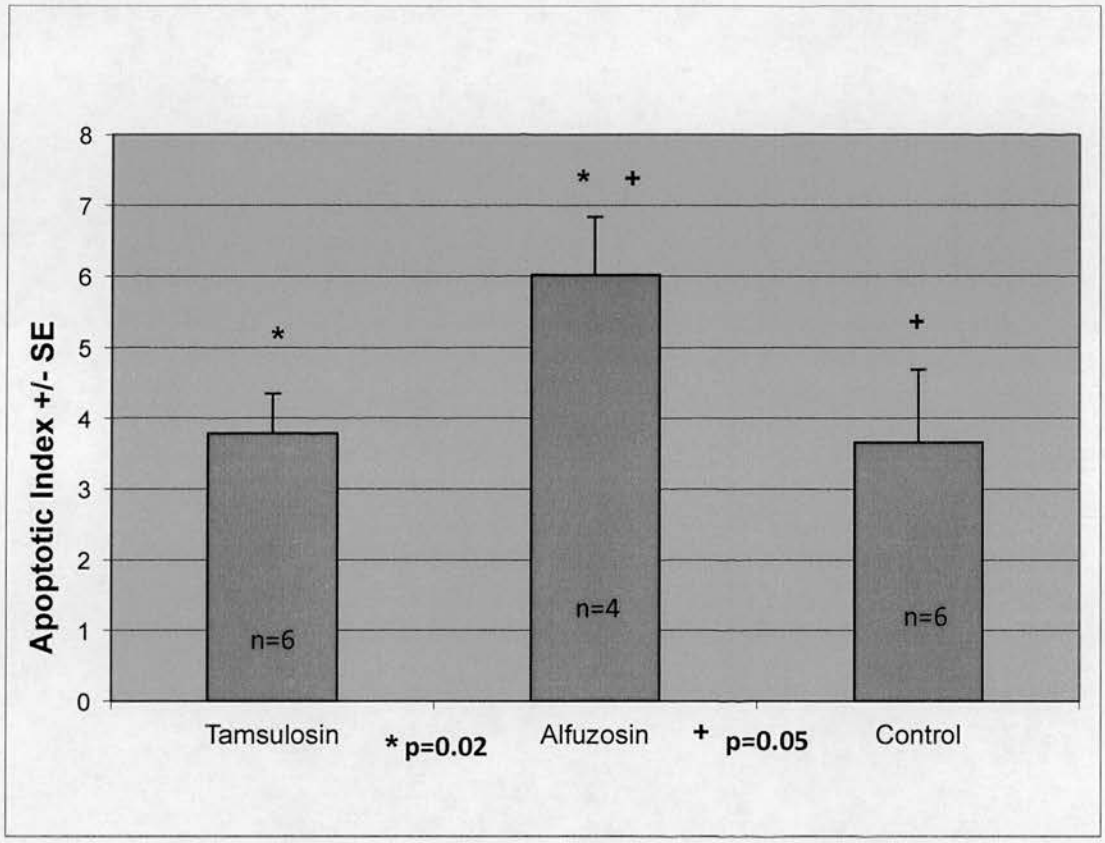

Fig 5.1 – The apoptotic index in TURP tissues using Caspase-3 assay.

The results of the study of apoptotic activity as assessed by the Caspase-3 assay in TURP tissues are presented in Figure 5.1. The results show that there is a significant increase in apoptotic activity within the TURP group treated with Alfuzosin compared with the group treated with Tamsulosin (* p=0.02). There is a significant increase in apoptotic activity within the Alfuzosin group compared with the control (+ p=0.05). There was no significant difference between tamsulosin and the control (p>0.05). The raw data for this experiment is contained in Appendix III.

5.2.2. Measurement of apoptosis employing the TUNEL assay

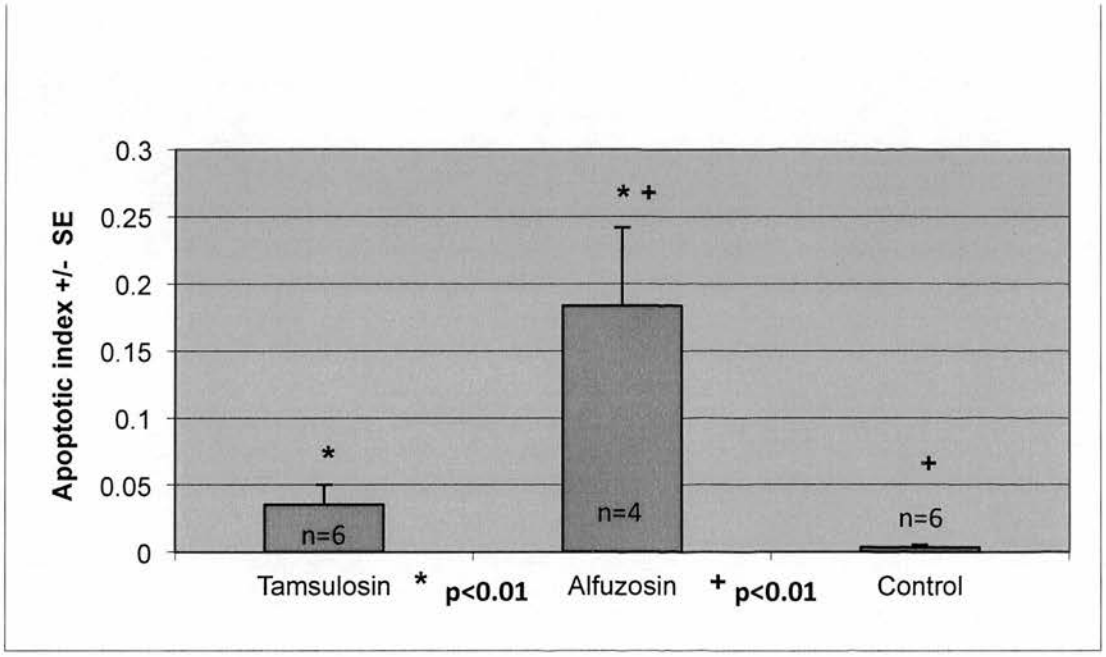

Figure 5.2 – The apoptotic index in TURP tissues using TUNEL assay.

The results of the study of apoptotic activity as assessed by TUNEL assay in TURP tissues are presented in Figure 5.2. The results show that there is a significant increase in apoptotic activity within the TURP group treated with Alfuzosin compared with the group treated with Tamsulosin (* $p<0.01$). There is a significant increase in apoptotic activity within the Alfuzosin group compared with the control (+ $p<0.01$). There was no significant difference between tamsulosin and the control ($p=0.07$).

The raw data for this experiment is contained in Appendix IV.

5.3. Morphometric and mechanical measurements in TURP tissues

To assess the morphology of the TURP tissues, prepared sections of tissue are subjected to immunohistochemical staining for anti-PSA and anti-smooth muscle antibodies to characterise the %ET and %SM within the tissue respectively. The quantitative analysis is described in section 2.5.3. The results of these experiments are presented in figures 5.3 and 5.4.

Prior to fixation and embedding in paraffin, the *ex vivo* prostate tissue resected at TURP is subjected to mechanical testing by applying a cyclic strain to the tissue using a 2mm macro-probe. The mechanical properties of the tissue are expressed by two values, $|E^*|$ and tan δ. $|E^*|$ represents tissue elasticity whereas tan δ represents tissue viscosity. The results of the mechanical testing are presented in figures 5.4 and 5.5.

5.3.1. Morphometric studies in TURP tissues

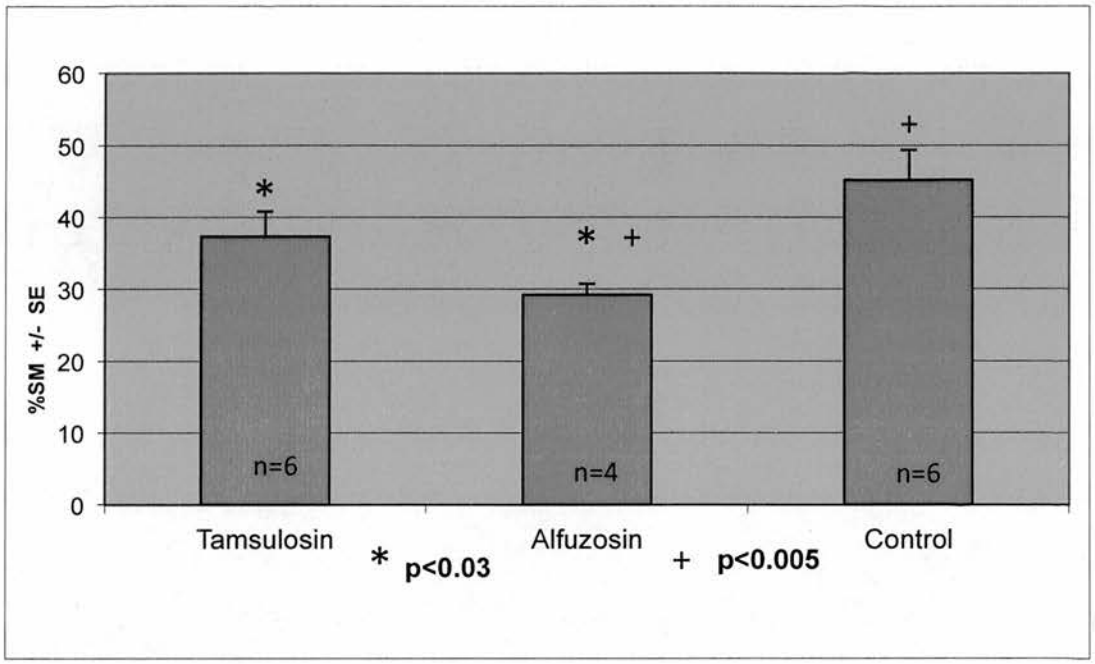

Figure 5.3 – %SM in TURP patients treated with tamsulosin, alfuzosin and control

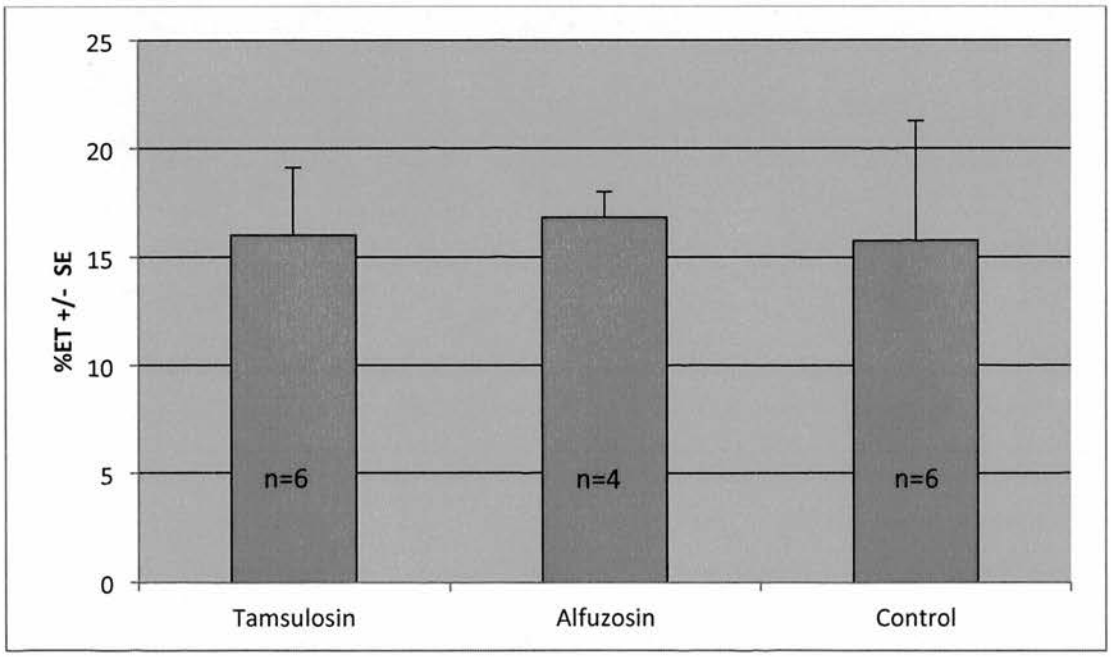

Figure 5.4 - %ET in TURP patients treated with tamsulosin, alfuzosin and control

The results of the morphometric studies are presented in figures 5.3 and 5.4. The %SM of the prostate tissue is shown in figure 5.3. These results show that the %SM in the alfuzosin group is significantly less than the tamsulosin ($p<0.03$) and control groups ($p<0.05$). There was no significant difference between the %SM content in the tamsulosin group and the control ($p=0.08$). The reduction in %SM can be attributed to the increase in apoptotic indices in the group treated with alfuzosin. Studies have confirmed the pro-apoptotic class effect of quinazoline-based alpha blockers but the literature is lacking in studies on alfuzosin. Therefore this work represents the first evidence for the pro-apoptotic effects of alfuzosin.

In figure 5.4, the %ET of the TURP tissue is shown. There are no significant differences in the epithelial content between the treatment groups and control group ($p>0.05$ for all groups). This may be a reflection of the low apoptotic rates within the epithelial compartment (which will be discussed later in this chapter).

5.3.2. Mechanical measurements in TURP tissues

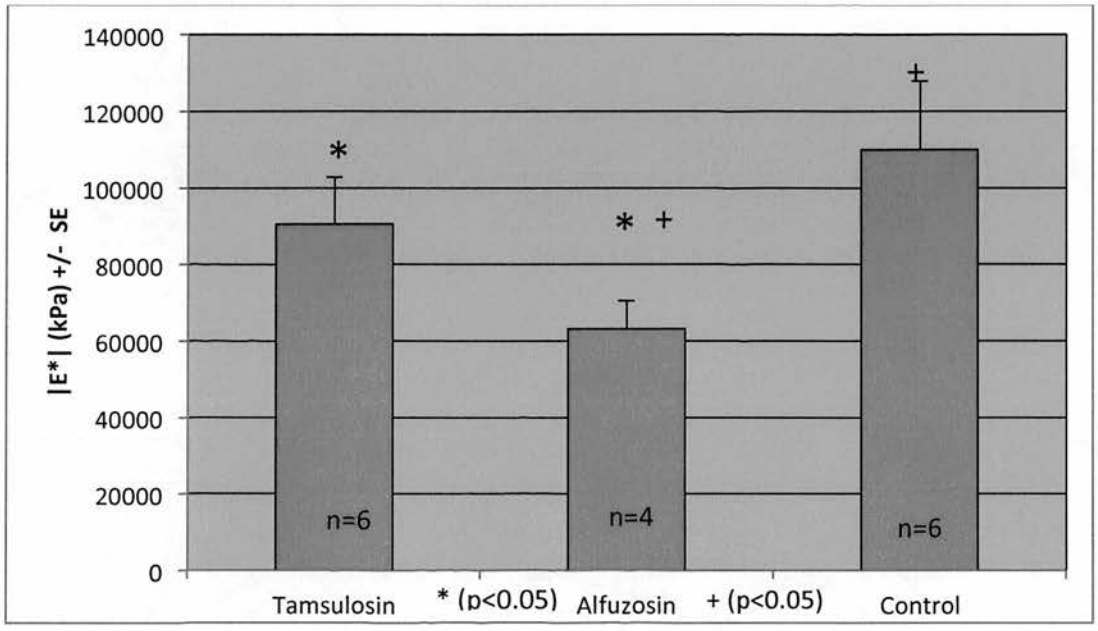

Figure 5.5 – |E*| in TURP patients treated with tamsulosin, alfuzosin and control

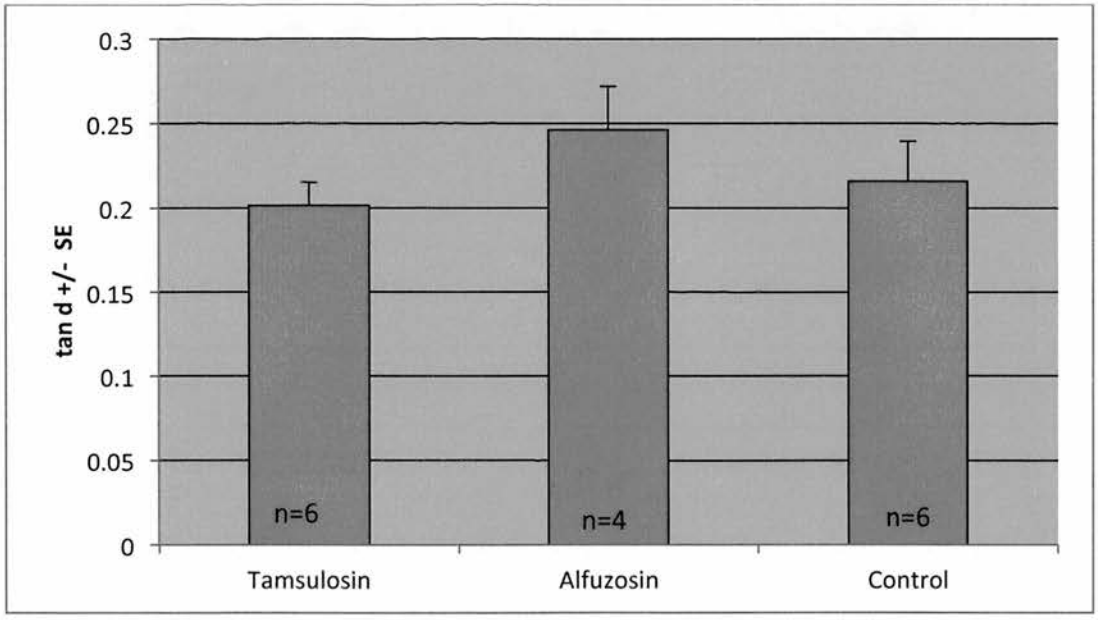

Figure 5.6 – Tan δ in TURP patients treated with tamsulosin, alfuzosin and control

The results of the mechanical testing in TURP tissues are shown in figures 5.5 and 5.6. In figure 5.5, there is a significant reduction in |E*|, tissue elasticity, in the group treated with alfuzosin compared with tamsulosin ($p<0.05$) and the control ($p<0.05$). There was no significant difference between tamsulosin and the control group ($p=0.2$). These results confirm that the effect of alfuzosin on prostate tissue has a significant and measureable difference in mechanical properties of the tissue.

In Figure 5.6, there are no significant differences in the mechanical measurement of tan δ between the tamsulosin and alfuzosin group ($p=0.07$), alfuzosin and control group ($p=0.22$) and tamsulosin and control group ($p=3.1$). This may be a reflection of the low rates of apoptotic activity within the epithelial areas.

5.4 Measurement of apoptosis indices in RRP tissues

RRP tissues were used as a comparative cohort to the TURP group. The apoptotic indices as assessed by the Caspase-3 assay and the TUNEL assay are presented in this section.

5.4.1. Measurement of apoptosis employing the Caspase-3 assay

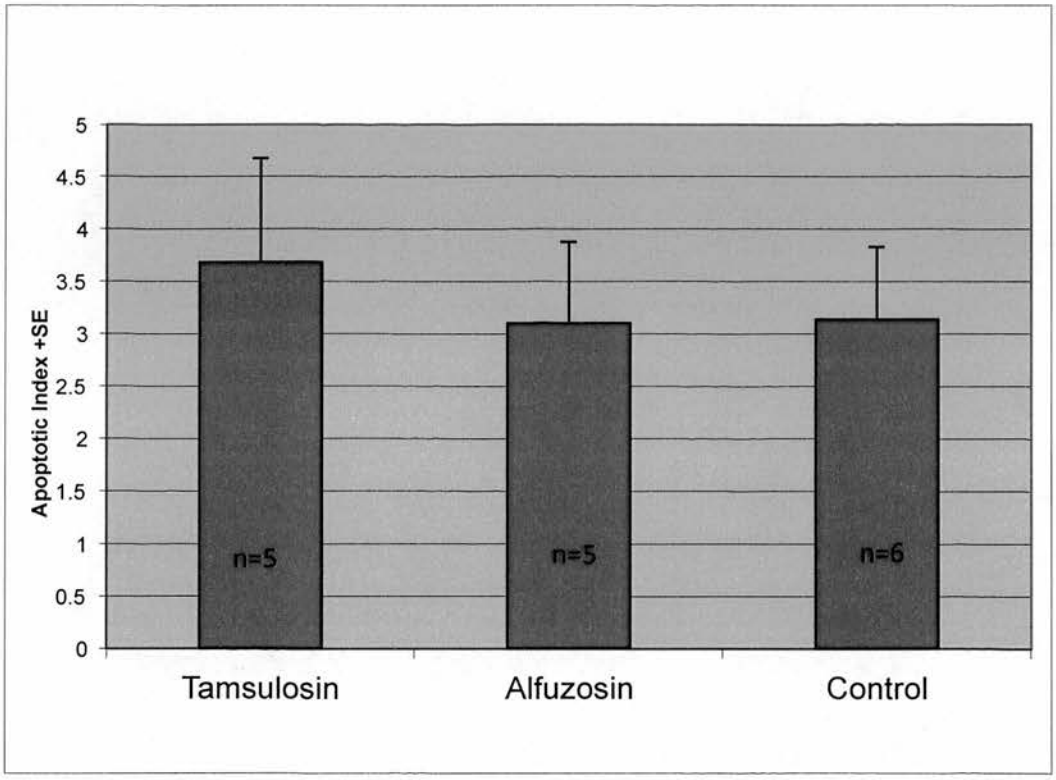

Figure 5.7 – Apoptotic index in RRP tissues assessed using Caspase-3.

Figure 5.7 demonstrates the apoptotic index measured using the Caspase-3 assay in RRP tissues in treated and non-treated patients. There was no significant difference between in the apoptotic index between the tamsulosin and alfuzosin group (p=0.32). No significant differences were found between tamsulosin and the control group (p=0.35) and alfuzosin and the control group (p=0.48).

5.4.2. Measurement of apoptosis employing the TUNEL assay

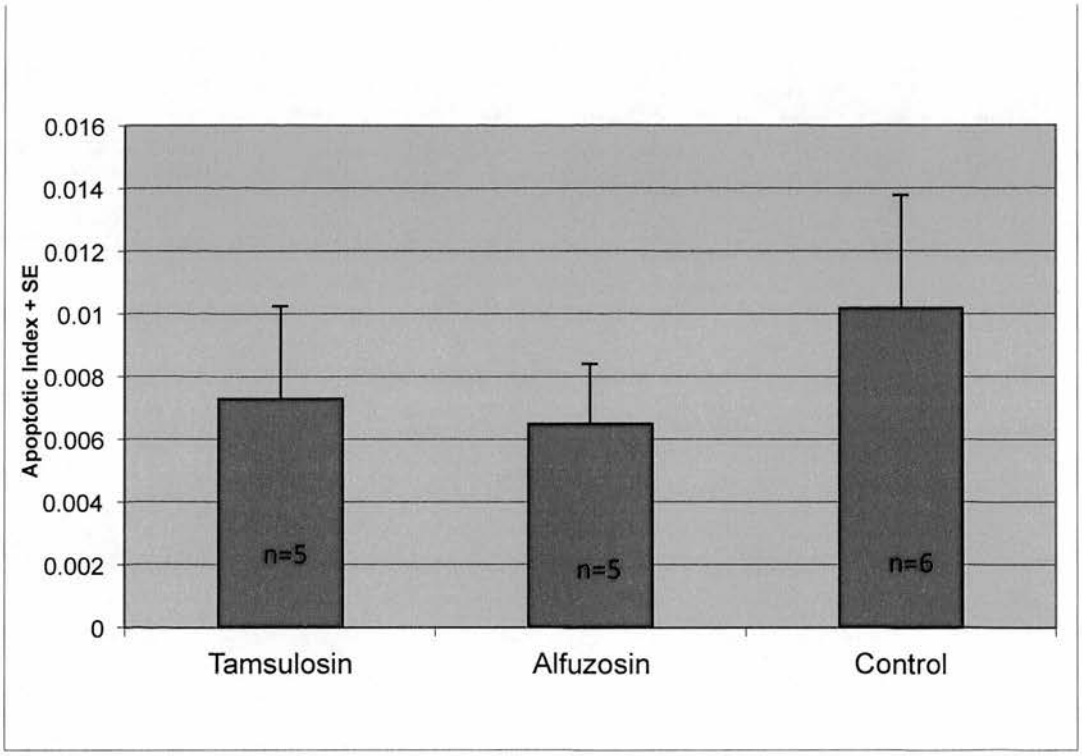

Figure 5.8 - Apoptotic index in RRP tissues assessed using TUNEL.

Figure 5.8 demonstrates the apoptotic index as measured using the TUNEL assay in RRP tissues in treated and non-treated patients. There was no significant difference between in the apoptotic index between the tamsulosin and alfuzosin group (p=0.41). No significant differences were found between tamsulosin and the control group (p=0.27) and alfuzosin and the control group (p=0.17).

5.5. Morphometric measurements in RRP tissues

The methodology for morphometric analysis of RRP tissues is identical to that of the TURP group. In the RRP group, no mechanical measurements are available due to the retrospective nature of these cases. The selection of cases was from archival material.

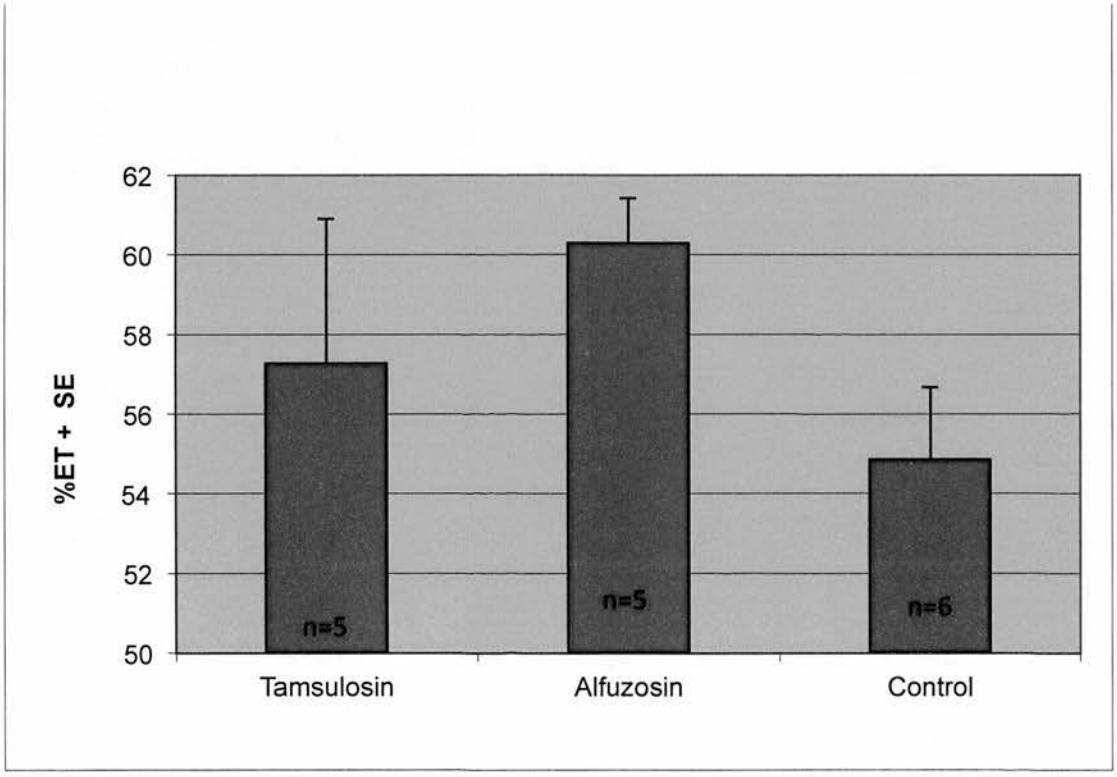

Figure 5.9 - %ET in RRP patients treated with tamsulosin, alfuzosin and control

Figure 5.9 demonstrates the mean epithelial content within treated and non-treated RRP patients. There was no significant difference in %ET between the tamsulosin

and alfuzosin group (p=0.21). No significant differences were found between tamsulosin and the control group (p=0.30) and alfuzosin and the control group (p=0.06).

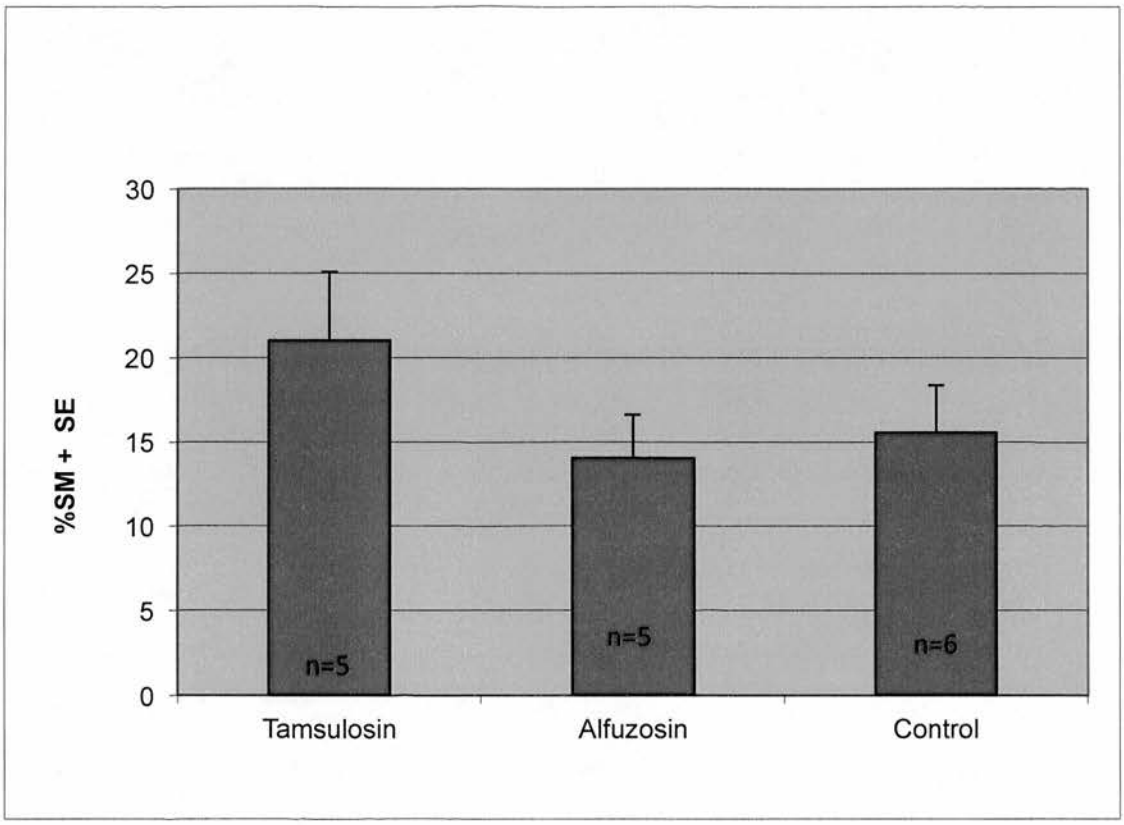

Figure 5.10 - %SM in RRP patients treated with tamsulosin, alfuzosin and control

Figure 5.10 demonstrates the mean %SM content in treated and non-treated RRP patients. There are no significant differences between the groups. The morphometric studies examining the %SM and %ET within RRP tissues do not show any significant difference between the treated groups and the control groups. There

was no significant difference in %SM between the tamsulosin and alfuzosin group (p=0.09). No significant differences were found between tamsulosin and the control group (p=0.13) and alfuzosin and the control group (p=0.35).

5.6. Discussion

The aim of this study is to examine the inter-relationship between apoptotic effects of alpha blocker therapy with the mechanical and morphological characteristics of the BPH tissue.

Two groups of patients were used to assess the relationship between alpha blocker therapy and its effect upon tissue composition and the rate of apoptotic events. The TURP group had come to surgery as medical therapy had failed whereas the RRP group had surgery for prostate cancer, but were responding to medical therapy at the time of their surgery. Patients in the TURP group were collected prospectively and underwent mechanical measurements prior to processing of the tissue. The RRP group lack mechanical measurements as these patients were selected retrospectively based upon their medical treatment.

TURP tissues

In section 5.2, the results show that within the TURP group, medical treatment with alfuzosin is associated with a significant increase in apoptotic activity within the tissues as assessed using both Caspase-3 assay and the TUNEL assay. In section

5.3.1, the morphometric analysis demonstrate that there is a significant reduction in %SM in the patients treated with alfuzosin. However, there were no significant differences seen in %ET between the groups. Within section 5.3.2, the mechanical measurements from the prostate tissue show that there was a significant reduction in |E*|, tissue elasticity, in patients treated with alfuzosin. There were no differences seen in tan δ, tissue viscosity, between the groups.

These sets of experiments confirm that in patients treated with alfuzosin, there is an increase in apoptotic activity which is associated with a reduction in smooth muscle composition of the tissue. The reduction in %SM is reflected in the mechanical measurements and a lower |E*| value is seen in the alfuzosin group.

Several studies have confirmed the pro-apoptotic effects of quinazoline-based alpha blockers, Doxazosin and Terazosin, in BPH tissues [87, 88, 141]. These studies show that an increase in apoptotic activity is associated with smooth muscle regression. However to date, there are no studies examining the pro-apoptotic effects of alfuzosin, a quinazoline-based alpha blocker. The work presented here supports the observation that alfuzosin appears to have similar pro-apoptotic effects as other quinazoline-based alpha blockers. The increase in apoptotic activity is seen primarily in the stroma and is associated with smooth muscle regression. This is in accordance with the findings from studies examining the agents, doxazosin and terazosin [43, 141]. Phipps *et al* have shown that the mechanical properties of TURP tissue are a function of smooth muscle content when measurements are made using a macro-probe [127]. The mechanical measurements (which were made using a

macro-probe indenter) presented in section 5.3.2 demonstrate the strong association with %SM and |E*|. Therefore, treatment with alfuzosin is shown to have a significant impact upon the mechanical properties of prostate tissue.

Despite a significant increase in apoptotic indices in patients treated with alfuzosin, no significant differences in %ET were observed in treated and non-treated prostates. In the TURP group, the mean %ET in all groups was 16% and the mean %SM was 35%. The TURP tissues were comprised mainly of smooth muscle. The remaining 50% comprise of the other constituents of the stroma such as fibroblasts, collagen and ground substance. Based upon previous work from this group, the epithelial and smooth muscle components of prostate tissue were found to be the most important determinants of the mechanical properties of the tissue. Therefore the remaining cellular constituents were not quantified in any manner.

Morphometric studies demonstrate that the %ET in patients (see figure 5.4) treated with alfuzosin is not significantly different to the tamsulosin and control group. Subsequently, there are no observed differences in tan δ, within all groups. This may be explained by the observation that apoptotic activity is much lower in the epithelial compartment. It was observed in the initial studies with doxazosin, that apoptotic activity within the glandular epithelium peaked at 4-5 months of treatment and returned to baseline after 11-13 months [87]. Subsequent studies have shown that apoptotic activity is reduced within the glandular epithelial compartment [141].

RRP tissues

Patients treated with alpha blocker therapy with low grade and low volume prostate cancers were identified from the local prostate cancer database. These patients had undergone RRP and the archival prostate tissue from this cohort provided a comparison group to the TURP group. Tissue blocks were taken from the base of the prostate to ensure adequate representation of the transitional zone of the prostate. From the microscopic and macroscopic histopathology report, blocks with known prostate cancer were avoided. The aim of using RRP tissue was two-fold. One was to increase our study numbers as the TURP cohort had only 4 patients treated with alfuzosin. Secondly, it was to assess whether there were differences in apoptotic indices in patients who have responded to or failed medical therapy.

The results from the apoptotic experiments shown in figures 5.7 and 5.8, demonstrate no significant difference in the apoptotic indices of treated and non-treated prostates. The apoptotic indices in all groups within the RRP cohort are comparable to the baseline apoptotic index of the control group in the TURP patients. The morphometric studies do not demonstrate significant differences in %ET and %SM composition between all groups as shown in figures 5.9 and 5.10.

The low apoptotic activity that is shown across all 3 groups may be explained by the differences in tissue composition. The mean %ET in the RRP cohort is 57% compared with 16% in the TURP group and the mean %SM is 17% in the RRP group compared with 37% in the TURP group. The histological composition of most

areas studied in the RRP group comprise mainly of glandular epithelium consisting of large acini separated by stroma containing tightly packed smooth muscle fibres. These sections were taken from the base of the prostate, close to the bladder neck, to ensure that the transitional zone was studied. However, despite this, the tissue architecture was significantly different to the morphology of tissue from TURP. This may be a reflection of prostate size, as proportions of ET and SM within specimens vary significantly depending upon the resected weight at TURP (which is a surrogate for prostate size) [33]. However, there is no data on the size of the prostates that underwent TURP. Histological reports for the RRP group confirm that the prostates weighed greater than 30g and this may explain the greater composition of ET in the RRP group.

The low rate of apoptosis within both smooth muscle and epithelial compartments may be explained by different cellular kinetics, i.e. the rate of cell death versus proliferation, exhibited by the RRP group. The morphology of tissue obtained from the RRP group show low smooth muscle content (mean %SM is 17%) and high epithelial content (mean %ET is 57%) as shown in figures 5.9 and 5.10. Several studies have observed increased expression of the anti-apoptotic factor bcl-2 in BPH epithelial cells. *Bcl-2* is a proto-oncogene that plays a role in blocking programmed cell death [142]. These studies observed a significant increase in *bcl-2* expression in basal epithelial and secretory cells but not stromal cells in BPH tissues [28, 143-145]. The increase in *bcl-2* expression may result in a reduction in apoptosis within epithelial cells and thereby maintain the cell population despite the pro-apoptotic effects of alfuzosin. A further cellular mechanism that may explain low apoptotic

activity is cellular senescence. Senescence describes the process by which somatic cells lose their ability to proliferate or to undergo apoptosis. The senescent cell remains metabolically active but in a growth arrested state. Studies have shown that larger prostates exhibit increased biomarkers of senescence and that these biomarkers were only expressed in the epithelial cells [146, 147]. Therefore, understanding the cell kinetics of this group may explain the observation of low apoptotic activity seen in mainly epithelial tissue.

Summary

Despite the small sample size of this study, the findings suggest that alfuzosin shares the same class effect of pro-apoptotic activity as doxazosin and terazosin. The results clearly show that treatment with alfuzosin is associated with an increase in apoptotic activity in BPH tissues. The increase in apoptotic activity is associated with a significant reduction in smooth muscle. The mechanical properties are a function of the underlying morphology and the work presented here show that alfuzosin therapy can have a significant impact upon the mechanical measurements. These measurements taken *in vivo*, may have great potential in aiding the urologist in the assessment and management of patients with prostatic disease.

These experiments are the first evidence that alfuzosin shares the class effect of other quinazoline-based agents. Over the last few years, the focus has been on elucidating the exact molecular mechanisms that underpin the pro-apoptotic properties of these agents. Much interest has been placed upon their potential role in the treatment of

prostate cancer [148, 149]. The work presented here is the first step in understanding the pro-apoptotic effects of alfuzosin. Understanding the apoptotic activity in the prostate tells only half the story. Further work is required in characterising the cellular kinetics with respect to proliferation markers such as bcl-2, TGF-1β, ki-67 to name a few will allow for a more complete picture of the dynamics within the tissue. Biomarkers of senescence should be examined, especially in samples composed mainly of epithelial tissue, to understand why there are such low levels of apoptosis in certain tissue compartments.

Chapter Six

General discussion and Conclusions

6.1. Development of the viscoelastic model of the prostate

This thesis builds upon the previous studies in the characterisation of the structure-property relationship of prostate tissue. The mechanical properties of prostate tissue from TURP have been shown to be a function of the underlying morphology [127, 128]. The structure-property relationship of TURP chippings follow a viscoelastic model with the smooth muscle component acting as springs (|E*| or amplitude ratio) and the epithelial component acting as dampers (tan δ or phase lag).

The main body of this work examines the morphological and mechanical properties of prostate tissue from radical cystoprostatectomy patients. TURP chippings mainly originate from the transitional zone of the prostate or from around the bladder neck. The use of transverse slices of whole prostates allow for the examination of the morphology of the whole prostate rather than restricting morphological analysis to a single zone of the prostate. The understanding of the morphological and mechanical characteristics of different areas within the whole prostate will further our knowledge of the structure-property relationship of prostatic tissue in respect of the whole gland.

Morphometric analysis

Protocols for the morphometric analysis of TURP chippings yielded on average 60-100 individual images per TURP chipping for computerised analysis. In the morphometric analysis of a section of a whole prostate, the processed and embedded specimen was required to be divided into four sections so that it can be mounted on

standard 25 × 75 mm glass slides as described in section 2.4. Subsequent application of these protocols to the analysis of whole prostates resulted in 3600 – 4000 images per section of a whole prostate at ×200 magnification. Composite images were reconstructed using image stitching software to create a "histological map" of the section. Discrete histological areas such as nodules comprising mainly of epithelial or stromal tissue were identified on the "histological map". Price *et al*, described these areas in a quantitative manner in their work with prostate tissue from both TURP and enucleations [32]. The work presented in section 2.1 show that there are significant histological differences in %ET and %SM between nodular and stromal areas. Nodular areas are comprised mainly of epithelial tissue whereas in stromal areas, smooth muscle is the main constituent (see section 2.6.4). Also in accordance to the work by Price *et al*, there are significant differences between the histological information from TURP chippings and from a transverse section of a whole prostate. This is most apparent in the data presented in Chapter 5. In section 5.3.1 the morphometric results from TURP tissues differ significantly from that of RRP tissues shown in section 5.5.

The volume of information generated from the morphometric analysis of a section of a whole prostate is 40-fold greater than from a single TURP chipping. The work with the whole prostates required modification of the original protocol used in the analysis of TURP chippings. Using a motorised stage and specialist scanning and stitching software, as detailed in Section 2.2, a mosaic or "map" of a section of prostate is captured at low magnification. The user can then pinpoint areas of

interest, such as areas subjected to mechanical testing, and capture histological information at high magnification. Marking of the area using ink and a pin embedded into the tissue allowed the area subjected to mechanical testing to be localised. This methodology enabled the study of loco-regional morphology and its associated mechanical properties. Recent studies by Ahn *et al* examined the mechanical properties of malignant prostate tissue from RRP patients [150, 151]. The methodology employed in the analysis of histology and the associated mechanical measurement was acknowledged to be flawed as a result of uncertainty in the localisation of the area subjected to mechanical testing. The authors arbitrarily divided the prostate into zones and subjected these areas of mechanical testing without employing any means to accurately mark the areas tested. However, in comparison, the methodology presented in this work enables a more accurate localisation of the area of tissue subjected to mechanical testing and provides a means to perform loco-regional morphometric analysis upon these areas.

Macro-point probing

Initial studies examining the relationship between the loco-regional morphology and the underlying mechanical properties used a macro sized 2mm diameter ball end probe for the mechanical testing. The loco-regional morphology was classified into nodular or stromal areas without prior knowledge of the associated mechanical measurements. The results presented in Section 3.2 show that the amplitude ratio, $|E^*|$, is significantly higher (>150 kPa) in the nodular group compared with the

stromal group. The phase lag, tan δ, was found to be significantly lower in the nodular group compared with the stromal group. That is, nodules are "stiffer" and less "viscous" than stromal areas respectively.

Despite these strong observations between these two morphologically distinct groups, individual correlations between morphological and mechanical parameters were found to be weak, as shown in sections 3.3 to 3.4. Initial statistical analysis utilised linear regression analysis which yielded weak correlations. Multiple linear regression analysis was employed to assess the impact of mean acinar area upon the relationships between the morphological and mechanical variables but these relationships did not follow a simple regression model. However, the correlations are strengthened when mean acinar area is considered in the multivariate analysis which suggests that taken individually, %SM and %ET values seem to be poor discriminators between stromal and nodular areas. However, the majority of the areas tested comprised of mixed epithelial and smooth muscle content of varying proportions. In figure 3.3, a histogram depicts the distribution of points according to the epithelial to smooth muscle ratio. The majority of nodular areas were comprised of tissue containing a higher epithelial to smooth muscle ratio. However, when the data was stratified according to epithelial and smooth muscle ratio, the relationships were still weak. Artificial neural networks are able to recognise complex relationships which a regression analysis may not be able to identify.

Artificial neural networks require a training stage and validation stage to be performed before the final analysis stage. This is explained in section 2.9.5. Within

each stage, a proportion of the dataset is used to set up the system before the final analysis and so, as the program progresses through the stages, the pool of data points is reduced. In figure 3.7, within the nodular group, the correlation between the single variables of |E*| and %ET shows a strong positive relationship (R=0.62). The next figure, 3.8, shows a similar strong positive relationship between tan δ and %ET (R=0.74). If both morphometric (%ET and %SM) and mechanical (|E*| and tan δ) datasets are used in the analysis, the relationship between these variables are further strengthened (R=0.85).

The disadvantage of ANN is that it does not show the analysis pathway used to reach its conclusion and therefore the system is unable to explain which parameters are the most influential in its analysis. However, despite this, the statistical analyses suggest that the viscoelastic model for the whole prostate does not follow a linear relationship between the ET and SM components with its corresponding mechanical measurement. Previous work on TURP chippings assumed the morphology of prostatic tissue to be homogenous and isotropic [138]. This work undoubtedly demonstrates that the structure-property of TURP chippings does not apply to the prostate when taken as a whole. Examination of a composite image of section of a whole prostate as shown in figure 2.3 clearly demonstrates the heterogeneous nature of the morphology. The histological parameters of %ET and %SM are unable to fully represent the inherent complexity of the morphology when examining the whole gland. Inspection of the simple linear correlation graphs between %ET and %SM within nodular and stromal groups (see figures 3.1 and 3.2) show that there is a significant amount of prostatic tissue unaccounted for. Within the stromal

environment, it has been shown that collagen and fibroblasts can comprise up to 30-35% of this compartment [33] and with advances in immunohistochemical techniques, localisation of fibroblasts has recently become feasible [140]. Within the glandular compartment, the basal cell layer is not stained. The epithelial cells are stained with anti-PSA antibody whereas the basal cell layer can be localised with stains for high molecular weight cytokeratins or p63 [152]. With these new developments, it may be that once the morphology of the prostate can be characterised fully, strong relationships between the mechanical properties can be found.

Micro-point probing

In chapter 4, the mechanical studies were performed using a micro-sized probe measuring 400μm × 500μm. The area of prostate tissue subjected to point probing by the macro probe is 9.86mm^2 compared with 0.2mm^2 of the micro probe. The aim of this work is to understand the effect of using a micro-indenter upon the mechanical measurements obtained and to relate this to the underlying prostate morphology. The rationale for micro testing resulted from a parallel project with a micro-engineering facility to develop a micro-engineered palpation device for measuring mechanical properties of biological tissues. The reduction in size of the indenter allows for the study of mechanical properties at a scale that approaches microscopic feature size.

The methodology used in the analysis of loco-regional morphology in the studies presented in Chapter 3 is again used for the micro-point probing studies. The

histological areas of interest were classified into stromal and nodular areas. Significant differences were observed with the nodular areas containing a greater amount of epithelial tissue compared with stromal areas, as shown in Table 4.1. Within the nodular group, as the %ET increased within the nodule, the greater the mean acinar area of the glands. The mechanical properties of nodular areas were significantly different compared with stromal areas. The mean |E*| was found to be significantly greater in the nodular group ($p=0.03$) but there was no significant difference in tan δ between the groups ($p=0.31$).

Simple linear regression analysis was used initially to examine the relationships between morphology and mechanical properties. Within the nodular group, as shown in figure 4.7, the relationship between the mean acinar area and tan δ was the strongest ($R^2=0.2$ $p<0.005$). As mean acinar size of the glands increased, this was paralleled with an increase in "viscosity" (tan δ). This correlation suggests that tan δ is sensitive to gland size as measured using a micro-probe indenter. However, there were weak linear correlations between %SM, %ET and ET:SM ratio with the mechanical measurements. Multiple linear regression analysis was used to examine the various parameters and their effect upon the mechanical properties. Furthermore, the data was stratified based upon the %SM and %ET content. However, the correlations between the remaining parameters with the mechanical properties were weak.

Artificial neural networks were used to analyse the data from both the nodular and stromal groups. There were no significant results from the analysis of the stromal

group data. In figures 4.13 and 4.14, the ANN analysis of the relationship between |E*| and the individual parameters of %ET and %SM yielded weak results. In figures 4.15 and 4.16, the analysis of the relationship between tan δ and the individual parameters of %ET and %SM show that there is a strong positive correlation between %ET (R^2=0.625) but not between %SM (R^2=0.226). The mean results of both morphometric and mechanical data points were assessed together and a strong positive relationship was seen (R^2=0.697). It appears that tan δ is a more sensitive discriminator between stromal and nodular areas than |E*|.

The lack of correlation seen between the individual parameters of |E*| and %ET and %SM; tan δ and %SM demonstrate the difficulties in the comparison of loco-regional morphology with the mechanical data generated from the use of micro-sized indenter. The primary area of difficulty was to accurately pinpoint the area subjected to mechanical testing. The area covered by the indenter is 0.2mm^2 and modification of the protocol described in 2.7 was explored. At the micro-level of histological analysis, moving just 500 μm away from the "origin" of the site of point probing may yield a result at the extreme ends of the scale. Use of a smaller matrix of captured images, such as 3 x 3 or even individual high powered frames, has the advantage of being closer in size to the actual area under the indenter. However with a smaller matrix size, there was increased uncertainty that the area selected was truly representative of the area tested. Initial attempts to represent the histological data as a set of individual variables corresponding to different matrix sizes (e.g. 3 x 3 matrix would yield 9 individual measurements) did not yield strong relationships with the mechanical parameters using linear regression analysis. Therefore a mean value of

the histological data from a matrix of 7 x 7 high powered fields per point probed was used to describe a single point. The weak correlations from the linear, multivariate and ANN analyses may be a reflection of the inaccurate localisation of morphological area subjected to micro-point probing. A possible future solution would be to use a laser fixed to the testing rig to mark a point adjacent to the tissue tested ensuring that the resulting damage to the surface of the tissue will not interfere with subsequent histological analysis. Lasers can penetrate to less than 1mm of the tissue surface. The tissue marking will not be lost through the fixation and embedding of the tissue.

The work presented here considers the prostate as a heterogonous organ, based upon the studies by McNeal [9]. It cannot be accepted that prostate tissue examined in this fashion is homogenous and isotropic. Instead, the results clearly demonstrate the heterogeneity and anisotropy of whole sections of prostate tissue. Both the macro-point and micro-point probing data show a significantly higher |E*| readings compared to Phipps's work [127]. These areas of increased |E*| are associated with large glandular nodules as illustrated in figure 4.23. One may postulate that these glands are under tension due to the constricting tension of the surrounding stroma. These studies may indicate that nodules may contribute not only to the static element of obstruction but also to the dynamic element. Recent *in vivo* studies have shown that intracellular tissue pressure has a positive effect upon shear modulus as measured using MR elastography [153]. In addition to further characterising the morphology of the prostate, the measurement of interstitial tissue pressure may provide further insight into the structure-property relationships of the prostate.

Summary

The macro and micro-probing data presented here demonstrate that there are measureable and quantifiable differences between the two methods of mechanical testing. In the macro-point probing experiments, there were significant relationships seen between the morphological parameters of SM and ET with the mechanical parameters of |E*| and tan δ. However, these relationships were difficult to elucidate, requiring the non linear analysis expertise of an ANN. This perhaps is a reflection of the lack of histological description obtained from just two variables, ET and SM.

In the micro-point probing experiments, strong relationships between the morphological and mechanical parameters were significantly more difficult to elucidate. In addition to the problems encountered in the macro-probing experiments, it was found to be very difficult to accurately pin point the area of tissue that was subjected to mechanical testing. This factor may have added an additional confounding element to the data analysis and is reflected in the weak correlations seen in the ANN analysis.

These findings have implications for the consideration of a suitable sized remote palpation device to conduct mechanical measurements *in vivo*. A micro sized probe may be an ideal tool for the urologist to deploy within a cystoscope to obtain mechanical measurements from the prostate. However, the average |E*| values in micro-probing is 25,000 kPa compared with 220 kPa in the macro-probing

experiments. This significant and exponential rise in |E*| values may preclude the use of a micro-piston to assess tissue mechanics as the sensitivity in detecting nodules and stromal areas is decreased [154]. These findings will have a significant impact upon the design and manufacture of a remote device capable of measuring these high pressures. Based upon these findings, the recommendation would be to utilise and develop the macro-point probing device for the measurement of mechanical properties in prostate tissue.

6.2. Alpha blocker therapy and morphology and mechanical measurements of the prostate

Since the early work by Kyprianou, the current focus of research is to elucidate the mechanisms by which quinazoline-based alpha blockers exert their pro-apoptotic effects and recent reports show promising results [92, 155, 156]. To date, there are no reports in the literature examining the potential class effect of pro-apoptotic activity of alfuzosin, a quinazoline-based alpha blocker.

TURP tissues

The apoptotic indices were measured using a TUNEL assay and a Caspase-3 assay in patients who have undergone a TURP. The treatment group was compared with a control group and a group taking tamsulosin, a non-quinazoline based alpha blocker. The results shown in figure 5.1 and 5.2 show a significant induction in apoptotic activity in the alfuzosin group compared to the control and tamsulosin groups. There was no significant difference between the tamsulosin and control groups. These results confirm that alfuzosin share this class-related effect of apoptotic induction in prostatic tissue.

Morphometric analysis, to determine the proportion of SM and ET, was performed on all three groups. In figure 5.3, there is a significant reduction in smooth muscle content in the alfuzosin group compared with the control and tamsulosin groups. There was no significant difference in %ET between all three groups. The mechanical properties, $|E^*|$ and tan δ were assessed for all specimens. Figure 5.5 demonstrate that $|E^*|$ is significantly reduced in the alfuzosin group compared with the control and tamsulosin groups. There is no significant difference in tan δ seen

between the groups. This may be explained by the observation that apoptotic activity is reduced within the glandular epithelial compartment [141].

The results presented here confirm that in patients treated with alfuzosin, there is an increase in apoptotic activity which is associated with a reduction in smooth muscle composition of the tissue. The reduction in %SM causes a significant and measureable change in the mechanical properties of the tissue. This is reflected in a lower |E*| value seen within in the alfuzosin group. These results represent the first evidence of the pro-apoptotic ability of alfuzosin. Early studies examining the quinazoline based agents, doxazosin and terazosin, show that these agents exhibit pro-apoptotic qualities which is associated with smooth muscle regression [87, 88]. This data from this study are in accordance with this early work, and confirm that alfuzosin shares this class-related effect of apoptotic induction in prostatic tissue.

RRP tissues

Patients treated with alpha blocker therapy who subsequently underwent RRP for localised prostate cancer were retrospectively identified. The aim of using RRP tissue was two-fold. One was to increase our study numbers as the TURP cohort had only 4 patients treated with alfuzosin. Secondly, it was to assess whether there were differences in apoptotic indices in patients who have responded to or failed medical therapy.

The experimental methodology to assess apoptotic activity and morphometric analysis in RRP tissue is similar to that used in TURP tissues. No mechanical measurements were available as these patients were retrospectively identified. The results from the apoptotic experiments shown in figures 5.7 and 5.8, demonstrate no significant difference in the apoptotic indices of treated and non-treated prostates. The low rate of apoptosis within both smooth muscle and epithelial compartments may be explained by different cellular kinetics, i.e. the rate of cell death versus proliferation, exhibited by the RRP group. The mean %ET in the RRP cohort is 57% compared with 16% in the TURP cohort. The mean %SM is 17% in the RRP group compared with 37% in the TURP group. The tissue composition between the two groups is significantly different and may explain the difference in response to alfuzosin. Studies have shown that epithelial and secretory cells exhibit an increase in expression of the anti-apoptotic factor bcl-2. This is an important proto-oncogene that has a role in blocking apoptosis [10, 28, 143, 144]. Therefore, it would be important not only to study the apoptotic activity within the tissue but to quantify the anti-apoptotic activity.

The tissue was selected under the guidance of a uro-pathologist to mirror as close as possible to the tissue that would be resected at TURP. However, the tissues used in the RRP cohort are composed mainly of glandular tissue and therefore, most likely, represent larger prostates than the TURP group. In future work, if RRP tissues are to be utilised in studies with TURP tissues, prostate size and weight must similar as proportions of ET and SM within specimens will vary significantly [33]

Summary

The work presented here comprises the initial step in the understanding of the pro-apoptotic effects of alfuzosin in BPH tissues. In future work, measurements of the apoptotic activity should be performed in tandem with measurements of cell proliferation to fully understand the cellular dynamics within the tissue studied. This then may offer an explanation as to the observed low rate of apoptotic activity within the RRP cohort. Further studies are required to elucidate the mechanisms involved in the pro-apoptotic effects of alfuzosin. Based upon the initial studies presented here, alfuzosin is an agent that researchers should examine more closely, as it may have a possible role in other novel areas such as cancer treatment [148].

6.3. Future work

The results from this work have highlighted several areas for improvement and further research. Further work and refinement of the techniques used for morphometric analysis is required. With the advent of laser micro-dissection of tissues, similar techniques may be used to increase the accuracy in localisation of areas of interest within the tissue, whether the tissue is a prostatic chipping from TURP or a whole mount prostate from open surgery. Improvements in the sophistication and automation of morphometric analysis systems may decrease user workload and improve accuracy.

Improvements in the antibodies available for immunohistochemical analysis of the glandular and stromal components of prostate tissue will enable a richer and more complete description of prostate morphology than is otherwise available using just anti-PSA and anti-smooth muscle myosin. This work has suggested that other components of the prostate stromal matrix may well be important in further understanding the morphological make-up of the prostate.

This work is only just beginning to understand the complex relationships between structures such as glandular nodules and their mechanical properties. The studies demonstrate that nodules are stiffer than surrounding stromal areas. The studies are really two-dimensional in nature and to fully understand the role these nodules play in the dynamics of bladder outflow obstruction, an appreciation and understanding of its three-dimensional structure is required. Parker *et al* have utilised

sonoelastography to examine the viscoelastic properties of prostate tissue. Recent work from this unit have combined the quasi-static measurements obtained from sonographical Doppler images with quantitative stress relaxation measurements to characterise prostate tissue [126, 157]. The value of elastography is that the 3-D image of the whole prostate that is available and combining modalities, the structural make-up of the prostate may be elucidated.

This work presented here is the first evidence that alfuzosin exhibits pro-apoptotic activity within prostate tissue. Continued work in the scientific community in understanding the pathways in which these quinazoline-based alpha blockers act, may provide novel therapies in the treatment of prostate diseases. Further work in this area would be to study the cellular kinetics of patients treated with alfuzosin to fully understand its effect upon prostate tissue. Archival material could be utilised in this future work with careful selection.

The framework and ultimate aim of this research is to develop a tactile remote palpation device that can be passed via the urethra to obtain mechanical measurements within the prostatic urethra. In order to replicate the testing conditions *in vivo*, the apparatus used to measure mechanical properties should be modified so that it can be deployed within a prostate. Work is continuing with mechanical engineers within this project to fabricate a device suitable to be used within the urethra or passed through a cystoscope. In the development of this device, various techniques of sensing pressure e.g. using hydraulic actuation or piezoelectric actuation, remains to be fabricated and tested. Once these tools are available, further

dynamic mechanical testing within a whole prostate will examine the relationships between regional morphology and local mechanical measurements and thereby expanding our knowledge of the structure-property relationship of this heterogeneous organ. Understanding these relationships may be useful in the further diagnosis and management and treatment of prostate diseases.

References

1. Thomson, A.A., *Mesenchymal mechanisms in prostate organogenesis.* Differentiation, 2008. **76**(6): p. 587-98.
2. Cunha, G.R., *Role of mesenchymal-epithelial interactions in normal and abnormal development of the mammary gland and prostate.* Cancer, 1994. **74**(3 Suppl): p. 1030-44.
3. Cunha, G.R., M. Sekkingstad, and B.A. Meloy, *Heterospecific induction of prostatic development in tissue recombinants prepared with mouse, rat, rabbit and human tissues.* Differentiation, 1983. **24**(2): p. 174-80.
4. Stewart, D.A., C.R. Cooper, and R.A. Sikes, *Changes in extracellular matrix (ECM) and ECM-associated proteins in the metastatic progression of prostate cancer.* Reprod Biol Endocrinol, 2004. **2**: p. 2.
5. Thomson, A.A., *Role of androgens and fibroblast growth factors in prostatic development.* Reproduction, 2001. **121**(2): p. 187-95.
6. Leong, K.G. and W.Q. Gao, *The Notch pathway in prostate development and cancer.* Differentiation, 2008. **76**(6): p. 699-716.
7. Matusik, R.J., et al., *Prostate epithelial cell fate.* Differentiation, 2008. **76**(6): p. 682-98.
8. McNeal, J.E., *The zonal anatomy of the prostate.* Prostate, 1981. **2**(1): p. 35-49.
9. McNeal, J., *Pathology of benign prostatic hyperplasia. Insight into etiology.* Urol Clin North Am, 1990. **17**(3): p. 477-86.
10. Kyprianou, N., H. Tu, and S.C. Jacobs, *Apoptotic versus proliferative activities in human benign prostatic hyperplasia.* Hum Pathol, 1996. **27**(7): p. 668-75.
11. Walsh, P.C. and J.D. Wilson, *The induction of prostatic hypertrophy in the dog with androstanediol.* J Clin Invest, 1976. **57**(4): p. 1093-7.
12. de Voogt, H.J., et al., *Androgen action blockade does not result in reduction in size but changes histology of the normal human prostate.* Prostate, 1987. **11**(4): p. 305-11.
13. Harkonen, P.L. and S.I. Makela, *Role of estrogens in development of prostate cancer.* J Steroid Biochem Mol Biol, 2004. **92**(4): p. 297-305.
14. Mobbs, B.G., I.E. Johnson, and Y. Liu, *Quantitation of cytosolic and nuclear estrogen and progesterone receptor in benign, untreated, and treated malignant human prostatic tissue by radioligand binding and enzyme-immunoassays.* Prostate, 1990. **16**(3): p. 235-44.
15. Nicholson, T.M. and W.A. Ricke, *Androgens and estrogens in benign prostatic hyperplasia: past, present and future.* Differentiation, 2011. **82**(4-5): p. 184-99.
16. Getzenberg, R.H., K.J. Pienta, and D.S. Coffey, *The tissue matrix: cell dynamics and hormone action.* Endocr Rev, 1990. **11**(3): p. 399-417.
17. Lee, K.L. and D.M. Peehl, *Molecular and cellular pathogenesis of benign prostatic hyperplasia.* J Urol, 2004. **172**(5 Pt 1): p. 1784-91.

18. Ezzat, S. and S.L. Asa, *FGF receptor signaling at the crossroads of endocrine homeostasis and tumorigenesis.* Horm Metab Res, 2005. **37**(6): p. 355-60.
19. Schwertfeger, K.L., *Fibroblast growth factors in development and cancer: insights from the mammary and prostate glands.* Curr Drug Targets, 2009. **10**(7): p. 632-44.
20. Cunha, G.R., et al., *Hormonal, cellular, and molecular regulation of normal and neoplastic prostatic development.* J Steroid Biochem Mol Biol, 2004. **92**(4): p. 221-36.
21. Sherwood, E.R. and C. Lee, *Epidermal growth factor-related peptides and the epidermal growth factor receptor in normal and malignant prostate.* World J Urol, 1995. **13**(5): p. 290-6.
22. Mori, H., et al., *Increased expression of genes for basic fibroblast growth factor and transforming growth factor type beta 2 in human benign prostatic hyperplasia.* Prostate, 1990. **16**(1): p. 71-80.
23. Peehl, D.M., P. Cohen, and R.G. Rosenfeld, *The insulin-like growth factor system in the prostate.* World J Urol, 1995. **13**(5): p. 306-11.
24. Gleason, P.E., et al., *Platelet derived growth factor (PDGF), androgens and inflammation: possible etiologic factors in the development of prostatic hyperplasia.* J Urol, 1993. **149**(6): p. 1586-92.
25. McNeal, J.E., *Origin and evolution of benign prostatic enlargement.* Invest Urol, 1978. **15**(4): p. 340-5.
26. Isaacs, J.T., *Prostate stem cells and benign prostatic hyperplasia.* Prostate, 2008. **68**(9): p. 1025-34.
27. Isaacs J, C.D., *Etiology and disease process of benign prostatic hyperplasia.* Prostate, 1987. **Suppl 2**: p. 33–50.
28. Colombel, M., et al., *Zonal variation of apoptosis and proliferation in the normal prostate and in benign prostatic hyperplasia.* Br J Urol, 1998. **82**(3): p. 380-5.
29. Isaacs, J.T., *Antagonistic effect of androgen on prostatic cell death.* Prostate, 1984. **5**(5): p. 545-57.
30. Franks, L.M., *Benign nodular hyperplasia of the prostate: A review.* Ann R Coll Surg Engl, 1954. **14**: p. 92-106.
31. Arenas, M.I., et al., *Morphometric evaluation of the human prostate.* Int J Androl, 2001. **24**(1): p. 37-47.
32. Price, H., J.E. McNeal, and T.A. Stamey, *Evolving patterns of tissue composition in benign prostatic hyperplasia as a function of specimen size.* Hum Pathol, 1990. **21**(6): p. 578-85.
33. Schuster, G.A. and T.G. Schuster, *The relative amount of epithelium, muscle, connective tissue and lumen in prostatic hyperplasia as a function of the mass of tissue resected.* J Urol, 1999. **161**(4): p. 1168-73.
34. Ishigooka, M., et al., *Relative and total volume of histological components in benign prostatic hyperplasia: relationships between histological components and clinical findings.* Prostate, 1996. **29**(2): p. 77-82.
35. Shapiro, E., et al., *The relative proportion of stromal and epithelial hyperplasia is related to the development of symptomatic benign prostate hyperplasia.* J Urol, 1992. **147**(5): p. 1293-7.

36. Chagas, M.A., et al., *Stromal and acinar components of the transition zone in normal and hyperplastic human prostate.* BJU Int, 2002. **89**(7): p. 699-702.
37. Isaacs, J.T. and D.S. Coffey, *Etiology and disease process of benign prostatic hyperplasia.* Prostate Suppl, 1989. **2**: p. 33-50.
38. Hakenberg, O.W., C.B. Pinnock, and V.R. Marshall, *Does evaluation with the International Prostate Symptom Score predict the outcome of transurethral resection of the prostate?* J Urol, 1997. **158**(1): p. 94-9.
39. Caine, M., A. Pfau, and S. Perlberg, *The use of alpha-adrenergic blockers in benign prostatic obstruction.* Br J Urol, 1976. **48**(4): p. 255-63.
40. Caine, M., S. Raz, and M. Zeigler, *Adrenergic and cholinergic receptors in the human prostate, prostatic capsule and bladder neck.* Br J Urol, 1975. **47**(2): p. 193-202.
41. Lepor, H., R. Tang, and E. Shapiro, *The alpha-adrenoceptor subtype mediating the tension of human prostatic smooth muscle.* Prostate, 1993. **22**(4): p. 301-7.
42. Shapiro, E., V. Hartanto, and H. Lepor, *The response to alpha blockade in benign prostatic hyperplasia is related to the percent area density of prostate smooth muscle.* Prostate, 1992. **21**(4): p. 297-307.
43. Kyprianou, N., *Doxazosin and terazosin suppress prostate growth by inducing apoptosis: clinical significance.* J Urol, 2003. **169**(4): p. 1520-5.
44. Berry, S.J., et al., *The development of human benign prostatic hyperplasia with age.* J Urol, 1984. **132**(3): p. 474-9.
45. Chapple, C.R., et al., *Lower urinary tract symptoms revisited: a broader clinical perspective.* Eur Urol, 2008. **54**(3): p. 563-9.
46. Jacobsen, S.J., et al., *Natural history of prostatism: longitudinal changes in voiding symptoms in community dwelling men.* J Urol, 1996. **155**(2): p. 595-600.
47. Garraway, W.M., G.N. Collins, and R.J. Lee, *High prevalence of benign prostatic hypertrophy in the community.* Lancet, 1991. **338**(8765): p. 469-71.
48. Jacobsen, S.J., C.J. Girman, and M.M. Lieber, *Natural history of benign prostatic hyperplasia.* Urology, 2001. **58**(6 Suppl 1): p. 5-16; discussion 16.
49. Roberts, R.O., et al., *Longitudinal changes in peak urinary flow rates in a community based cohort.* J Urol, 2000. **163**(1): p. 107-13.
50. Kaplan, S.A., et al., *Urinary retention and post-void residual urine in men: separating truth from tradition.* J Urol, 2008. **180**(1): p. 47-54.
51. Jacobsen, S.J., et al., *Natural history of prostatism: risk factors for acute urinary retention.* J Urol, 1997. **158**(2): p. 481-7.
52. McConnell, J.D., et al., *The effect of finasteride on the risk of acute urinary retention and the need for surgical treatment among men with benign prostatic hyperplasia. Finasteride Long-Term Efficacy and Safety Study Group.* N Engl J Med, 1998. **338**(9): p. 557-63.
53. McConnell, J.D., et al., *The long-term effect of doxazosin, finasteride, and combination therapy on the clinical progression of benign prostatic hyperplasia.* N Engl J Med, 2003. **349**(25): p. 2387-98.
54. Barry, M.J., et al., *Relationship of symptoms of prostatism to commonly used physiological and anatomical measures of the severity of benign prostatic hyperplasia.* J Urol, 1993. **150**(2 Pt 1): p. 351-8.

55. Yalla, S.V., et al., *Correlation of American Urological Association symptom index with obstructive and nonobstructive prostatism.* J Urol, 1995. **153**(3 Pt 1): p. 674-9; discussion 679-80.
56. Ezz el Din, K., et al., *The predictive value of microscopic haematuria in patients with lower urinary tract symptoms and benign prostatic hyperplasia.* Eur Urol, 1996. **30**(4): p. 409-13.
57. Barry, M.J., et al., *The American Urological Association symptom index for benign prostatic hyperplasia. The Measurement Committee of the American Urological Association.* J Urol, 1992. **148**(5): p. 1549-57; discussion 1564.
58. el Din, K.E., et al., *The correlation between bladder outlet obstruction and lower urinary tract symptoms as measured by the international prostate symptom score.* J Urol, 1996. **156**(3): p. 1020-5.
59. NICE. *The management of lower urinary tract symptoms in men.* NICE Clinical guideline 97 2010; Available from: http://guidance.nice.org.uk/CG97/Guidance.
60. Mebust, W.K., et al., *Transurethral prostatectomy: immediate and postoperative complications. A cooperative study of 13 participating institutions evaluating 3,885 patients.* J Urol, 1989. **141**(2): p. 243-7.
61. Roehrborn, C.G., et al., *Serum prostate-specific antigen as a predictor of prostate volume in men with benign prostatic hyperplasia.* Urology, 1999. **53**(3): p. 581-9.
62. Roehrborn, C.G., et al., *Serum prostate specific antigen is a strong predictor of future prostate growth in men with benign prostatic hyperplasia. PROSCAR long-term efficacy and safety study.* J Urol, 2000. **163**(1): p. 13-20.
63. Roehrborn, C.G., et al., *Serum prostate-specific antigen and prostate volume predict long-term changes in symptoms and flow rate: results of a four-year, randomized trial comparing finasteride versus placebo. PLESS Study Group.* Urology, 1999. **54**(4): p. 662-9.
64. Crawford, E.D., et al., *Baseline factors as predictors of clinical progression of benign prostatic hyperplasia in men treated with placebo.* J Urol, 2006. **175**(4): p. 1422-6; discussion 1426-7.
65. Gleason, D.M., et al., *Urinary flow velocity as an index of male voiding function.* J Urol, 1982. **128**(6): p. 1363-7.
66. Chancellor, M.B., et al., *Bladder outlet obstruction versus impaired detrusor contractility: the role of outflow.* J Urol, 1991. **145**(4): p. 810-2.
67. Bruskewitz, R.C., P. Iversen, and P.O. Madsen, *Value of postvoid residual urine determination in evaluation of prostatism.* Urology, 1982. **20**(6): p. 602-4.
68. Kranse, R. and R. van Mastrigt, *Weak correlation between bladder outlet obstruction and probability to void to completion.* Urology, 2003. **62**(4): p. 667-71.
69. Rosier, P.F., et al., *Variability of pressure-flow analysis parameters in repeated cystometry in patients with benign prostatic hyperplasia.* J Urol, 1995. **153**(5): p. 1520-5.

70. Yap, T.L., et al., *The impact of self-management of lower urinary tract symptoms on frequency-volume chart measures.* BJU Int, 2009. **104**(8): p. 1104-8.
71. Brown, C.T., et al., *Self management for men with lower urinary tract symptoms: randomised controlled trial.* BMJ, 2007. **334**(7583): p. 25.
72. Caine, M., *The present role of alpha-adrenergic blockers in the treatment of benign prostatic hypertrophy.* J Urol, 1986. **136**(1): p. 1-4.
73. Civantos Calzada, B. and A. Aleixandre de Artinano, *Alpha-adrenoceptor subtypes.* Pharmacol Res, 2001. **44**(3): p. 195-208.
74. Hieble, J.P., et al., *International Union of Pharmacology. X. Recommendation for nomenclature of alpha 1-adrenoceptors: consensus update.* Pharmacol Rev, 1995. **47**(2): p. 267-70.
75. Price, D.T., et al., *Identification, quantification, and localization of mRNA for three distinct alpha 1 adrenergic receptor subtypes in human prostate.* J Urol, 1993. **150**(2 Pt 1): p. 546-51.
76. Walden, P.D., et al., *Localization of mRNA and receptor binding sites for the alpha 1a-adrenoceptor subtype in the rat, monkey and human urinary bladder and prostate.* J Urol, 1997. **157**(3): p. 1032-8.
77. Kobayashi, S., et al., *Localization of endothelin receptors in the human prostate.* J Urol, 1994. **151**(3): p. 763-6.
78. Abrams, P.H., et al., *Bladder outflow obstruction treated with phenoxybenzamine.* Br J Urol, 1982. **54**(5): p. 527-30.
79. Caine, M., S. Perlberg, and A. Shapiro, *Phenoxybenzamine for benign prostatic obstruction. Review of 200 cases.* Urology, 1981. **17**(6): p. 542-6.
80. Akduman, B. and E.D. Crawford, *Terazosin, doxazosin, and prazosin: current clinical experience.* Urology, 2001. **58**(6 Suppl 1): p. 49-54.
81. Lefevre-Borg, F., et al., *Alfuzosin, a selective alpha 1-adrenoceptor antagonist in the lower urinary tract.* Br J Pharmacol, 1993. **109**(4): p. 1282-9.
82. Martin, D.J., et al., *Comparative alpha-1 adrenoceptor subtype selectivity and functional uroselectivity of alpha-1 adrenoceptor antagonists.* J Pharmacol Exp Ther, 1997. **282**(1): p. 228-35.
83. Michel, M.C., M.T. Flannery, and P. Narayan, *Worldwide experience with alfuzosin and tamsulosin.* Urology, 2001. **58**(4): p. 508-16.
84. Noble, A.J., et al., *The effects of tamsulosin, a high affinity antagonist at functional alpha 1A- and alpha 1D-adrenoceptor subtypes.* Br J Pharmacol, 1997. **120**(2): p. 231-8.
85. Lepor, H., *Phase III multicenter placebo-controlled study of tamsulosin in benign prostatic hyperplasia. Tamsulosin Investigator Group.* Urology, 1998. **51**(6): p. 892-900.
86. Djavan, B., et al., *State of the art on the efficacy and tolerability of alpha1-adrenoceptor antagonists in patients with lower urinary tract symptoms suggestive of benign prostatic hyperplasia.* Urology, 2004. **64**(6): p. 1081-8.
87. Kyprianou, N., et al., *Induction of prostate apoptosis by doxazosin in benign prostatic hyperplasia.* J Urol, 1998. **159**(6): p. 1810-5.

88. Chon, J.K., et al., *Alpha 1-adrenoceptor antagonists terazosin and doxazosin induce prostate apoptosis without affecting cell proliferation in patients with benign prostatic hyperplasia.* J Urol, 1999. **161**(6): p. 2002-8.
89. Kyprianou, N. and C.M. Benning, *Suppression of human prostate cancer cell growth by alpha1-adrenoceptor antagonists doxazosin and terazosin via induction of apoptosis.* Cancer Res, 2000. **60**(16): p. 4550-5.
90. Glassman, D.T., et al., *Combined effect of terazosin and finasteride on apoptosis, cell proliferation, and transforming growth factor-beta expression in benign prostatic hyperplasia.* Prostate, 2001. **46**(1): p. 45-51.
91. Partin, J.V., I.E. Anglin, and N. Kyprianou, *Quinazoline-based alpha 1-adrenoceptor antagonists induce prostate cancer cell apoptosis via TGF-beta signalling and I kappa B alpha induction.* Br J Cancer, 2003. **88**(10): p. 1615-21.
92. Keledjian, K., J.B. Garrison, and N. Kyprianou, *Doxazosin inhibits human vascular endothelial cell adhesion, migration, and invasion.* J Cell Biochem, 2005. **94**(2): p. 374-88.
93. Garrison, J.B., et al., *Novel quinazoline-based compounds impair prostate tumorigenesis by targeting tumor vascularity.* Cancer Res, 2007. **67**(23): p. 11344-52.
94. Andriole, G., et al., *Dihydrotestosterone and the prostate: the scientific rationale for 5alpha-reductase inhibitors in the treatment of benign prostatic hyperplasia.* J Urol, 2004. **172**(4 Pt 1): p. 1399-403.
95. Thigpen, A.E., et al., *Tissue distribution and ontogeny of steroid 5 alpha-reductase isozyme expression.* J Clin Invest, 1993. **92**(2): p. 903-10.
96. Boyle, P., A.L. Gould, and C.G. Roehrborn, *Prostate volume predicts outcome of treatment of benign prostatic hyperplasia with finasteride: meta-analysis of randomized clinical trials.* Urology, 1996. **48**(3): p. 398-405.
97. Andriole, G.L., et al., *Treatment with finasteride preserves usefulness of prostate-specific antigen in the detection of prostate cancer: results of a randomized, double-blind, placebo-controlled clinical trial. PLESS Study Group. Proscar Long-term Efficacy and Safety Study.* Urology, 1998. **52**(2): p. 195-201; discussion 201-2.
98. Clark, R.V., et al., *Marked suppression of dihydrotestosterone in men with benign prostatic hyperplasia by dutasteride, a dual 5alpha-reductase inhibitor.* J Clin Endocrinol Metab, 2004. **89**(5): p. 2179-84.
99. Roehrborn, C.G., et al., *Efficacy and safety of a dual inhibitor of 5-alpha-reductase types 1 and 2 (dutasteride) in men with benign prostatic hyperplasia.* Urology, 2002. **60**(3): p. 434-41.
100. Roehrborn, C.G., et al., *Clinical outcomes after combined therapy with dutasteride plus tamsulosin or either monotherapy in men with benign prostatic hyperplasia (BPH) by baseline characteristics: 4-year results from the randomized, double-blind Combination of Avodart and Tamsulosin (CombAT) trial.* BJU Int, 2011. **107**(6): p. 946-54.
101. Sairam, K., et al., *Sildenafil influences lower urinary tract symptoms.* BJU Int, 2002. **90**(9): p. 836-9.

102. Kohler, T.S. and K.T. McVary, *The relationship between erectile dysfunction and lower urinary tract symptoms and the role of phosphodiesterase type 5 inhibitors.* Eur Urol, 2009. **55**(1): p. 38-48.
103. Habib, F.K. and M.G. Wyllie, *Not all brands are created equal: a comparison of selected components of different brands of Serenoa repens extract.* Prostate Cancer Prostatic Dis, 2004. **7**(3): p. 195-200.
104. Buck, A.C., *Is there a scientific basis for the therapeutic effects of serenoa repens in benign prostatic hyperplasia? Mechanisms of action.* J Urol, 2004. **172**(5 Pt 1): p. 1792-9.
105. Tacklind, J., et al., *Serenoa repens for benign prostatic hyperplasia.* Cochrane Database Syst Rev, 2009(2): p. CD001423.
106. Varkarakis, I., et al., *Long-term results of open transvesical prostatectomy from a contemporary series of patients.* Urology, 2004. **64**(2): p. 306-10.
107. Emberton, M., et al., *The effect of prostatectomy on symptom severity and quality of life.* Br J Urol, 1996. **77**(2): p. 233-47.
108. Wasson, J.H., et al., *A comparison of transurethral surgery with watchful waiting for moderate symptoms of benign prostatic hyperplasia. The Veterans Affairs Cooperative Study Group on Transurethral Resection of the Prostate.* N Engl J Med, 1995. **332**(2): p. 75-9.
109. Rassweiler, J., et al., *Complications of transurethral resection of the prostate (TURP)--incidence, management, and prevention.* Eur Urol, 2006. **50**(5): p. 969-79; discussion 980.
110. Hoffman, R.M., et al., *Transurethral microwave thermotherapy vs transurethral resection for treating benign prostatic hyperplasia: a systematic review.* BJU Int, 2004. **94**(7): p. 1031-6.
111. Boyle, P., et al., *A meta-analysis of trials of transurethral needle ablation for treating symptomatic benign prostatic hyperplasia.* BJU Int, 2004. **94**(1): p. 83-8.
112. Naspro, R., et al., *A review of the recent evidence (2006-2008) for 532-nm photoselective laser vaporisation and holmium laser enucleation of the prostate.* Eur Urol, 2009. **55**(6): p. 1345-57.
113. Fung, Y.C., *Biomechanics. Mechanical Properties of Living Tissues*. 2nd ed. 1993, New York: Springer-Verlag.
114. Rajagopal, V., P.M. Nielsen, and M.P. Nash, *Modeling breast biomechanics for multi-modal image analysis--successes and challenges.* Wiley Interdiscip Rev Syst Biol Med, 2010. **2**(3): p. 293-304.
115. John, L.C., *Biomechanics of coronary artery and bypass graft disease: potential new approaches.* Ann Thorac Surg, 2009. **87**(1): p. 331-8.
116. Weiss, R.E., et al., *Prostate mechanical imaging: a new method for prostate assessment.* Urology, 2008. **71**(3): p. 425-9.
117. Erkamp, R.Q., et al., *Measuring the elastic modulus of small tissue samples.* Ultrason Imaging, 1998. **20**(1): p. 17-28.
118. Lanir, Y. and Y.C. Fung, *Two-dimensional mechanical properties of rabbit skin. I. Experimental system.* J Biomech, 1974. **7**(1): p. 29-34.
119. Vawter, D.L., Y.C. Fung, and J.B. West, *Elasticity of excised dog lung parenchyma.* J Appl Physiol, 1978. **45**(2): p. 261-9.

120. Krouskop, T.A., et al., *Elastic moduli of breast and prostate tissues under compression.* Ultrason Imaging, 1998. **20**(4): p. 260-74.
121. Lorenz, A., et al., *[Ultrasound elastography of the prostate. A new technique for tumor detection].* Ultraschall Med, 2000. **21**(1): p. 8-15.
122. Ophir, J., et al., *Elastography: a quantitative method for imaging the elasticity of biological tissues.* Ultrason Imaging, 1991. **13**(2): p. 111-34.
123. Konig, K., et al., *Initial experiences with real-time elastography guided biopsies of the prostate.* J Urol, 2005. **174**(1): p. 115-7.
124. Pallwein, L., et al., *Real-time elastography for detecting prostate cancer: preliminary experience.* BJU Int, 2007. **100**(1): p. 42-6.
125. Parker, K.J., et al., *Tissue response to mechanical vibrations for "sonoelasticity imaging".* Ultrasound Med Biol, 1990. **16**(3): p. 241-6.
126. Hoyt, K., et al., *Tissue elasticity properties as biomarkers for prostate cancer.* Cancer Biomark, 2008. **4**(4-5): p. 213-25.
127. Phipps, S., et al., *Measurement of the mechanical characteristics of benign prostatic tissue: a novel method for assessing benign prostatic disease.* Urology, 2005. **65**(5): p. 1024-8.
128. Phipps, S., et al., *Measurement of tissue mechanical characteristics to distinguish between benign and malignant prostatic disease.* Urology, 2005. **66**(2): p. 447-50.
129. Yang, T.H.J., *Structure-property relationship in biological tissues*, in *School of Engineering and Physical Sciences*. 2006, Heriot Watt University: Edinburgh.
130. Phipps, S., et al., *Measurement of the Mechanical Characteristics of Benign Prostatic Tissues: A Novel Method For Assessing Benign Prostatic Disease.* Urology, 2005. **65**: p. 1024-1028.
131. Phipps, S., et al., *The Measurement of Tissue Mechanical Characteristics to Distinguish between Benign and Malignant Prostatic Disease.* Urology, 2005. **66**: p. 447-450.
132. Barrett, K.L., et al., *Advances in cytochemical methods for detection of apoptosis.* J Histochem Cytochem, 2001. **49**(7): p. 821-32.
133. Allen, R.T., W.J. Hunter, 3rd, and D.K. Agrawal, *Morphological and biochemical characterization and analysis of apoptosis.* J Pharmacol Toxicol Methods, 1997. **37**(4): p. 215-28.
134. Gown, A.M. and M.C. Willingham, *Improved detection of apoptotic cells in archival paraffin sections: immunohistochemistry using antibodies to cleaved caspase 3.* J Histochem Cytochem, 2002. **50**(4): p. 449-54.
135. Phipps, S., F.K. Habib, and S.A. McNeill, *Quantitative Morphometric Analysis of Resected Prostatic Tissue Specimens using Immunohistochemical Staining and Colour Image Analysis.* BJU Int, 2004. **94**: p. 919-921.
136. Djavan, B., et al., *Novel artificial neural network for early detection of prostate cancer.* J Clin Oncol, 2002. **20**(4): p. 921-9.
137. Rodvold, D.M., et al., *Introduction to artificial neural networks for physicians: taking the lid off the black box.* Prostate, 2001. **46**(1): p. 39-44.
138. Phipps, S., F.K. Habib, and A. McNeill, *Quantitative morphometric analysis of individual resected prostatic tissue specimens, using immunohistochemical staining and colour-image analysis.* BJU Int, 2004. **94**(6): p. 919-21.

139. Chang, H.Y., et al., *Diversity, topographic differentiation, and positional memory in human fibroblasts.* Proc Natl Acad Sci U S A, 2002. **99**(20): p. 12877-82.
140. Goodpaster, T., et al., *An immunohistochemical method for identifying fibroblasts in formalin-fixed, paraffin-embedded tissue.* J Histochem Cytochem, 2008. **56**(4): p. 347-58.
141. Erdogru, T., et al., *Apoptotic and proliferative index after Alpha-1-adrenoceptor antagonist and/or finasteride treatment in benign prostatic hyperplasia.* Urol Int, 2002. **69**(4): p. 287-92.
142. Hockenbery, D., et al., *Bcl-2 is an inner mitochondrial membrane protein that blocks programmed cell death.* Nature, 1990. **348**(6299): p. 334-6.
143. Claus, S., et al., *Cell kinetic in epithelium and stroma of benign prostatic hyperplasia.* J Urol, 1997. **158**(1): p. 217-21.
144. Gandour-Edwards, R., et al., *Abnormalities of apoptotic and cell cycle regulatory proteins in distinct histopathologic components of benign prostatic hyperplasia.* Prostate Cancer Prostatic Dis, 2004. **7**(4): p. 321-6.
145. Tang, J., et al., *Does benign prostatic hyperplasia originate from the peripheral zone of the prostate? A preliminary study.* BJU Int, 2007. **100**(5): p. 1091-6.
146. Castro, P., et al., *Cellular senescence in the pathogenesis of benign prostatic hyperplasia.* Prostate, 2003. **55**(1): p. 30-8.
147. Choi, J., et al., *Expression of senescence-associated beta-galactosidase in enlarged prostates from men with benign prostatic hyperplasia.* Urology, 2000. **56**(1): p. 160-6.
148. Kyprianou, N., T.B. Vaughan, and M.C. Michel, *Apoptosis induction by doxazosin and other quinazoline alpha1-adrenoceptor antagonists: a new mechanism for cancer treatment?* Naunyn Schmiedebergs Arch Pharmacol, 2009. **380**(6): p. 473-7.
149. Sleebs, B.E., et al., *Quinazoline sulfonamides as dual binders of the proteins B-cell lymphoma 2 and B-cell lymphoma extra long with potent proapoptotic cell-based activity.* J Med Chem, 2011. **54**(6): p. 1914-26.
150. Ahn, B., et al., *Robotic palpation-based mechanical property mapping for diagnosis of prostate cancer.* J Endourol, 2011. **25**(5): p. 851-7.
151. Ahn, B.M., et al., *Mechanical property characterization of prostate cancer using a minimally motorized indenter in an ex vivo indentation experiment.* Urology, 2010. **76**(4): p. 1007-11.
152. Weinstein, M.H., S. Signoretti, and M. Loda, *Diagnostic utility of immunohistochemical staining for p63, a sensitive marker of prostatic basal cells.* Mod Pathol, 2002. **15**(12): p. 1302-8.
153. Weaver, J.B., Perrinez, P.R., Bergeron, J.A., Kennedy, F.E., Wang, H., Scott Lollis, S., Doyley, M.M., Hoopes, P.J., Paulsen, K.D., *The effects of interstitial tissue pressure on the measured shear modulus in vivo.* Proc SPIE, 2007. **6511**: p. 65111-A.
154. Yang, T.H., et al., *In-vitro dynamic micro-probing and the mechanical properties of human prostate tissues.* Technol Health Care, 2006. **14**(4-5): p. 281-96.

155. Eiras, S., et al., *Doxazosin induces activation of GADD153 and cleavage of focal adhesion kinase in cardiomyocytes en route to apoptosis.* Cardiovasc Res, 2006. **71**(1): p. 118-28.
156. Justulin, L.A., Jr., F.K. Delella, and S.L. Felisbino, *Doxazosin reduces cell proliferation and increases collagen fibers in rat prostatic lobes.* Cell Tissue Res, 2008. **332**(1): p. 171-83.
157. Zhang, M., et al., *Quantitative characterization of viscoelastic properties of human prostate correlated with histology.* Ultrasound Med Biol, 2008. **34**(7): p. 1033-42.

Appendix I. Clinical Data

Patient No	Age	PSA	Duration of medication (months)
Tamsulosin Group			
25	61	3.4	6
28	57	6.5	8
31	59	2.6	12
54	58	5.5	3
55	76	7.6	6
67	61	6	12
Alfuzosin Group			
3	71	3	6
30	75	5	12
74	80	1.8	36
76	68	8.9	3
Control Group			
24	68	2.3	No medication
51	71	6.3	No medication
53	71	5.6	No medication
56	60	1.2	No medication
63	62	6.2	No medication
75	72	10	No medication

Clinical characteristics of the TURP group

Patient No	Age	PSA	Duration of medication (months)
Tamsulosin Group			
12907	76	4.9	12
3800	76	n/a	10
799	68	7	8
1070	69	7.8	6
8324	77	6	14
Alfuzosin Group			
524	76	4.7	10
105719	72	1.2	7
17962	65	5	15
13566	69	15	9
3574	56	3.5	18
Control Group			
8489	64	n/a	No medication
5359	74	8.9	No medication
4559	64	12.3	No medication
2153	78	n/a	No medication
16921	71	n/a	No medication
11442	74	6.4	No medication

Clinical characteristics of the RRP control group

Appendix II. Raw data for morphological analysis

Point	% Myo (7x7)	%PSA (7x7)	Histology
P70 Q1 Pt1	28	60	Nodule
P70 Q1 Pt2	21.00	35.00	Stroma
P70 Q1 Pt3	20.00	57.00	Stroma
P70 Q1 Pt4	15	73	Nodule
P70 Q1 Pt5	11	55	Nodule
P70 Q2 Pt1	22	37.119	Stroma
P70 Q2 Pt2	11.00	37.796	Nodule
P70 Q2 Ot3	8.00	36.83	Nodule
P70 Q2 Pt4	21	52.007	Stroma
P70 Q2Pt 5	27	40.981	Stroma
P70 Q3 Pt1	20	45	Nodule
P70 Q3 Pt2	32.00	33.00	Stroma
P70 Q3 Pt3	28.00	48.00	Nodule
P70 Q3 Pt4	12	49	Nodule
P70 Q4 Pt1	12	50	Nodule
P70 Q4 Pt2	14.00	45.00	Nodule
P70 Q4 Pt3	19.00	23.00	Stroma
P70 Q4 Pt4	21	18	Stroma
P77 R Pt1	21	53.296	Stroma
P77 R Pt2	23.00	64.533	Stroma
P77 R Pt3	29.00	43.732	Stroma
P77 R Pt4	11	36.525	Nodule
P77 R Pt5	23	38.833	Nodule
P77 L Pt1	14	53.296	Nodule
P77 L Pt2	24.00	64.533	Nodule
P77 L Pt3	11.00	43.732	Stroma
P77 L Pt4	44	52	Nodule
P77 L Pt5	28	45	Nodule
P79 L Pt1	35.1	43	Nodule
P79 L Pt2	31.4	69.00	Nodule
P79 L Pt3	28.1	68.00	Nodule
P79 R Pt1	21.1	58	Nodule
P79 R Pt2	20.6	77.00	Nodule
P79 R Pt3	31.0	57.00	Nodule
P81 L Pt1	31	28	Stroma

Point	% Myo (7x7)	%PSA (7x7)	Histology
P81 L Pt2	20.00	35.00	Nodule
P81 L Pt3	21.00	37.00	Nodule
P81 L Pt4	23.1	55.31	Nodule
P81 L Pt5	40.46	63	Nodule
P81 R Pt6	27.33	43	Nodule
P81 R Pt7	13.66	45.00	Nodule
P81 R Pt8	30.22	56.00	Nodule
P81 R Pt9	15.7	55	Nodule
P81 R Pt10	29.08	14	Stroma
P81 R Pt11	26.98	10	Stroma
P82 R Pt1	11	40.66	Nodule
P82 R Pt2	23.00	66.00	Nodule
P82 R Pt3	15.00	45.00	Stroma
P82 R Pt4	21.00	41.424	Stroma
P82 R Pt5	40	4	Stroma
P82 R Pt6	22.00	11	Stroma
P82 R Pt7	40	6	Stroma
P82 R Pt8	22.00	47.972	Stroma
P82 L Pt9	22	56.255	Stroma
P82 L Pt10	38.00	23.083	Stroma
P82 L Pt11	30	0.119	Stroma
P82 L Pt12	32	22.003	Stroma
P82 L Pt13	38	12.89	Stroma
P82 L Pt14	29.00	25.1	Stroma
P82 L Pt15	24.00	31.1	Stroma
P82 L Pt16	27	16.864	Stroma
P82 L Pt17	30.00	24.1	Stroma
P82 L Pt18	23	26.238	Nodule
83-1 Pt1	31.25	25.9	Nodular
83-1 Pt2	19.92	43.46	Nodular
83-1 Pt3	36.01	5.16	Stroma
83-1 Pt4	30.02	12.84	Stroma
83-2 Pt5	19.61	64.23	Nodular
83-2 Pt6	23.74	27.84	Stroma
83-5 Pt7	38.4	22.03	Stroma
83-4 Pt8	11.69	60.31	Nodular
83-4 Pt9	15.64	60.27	Nodular
83-4 Pt10	17.67	69.25	Nodular

Point	% Myo (7x7)	%PSA (7x7)	Histology
83-3 Pt11	8.81	78.14	Nodular
83-3 Pt12	8.77	78.3	Nodular
83-5 Pt13	36.8	18.68	Stroma
84-3 Pt2	25.21	39.31	Stroma
84-3 Pt3	8.9	59.36	Nodular
84-4 Pt4	17.13	31.91	Nodular
84-3 Pt5	23.58	35.45	Stroma
84-4 Pt6	10.61	24.41	Nodular
84-3 Pt7	28.14	15.96	Stroma
84-4 Pt8	32.57	14.63	Stroma
84-3 Pt9	23.5	16.96	Stroma
84-2 Pt10	24.83	58.86	Nodular
84-2 Pt11	30.26	43.54	Nodular
84-1 Pt12	21.52	43.6	Stroma
84-2 Pt13	22.91	20.12	Stroma
85-1 Pt1	15.98	62.29	Nodular
85-1 Pt2	35.61	51.49	Nodular
85-1 Pt3	34	46.43	Nodular
85-2 Pt4	32	44.34	Stroma
85-2 Pt5	28.5	48.2	Nodular
85-2 Pt6	21.59	51.25	Stroma
85-3 Pt7	16.2	48.91	Nodular
85-3 Pt8	30.78	34.45	Nodular
85-4 Pt9	33.14	17.49	Stroma
85-4 Pt10	26.89	50.89	Nodular
85-4 Pt11	19.83	55.16	Stroma
85-3 Pt12	25.63	37.64	Nodular
86-1 Pt1	14.77	29.37	Stroma
86-1 Pt2	30.44	28.67	Stroma
86-2 Pt3	11.53	72.16	Nodular
86-1 Pt4	22.64	23.01	Stroma
86-2 Pt5	20.07	49.84	Nodular
86-2 Pt6	19.97	36.74	Nodular
86-2 Pt7	19.36	51.75	Nodular
86-4 Pt8	16.34	40.96	Stroma
86-4 Pt9	10.21	40.54	Nodular
86-4 Pt10	19.06	53.17	Nodular

Point	% Myo (7x7)	%PSA (7x7)	Histology
86-3 Pt11	20.56	37.3	Stroma
86-3 Pt12	32.55	25.26	Stroma
87-1 Pt1	18.67		Stroma
87-1 Pt2	22.87		Nodular
87-1 Pt3	24.71		Nodular
87-2 Pt4	27.99	35.13	Stroma
87-2 Pt5	29.75	37.48	Nodular
87-2 Pt6	25.09	46.6	Nodular
88-1 Pt1	16	31.95	Stroma
88-1 Pt2	16.05	17.62	Stroma
88-1 Pt3	21.26	41.45	Nodular
88-1 Pt4	23.29	46.95	Nodular
88-2 Pt5	22.98	39.26	Stroma
88-2 Pt6	23.04	42.5	Stroma
88-3 Pt7	20.53	55.25	Nodular
88-3 Pt8	30.7	51.12	Nodular
89-2 Pt1	32.71	12.55	Stroma
89-1 Pt2	26.75	30.16	Stroma
89-2 Pt3	26.87	18.86	Nodular
89-1 Pt4	15.32	60.13	Nodular
89-1 Pt5	26.78	51.94	Nodular
89-3 Pt6	22.98	38.57	Stroma
89-3 Pt7	22.4	35.42	Stroma
89-4 Pt8	29.17	59.92	Nodular
89-4 Pt9	38.06	41.18	Stroma
89-3 Pt10	20.4	51.13	Nodular
89-4 Pt11	31.78	19.36	Stroma

Appendix III – Raw data for the capase-3 analysis of apoptosis in prostate tissue

TURP Patients taking Tamsulosin

	Total Cells	Apoptotic Cells	% Apoptotic Cells	Intensity	Apoptotic Score	**Total Cells/10 fields**	**Total Apoptotic Cells**	**Apoptotic Score**
25-7								
1	170	58	0.34	2	0.68	1914	1056	0.69
2	147	96	0.65	1	0.65			
3	244	148	0.61	1	0.61			
4	260	135	0.52	1	0.52			
5	230	132	0.57	1	0.57			
6	149	66	0.44	1	0.44			
7	306	120	0.39	1	0.39			
8	245	177	0.72	1	0.72			
9	114	86	0.75	2	1.51			
10	49	38	0.78	1	0.78			
25-8								
1	172	136	0.79	2	1.58	1663	1076	1.56
2	221	79	0.36	2	0.71			
3	136	116	0.85	2	1.71			
4	179	121	0.68	3	2.03			
5	151	127	0.84	2	1.68			
6	42	24	0.57	2	1.14			
7	165	116	0.70	3	2.11			
8	234	120	0.51	3	1.54			
9	162	82	0.51	3	1.52			
10	201	155	0.77	2	1.54			
28-1								
1	229	103	0.45	1	0.45	2413	1291	0.64
2	253	109	0.43	1	0.43			
3	284	184	0.65	1	0.65			
4	240	190	0.79	1	0.79			
5	211	121	0.57	1	0.57			
6	213	141	0.66	1	0.66			
7	281	108	0.38	1	0.38			
8	207	160	0.77	1	0.77			
9	223	98	0.44	2	0.88			
10	272	77	0.28	3	0.85			
28-2								
1	251	106	0.42	2	0.84	2108	644	0.49
2	193	78	0.40	2	0.81			
3	171	81	0.47	3	1.42			
4	254	56	0.22	1	0.22			
5	163	52	0.32	1	0.32			
6	159	43	0.27	1	0.27			
7	175	42	0.24	1	0.24			
8	228	68	0.30	1	0.30			

	Total Cells	Apoptotic Cells	% Apoptotic Cells	Intensity	Apoptotic Score	**Total Cells/10 fields**	**Total Apoptotic Cells**	**Apoptotic Score**
9	251	35	0.14	1	0.14			
10	263	83	0.32	1	0.32			
31-2								
1	179	172	0.96	1	0.96	1497	1319	1.39
2	173	151	0.87	2	1.75			
3	129	106	0.82	2	1.64			
4	149	124	0.83	2	1.66			
5	172	152	0.88	2	1.77			
6	138	129	0.93	1	0.93			
7	168	141	0.84	1	0.84			
8	144	138	0.96	1	0.96			
9	118	102	0.86	2	1.73			
10	127	104	0.82	2	1.64			
31-5								
1	292	278	0.95	2	1.90	1768	530	0.35
2	151	0	0.00	0	0.00			
3	158	0	0.00	0	0.00			
4	164	0	0.00	0	0.00			
5	132	91	0.69	1	0.69			
6	173	98	0.57	1	0.57			
7	180	46	0.26	1	0.26			
8	135	0	0.00	0	0.00			
9	172	0	0.00	0	0.00			
10	211	17	0.08	1	0.08			
54-1								
1	138	0	0.00	0	0.00	1918	0	0.00
2	153	0	0.00	0	0.00			
3	194	0	0.00	0	0.00			
4	240	0	0.00	0	0.00			
5	231	0	0.00	0	0.00			
6	261	0	0.00	0	0.00			
7	197	0	0.00	0	0.00			
8	198	0	0.00	0	0.00			
9	161	0	0.00	0	0.00			
10	145	0	0.00	0	0.00			
54-3								
1	220	93	0.42	2	0.85	1652	857	1.04
2	87	55	0.63	2	1.26			
3	165	113	0.68	2	1.37			
4	193	64	0.33	2	0.66			
5	222	141	0.64	1	0.64			
6	154	104	0.68	1	0.68			
7	216	138	0.64	3	1.92			
8	143	62	0.43	3	1.30			
9	139	49	0.35	3	1.06			

	Total Cells	Apoptotic Cells	% Apoptotic Cells	Intensity	Apoptotic Score	**Total Cells/10 fields**	**Total Apoptotic Cells**	**Apoptotic Score**
10	113	38	0.34	2	0.67			
55-5								
1	278	181	0.65	1	0.65	1928	819	0.66
2	234	70	0.30	2	0.60			
3	232	93	0.40	2	0.80			
4	118	83	0.70	1	0.70			
5	172	75	0.44	1	0.44			
6	211	51	0.24	2	0.48			
7	191	105	0.55	2	1.10			
8	200	87	0.44	2	0.87			
9	115	43	0.37	2	0.75			
10	177	31	0.18	1	0.18			
55-6								
1	148	85	0.57	2	1.15	1013	732	1.02
2	105	71	0.68	1	0.68			
3	83	64	0.77	1	0.77			
4	78	33	0.42	1	0.42			
5	98	75	0.77	1	0.77			
6	87	58	0.67	2	1.33			
7	115	92	0.80	1	0.80			
8	102	82	0.80	1	0.80			
9	88	79	0.90	2	1.80			
10	109	93	0.85	2	1.71			
67-3								
1	124	87	0.70	1	0.70	1693	1025	0.98
2	96	82	0.85	1	0.85			
3	177	96	0.54	1	0.54			
4	179	87	0.49	2	0.97			
5	136	100	0.74	2	1.47			
6	155	89	0.57	1	0.57			
7	216	138	0.64	2	1.28			
8	240	125	0.52	2	1.04			
9	182	73	0.40	2	0.80			
10	188	148	0.79	2	1.57			
67-5								
1	176	92	0.52	1	0.52	2237	1011	0.76
2	326	87	0.27	1	0.27			
3	302	119	0.39	1	0.39			
4	289	98	0.34	2	0.68			
5	269	79	0.29	2	0.59			
6	216	134	0.62	1	0.62			
7	211	97	0.46	1	0.46			
8	139	116	0.83	2	1.67			
9	151	68	0.45	2	0.90			
10	158	121	0.77	2	1.53			

						21804	**10360**	**9.58**
TURP Patients taking Alfuzosin								
	Total Cells	Apoptotic Cells	% Apoptotic Cells	Intensity	Apoptotic Score	**Total Cells/10 fields**	**Total Apoptotic Cells**	**Apoptotic Score**
3-1								
1	229	90	0.393013	2	0.786026	1944	876	8.59
2	119	82	0.689076	1	0.689076			
3	228	58	0.254386	1	0.254386			
4	191	103	0.539267	2	1.078534			
5	197	152	0.771574	2	1.543147			
6	206	118	0.572816	2	1.145631			
7	115	53	0.46087	2	0.921739			
8	250	0	0	0	0			
9	211	81	0.383886	2	0.767773			
10	198	139	0.70202	2	1.40404			
30-2								
1	171	150	0.877193	2	1.754386	1802	1265	14.35
2	178	143	0.803371	2	1.606742			
3	124	119	0.959677	2	1.919355			
4	186	0	0	0	0			
5	189	172	0.910053	2	1.820106			
6	198	164	0.828283	2	1.656566			
7	158	148	0.936709	2	1.873418			
8	169	102	0.60355	2	1.207101			
9	203	149	0.73399	2	1.46798			
10	226	118	0.522124	2	1.044248			
30-3								
1	92	65	0.706522	2	1.413043	975	776	15.79
2	89	62	0.696629	2	1.393258			
3	114	96	0.842105	2	1.684211			
4	125	105	0.84	2	1.68			
5	112	102	0.910714	2	1.821429			
6	79	58	0.734177	2	1.468354			
7	108	86	0.796296	2	1.592593			
8	74	61	0.824324	2	1.648649			
9	79	59	0.746835	2	1.493671			
10	103	82	0.796117	2	1.592233			
74-3								
1	112	73	0.651786	3	1.955357	1541	1039	16.61
2	124	75	0.604839	3	1.814516			
3	199	171	0.859296	3	2.577889			
4	167	105	0.628743	3	1.886228			
5	169	75	0.443787	3	1.331361			
6	151	102	0.675497	2	1.350993			

	Total Cells	Apoptotic Cells	% Apoptotic Cells	Intensity	Apoptotic Score	**Total Cells/10 fields**	**Total Apoptotic Cells**	**Apoptotic Score**
7	118	81	0.686441	2	1.372881			
8	144	121	0.840278	2	1.680556			
9	179	142	0.793296	2	1.586592			
10	178	94	0.52809	2	1.05618			
74-4								
1	204	168	0.823529	1	0.823529	1619	1075	10.14
2	144	108	0.75	1	0.75			
3	233	173	0.742489	1	0.742489			
4	113	61	0.539823	2	1.079646			
5	124	70	0.564516	2	1.129032			
6	116	78	0.672414	2	1.344828			
7	189	107	0.566138	2	1.132275			
8	155	76	0.490323	2	0.980645			
9	180	143	0.794444	2	1.588889			
10	161	91	0.565217	1	0.565217			
76-5								
1	184	52	0.282609	1	0.282609	2093	655	3.23
2	213	139	0.652582	1	0.652582			
3	137	0	0	0	0			
4	158	92	0.582278	1	0.582278			
5	256	69	0.269531	1	0.269531			
6	226	0	0	0	0			
7	248	0	0	0	0			
8	251	72	0.286853	1	0.286853			
9	185	153	0.827027	1	0.827027			
10	235	78	0.331915	1	0.331915			
76-8								
1	138	124	0.898551	2	1.797101	1423	1007	14.92
2	186	139	0.747312	2	1.494624			
3	177	96	0.542373	2	1.084746			
4	167	119	0.712575	3	2.137725			
5	117	81	0.692308	2	1.384615			
6	137	95	0.693431	2	1.386861			
7	115	58	0.504348	2	1.008696			
8	94	71	0.755319	2	1.510638			
9	164	112	0.682927	2	1.365854			
10	128	112	0.875	2	1.75			

TURP Patients not receiving medication

	Total Cells	Apoptotic Cells	% Apoptotic Cells	Intensity	Apoptotic Score	**Total Cells/10 fields**	**Total Apoptotic Cells**	**Apop Score**
24-2								
1	82	0	0	0	0	1070	484	4.19
2	69	0	0	0	0			
3	134	0	0	0	0			
4	105	0	0	0	0			
5	126	92	0.730159	1	0.730159			
6	136	121	0.889706	1	0.889706			
7	124	91	0.733871	1	0.733871			
8	94	58	0.617021	1	0.617021			
9	82	51	0.621951	1	0.621951			
10	118	71	0.601695	1	0.601695			
51-5								
1	130	116	0.892308	1	0.892308	1750	1157	9.22
2	187	137	0.73262	1	0.73262			
3	251	58	0.231076	1	0.231076			
4	238	153	0.642857	1	0.642857			
5	179	108	0.603352	1	0.603352			
6	146	91	0.623288	2	1.246575			
7	151	124	0.821192	2	1.642384			
8	114	90	0.789474	1	0.789474			
9	159	109	0.685535	1	0.685535			
10	195	171	0.876923	2	1.753846			
53-4								
1	143	59	0.412587	1	0.412587	1395	813	8.51
2	115	75	0.652174	1	0.652174			
3	120	106	0.883333	1	0.883333			
4	176	102	0.579545	2	1.159091			
5	159	68	0.427673	1	0.427673			
6	129	98	0.75969	1	0.75969			
7	86	63	0.732558	2	1.465116			
8	91	83	0.912088	2	1.824176			
9	172	159	0.924419	1	0.924419			
10	204	0	0	0	0			
56-4								
1	194	78	0.402062	1	0.402062	1834	1018	4.76
2	144	91	0.631944	1	0.631944			
3	177	143	0.80791	1	0.80791			
4	164	121	0.737805	1	0.737805			
5	156	106	0.679487	1	0.679487			
6	218	108	0.495413	1	0.495413			
7	224	98	0.4375	1	0.4375			
8	154	0	0	0	0			
9	248	142	0.572581	1	0.572581			

	Total Cells	Apoptotic Cells	% Apoptotic Cells	Intensity	Apoptotic Score	**Total Cells/10 fields**	**Total Apoptotic Cells**	**Apop Score**
10	155	131	0.845161	0	0			
63-3								
1	112	94	0.839286	2	1.678571	1572	877	11.60
2	202	96	0.475248	1	0.475248			
3	190	72	0.378947	2	0.757895			
4	139	89	0.640288	2	1.280576			
5	89	71	0.797753	2	1.595506			
6	201	83	0.412935	2	0.825871			
7	212	81	0.382075	2	0.764151			
8	166	70	0.421687	2	0.843373			
9	135	119	0.881481	2	1.762963			
10	126	102	0.809524	2	1.619048			
63-4								
1	163	79	0.484663	2	0.969325	1593	1052	11.35
2	178	98	0.550562	2	1.101124			
3	150	119	0.793333	1	0.793333			
4	243	216	0.888889	1	0.888889			
5	181	126	0.696133	2	1.392265			
6	118	73	0.618644	2	1.237288			
7	158	94	0.594937	2	1.189873			
8	93	71	0.763441	2	1.526882			
9	142	68	0.478873	2	0.957746			
10	167	108	0.646707	2	1.293413			
75-1								
1	67	46	0.686567	2	1.373134	1242	816	14.57
2	189	59	0.312169	1	0.312169			
3	88	72	0.818182	2	1.636364			
4	72	51	0.708333	3	2.125			
5	159	105	0.660377	3	1.981132			
6	106	58	0.54717	2	1.09434			
7	146	115	0.787671	2	1.575342			
8	154	120	0.779221	2	1.558442			
9	129	112	0.868217	2	1.736434			
10	132	78	0.590909	2	1.181818			
75-4								
1	205	0	0	0	0	1999	618	3.02
2	153	0	0	0	0			
3	176	0	0	0	0			
4	205	0	0	0	0			
5	241	0	0	0	0			
6	137	64	0.467153	1	0.467153			
7	227	175	0.770925	1	0.770925			
8	165	122	0.739394	1	0.739394			
9	223	108	0.484305	1	0.484305			
10	267	149	0.558052	1	0.558052			

Radical Prostatectomy Patients taking Tamsulosin

	Total Cells	Apoptotic Cells	% Apoptotic Cells	Intensity	Apoptotic Score	**Total Cells/10 fields**	**Total Apoptotic Cells**	**Apop Score**
1070J								
1	139	83	0.597122	2	1.194245	1547	1171	14.90
2	143	119	0.832168	2	1.664336			
3	163	123	0.754601	1	0.754601			
4	147	102	0.693878	2	1.387755			
5	154	125	0.811688	2	1.623377			
6	158	134	0.848101	2	1.696203			
7	152	131	0.861842	2	1.723684			
8	139	114	0.820144	2	1.640288			
9	179	154	0.860335	2	1.72067			
10	173	86	0.49711	3	1.491329			
1070L								
1	131	122	0.931298	1	0.931298	1455	1145	11.19
2	152	114	0.75	1	0.75			
3	150	120	0.8	2	1.6			
4	136	85	0.625	1	0.625			
5	154	142	0.922078	2	1.844156			
6	125	95	0.76	1	0.76			
7	142	102	0.71831	1	0.71831			
8	136	98	0.720588	1	0.720588			
9	148	118	0.797297	2	1.594595			
10	181	149	0.823204	2	1.646409			
12097J								
1	76	76	1	1	1	1127	779	10.31
2	109	78	0.715596	1	0.715596			
3	160	114	0.7125	1	0.7125			
4	120	76	0.633333	2	1.266667			
5	98	54	0.55102	2	1.102041			
6	131	102	0.778626	1	0.778626			
7	101	38	0.376238	1	0.376238			
8	119	88	0.739496	2	1.478992			
9	108	72	0.666667	2	1.333333			
10	105	81	0.771429	2	1.542857			
12097K								
1	163	101	0.619632	2	1.239264	1500	981	11.02
2	180	152	0.844444	2	1.688889			
3	124	81	0.653226	2	1.306452			
4	188	153	0.81383	2	1.62766			
5	158	125	0.791139	2	1.582278			
6	176	121	0.6875	2	1.375			
7	168	0	0	0	0			
8	125	93	0.744	1	0.744			
9	89	73	0.820225	1	0.820225			

	Total Cells	Apoptotic Cells	% Apoptotic Cells	Intensity	Apoptotic Score	**Total Cells/10 fields**	**Total Apoptotic Cells**	**Apop Score**
10	129	82	0.635659	1	0.635659			
3800F								
1	95	63	0.663158	1	0.663158	1331	678	6.60
2	116	94	0.810345	1	0.810345			
3	97	69	0.71134	2	1.42268			
4	138	0	0	0	0			
5	127	0	0	0	0			
6	102	89	0.872549	1	0.872549			
7	129	119	0.922481	0	0			
8	198	86	0.434343	2	0.868687			
9	136	74	0.544118	2	1.088235			
10	193	84	0.435233	2	0.870466			
3800I								
1	93	81	0.870968	1	0.870968	983	774	9.57
2	89	75	0.842697	1	0.842697			
3	133	129	0.969925	1	0.969925			
4	47	42	0.893617	1	0.893617			
5	79	64	0.810127	1	0.810127			
6	87	65	0.747126	2	1.494253			
7	104	81	0.778846	1	0.778846			
8	88	61	0.693182	1	0.693182			
9	129	112	0.868217	2	1.736434			
10	134	64	0.477612	1	0.477612			
799K								
1	95	75	0.789474	2	1.578947	1350	528	5.09
2	106	0	0	0	0			
3	174	168	0.965517	1	0.965517			
4	152	0	0	0	0			
5	141	98	0.695035	1	0.695035			
6	133	0	0	0	0			
7	173	0	0	0	0			
8	170	0	0	0	0			
9	75	75	1	1	1			
10	131	112	0.854962	1	0.854962			
799N								
1	96	86	0.895833	2	1.791667	1278	1088	14.43
2	84	71	0.845238	2	1.690476			
3	158	138	0.873418	2	1.746835			
4	138	119	0.862319	2	1.724638			
5	112	92	0.821429	2	1.642857			
6	105	88	0.838095	2	1.67619			
7	194	146	0.752577	2	1.505155			
8	95	81	0.852632	1	0.852632			
9	169	154	0.911243	1	0.911243			
10	127	113	0.889764	1	0.889764			

	Total Cells	Apoptotic Cells	% Apoptotic Cells	Intensity	Apoptotic Score	**Total Cells/10 fields**	**Total Apoptotic Cells**	**Apop Score**
8324E								
1	123	0	0	0	0	1539	175	0.94
2	183	0	0	0	0			
3	217	0	0	0	0			
4	188	152	0.808511	1	0.808511			
5	181	23	0.127072	1	0.127072			
6	168	0	0	0	0			
7	145	0	0	0	0			
8	121	0	0	0	0			
9	96	0	0	0	0			
10	117	0	0	0	0			
8324I								
1	94	42	0.446809	2	0.893617	1650	995	9.38
2	178	138	0.775281	2	1.550562			
3	193	154	0.797927	2	1.595855			
4	185	119	0.643243	1	0.643243			
5	161	64	0.397516	1	0.397516			
6	166	72	0.433735	1	0.433735			
7	218	154	0.706422	1	0.706422			
8	142	72	0.507042	2	1.014085			
9	181	142	0.78453	2	1.569061			
10	132	38	0.287879	2	0.575758			

Radical Prostatectomy Patients taking Alfuzosin

	Total Cells	Apoptotic Cells	% Apoptotic Cells	Intensity	Apoptotic Score	**Total Cells/10 fields**	**Total Apoptotic Cells**	**Apop Score**
524L								
1	168	0	0	0	0	1517	261	2.00
2	151	0	0	0	0			
3	118	0	0	0	0			
4	169	0	0	0	0			
5	128	38	0.296875	1	0.296875			
6	171	0	0	0	0			
7	165	0	0	0	0			
8	185	0	0	0	0			
9	124	102	0.822581	1	0.822581			
10	138	121	0.876812	1	0.876812			
524M								
1	138	124	0.898551	2	1.797101	1897	498	4.84
2	241	38	0.157676	1	0.157676			
3	217	16	0.073733	1	0.073733			
4	133	121	0.909774	1	0.909774			
5	227	10	0.044053	1	0.044053			
6	232	24	0.103448	2	0.206897			
7	213	39	0.183099	2	0.366197			
8	188	53	0.281915	2	0.56383			
9	190	49	0.257895	2	0.515789			
10	118	24	0.20339	1	0.20339			
3574I								
1	203	152	0.748768	1	0.748768	1776	524	5.14
2	142	69	0.485915	1	0.485915			
3	165	102	0.618182	2	1.236364			
4	172	6	0.034884	1	0.034884			
5	224	0	0	0	0			
6	239	0	0	0	0			
7	183	121	0.661202	3	1.983607			
8	173	0	0	0	0			
9	161	0	0	0	0			
10	114	74	0.649123	1	0.649123			
3574L								
1	150	124	0.826667	2	1.653333	1408	1158	14.67
2	162	139	0.858025	1	0.858025			
3	169	145	0.857988	2	1.715976			
4	146	131	0.89726	1	0.89726			
5	131	94	0.717557	2	1.435115			
6	134	102	0.761194	2	1.522388			
7	114	98	0.859649	2	1.719298			
8	122	109	0.893443	2	1.786885			
9	142	114	0.802817	2	1.605634			
10	138	102	0.73913	2	1.478261			

	Total Cells	Apoptotic Cells	% Apoptotic Cells	Intensity	Apoptotic Score	**Total Cells/10 fields**	**Total Apoptotic Cells**	**Apop Score**
17962P								
1	197	164	0.832487	1	0.832487	1448	1045	11.29
2	148	107	0.722973	1	0.722973			
3	101	72	0.712871	2	1.425743			
4	189	127	0.671958	2	1.343915			
5	132	87	0.659091	2	1.318182			
6	131	92	0.70229	2	1.40458			
7	134	78	0.58209	1	0.58209			
8	131	72	0.549618	2	1.099237			
9	108	91	0.842593	2	1.685185			
10	177	155	0.875706	1	0.875706			
17962O								
1	227	68	0.299559	2	0.599119	1541	806	14.45
2	171	119	0.695906	3	2.087719			
3	162	66	0.407407	3	1.222222			
4	83	40	0.481928	3	1.445783			
5	138	129	0.934783	2	1.869565			
6	129	71	0.550388	3	1.651163			
7	139	72	0.517986	3	1.553957			
8	154	103	0.668831	2	1.337662			
9	259	59	0.227799	3	0.683398			
10	79	79	1	2	2			
13566K								
1	113	94	0.831858	2	1.663717	1477	882	6.99
2	127	67	0.527559	1	0.527559			
3	143	87	0.608392	1	0.608392			
4	177	88	0.497175	1	0.497175			
5	161	134	0.832298	1	0.832298			
6	122	87	0.713115	1	0.713115			
7	181	93	0.513812	1	0.513812			
8	117	91	0.777778	1	0.777778			
9	154	78	0.506494	1	0.506494			
10	182	63	0.346154	1	0.346154			
13566J								
1	127	85	0.669291	2	1.338583	1389	895	11.74
2	142	68	0.478873	2	0.957746			
3	132	114	0.863636	2	1.727273			
4	139	108	0.776978	2	1.553957			
5	176	69	0.392045	2	0.784091			
6	154	104	0.675325	1	0.675325			
7	117	102	0.871795	2	1.74359			
8	141	54	0.382979	2	0.765957			
9	133	97	0.729323	2	1.458647			
10	128	94	0.734375	1	0.734375			

	Total Cells	Apoptotic Cells	% Apoptotic Cells	Intensity	Apoptotic Score	**Total Cells/10 fields**	**Total Apoptotic Cells**	**Apop Score**
10519K								
1	172	0	0	0	0	1487	542	3.78
2	139	0	0	0	0			
3	218	0	0	0	0			
4	117	0	0	0	0			
5	135	92	0.681481	1	0.681481			
6	147	118	0.802721	1	0.802721			
7	166	132	0.795181	1	0.795181			
8	128	0	0	0	0			
9	128	78	0.609375	1	0.609375			
10	137	122	0.890511	1	0.890511			
10519J								
1	156	132	0.846154	1	0.846154	1161	930	10.26
2	122	81	0.663934	1	0.663934			
3	88	79	0.897727	1	0.897727			
4	121	78	0.644628	1	0.644628			
5	82	39	0.47561	2	0.95122			
6	124	116	0.935484	1	0.935484			
7	95	92	0.968421	2	1.936842			
8	83	71	0.855422	2	1.710843			
9	149	124	0.832215	1	0.832215			
10	141	118	0.836879	1	0.836879			

Radical Prostatectomy Patients no medication

	Total Cells	Apoptotic Cells	% Apoptotic Cells	Intensity	Apoptotic Score	**Total Cells/10 fields**	**Total Apoptotic Cells**	**Apop Score**
11442O								
1	142	0	0	0	0	1510	685	6.75
2	150	92	0.613333	2	1.226667			
3	148	113	0.763514	1	0.763514			
4	154	116	0.753247	1	0.753247			
5	143	92	0.643357	2	1.286713			
6	151	53	0.350993	1	0.350993			
7	195	43	0.220513	2	0.441026			
8	120	42	0.35	2	0.7			
9	145	52	0.358621	2	0.717241			
10	162	82	0.506173	1	0.506173			
16921N								
1	80	0	0	0	0	1293	500	4.97
2	160	112	0.7	1	0.7			
3	122	110	0.901639	1	0.901639			
4	66	0	0	0	0			
5	104	0	0	0	0			
6	117	62	0.529915	1	0.529915			
7	180	0	0	0	0			
8	159	54	0.339623	2	0.679245			
9	129	78	0.604651	2	1.209302			
10	176	84	0.477273	2	0.954545			
2153G								
1	120	0	0	0	0	1420	616	6.60
2	129	84	0.651163	2	1.302326			
3	125	72	0.576	2	1.152			
4	244	81	0.331967	1	0.331967			
5	141	0	0	0	0			
6	197	110	0.558376	1	0.558376			
7	88	51	0.579545	2	1.159091			
8	99	40	0.40404	2	0.808081			
9	153	97	0.633987	1	0.633987			
10	124	81	0.653226	1	0.653226			
4559N								
1	165	58	0.351515	1	0.351515	1405	518	6.43
2	112	55	0.491071	2	0.982143			
3	147	81	0.55102	1	0.55102			
4	185	86	0.464865	2	0.92973			
5	156	52	0.333333	1	0.333333			
6	109	43	0.394495	2	0.788991			
7	102	64	0.627451	2	1.254902			
8	133	46	0.345865	2	0.691729			
9	121	33	0.272727	2	0.545455			
10	175	0	0	0	0			

	Total Cells	Apoptotic Cells	% Apoptotic Cells	Intensity	Apoptotic Score	**Total Cells/10 fields**	**Total Apoptotic Cells**	**Apop Score**
5359L								
1	188	96	0.510638	2	1.021277	1751	750	7.54
2	223	177	0.793722	2	1.587444			
3	107	58	0.542056	1	0.542056			
4	269	118	0.438662	2	0.877323			
5	87	62	0.712644	2	1.425287			
6	294	58	0.197279	1	0.197279			
7	181	62	0.342541	2	0.685083			
8	51	37	0.72549	1	0.72549			
9	190	32	0.168421	1	0.168421			
10	161	50	0.310559	1	0.310559			
8489W								
1	151	118	0.781457	1	0.781457	1373	639	7.14
2	142	78	0.549296	2	1.098592			
3	183	98	0.535519	1	0.535519			
4	86	51	0.593023	2	1.186047			
5	114	64	0.561404	2	1.122807			
6	129	94	0.728682	2	1.457364			
7	111	34	0.306306	1	0.306306			
8	172	0	0	0	0			
9	156	102	0.653846	1	0.653846			
10	129	0	0	0	0			

Appendix IV – Raw data for the TUNEL assay analysis of apoptosis in prostate tissue

TURP patients taking Tamsulosin

Patient	Cell Total	Apoptotic Cell Total	Apoptotic Index	Total Cells/10 fields	Total Apoptotic Cells	Apop Index
25-7						
1	236	2	0.008475	2333	58	0.02
2	167	13	0.077844			
3	237	10	0.042194			
4	187	4	0.02139			
5	176	11	0.0625			
6	187	7	0.037433			
7	129	1	0.007752			
8	421	0	0			
9	415	2	0.004819			
10	178	8	0.044944			
25-8						
1	126	10	0.079365	1777	316	0.18
2	118	19	0.161017			
3	218	95	0.43578			
4	222	63	0.283784			
5	196	82	0.418367			
6	176	0	0			
7	197	1	0.005076			
8	259	1	0.003861			
9	159	31	0.194969			
10	106	14	0.132075			
28-1						
1	223	2	0.008969	2353	233	0.10
2	269	12	0.04461			
3	149	33	0.221477			
4	204	70	0.343137			
5	325	23	0.070769			
6	262	14	0.053435			
7	169	12	0.071006			
8	308	30	0.097403			
9	287	31	0.108014			
10	157	6	0.038217			
28-2						
1	215	0	0	2694	0	0.00
2	255	0	0			
3	251	0	0			
4	218	0	0			
5	283	0	0			
6	233	0	0			
7	241	0	0			

Patient	Cell Total	Apoptotic Cell Total	Apoptotic Index	Total Cells/10 fields	Total Apoptotic Cells	Apop Index
8	279	0	0			
9	260	0	0			
10	459	0	0			
31-2						
1	213	4	0.018779	2209	81	0.04
2	221	12	0.054299			
3	169	6	0.035503			
4	246	13	0.052846			
5	121	9	0.07438			
6	228	10	0.04386			
7	143	3	0.020979			
8	228	6	0.026316			
9	224	7	0.03125			
10	416	11	0.026442			
31-5						
1	181	15	0.082873	2053	51	0.02
2	214	12	0.056075			
3	222	14	0.063063			
4	197	1	0.005076			
5	215	0	0			
6	253	3	0.011858			
7	176	0	0			
8	224	3	0.013393			
9	176	2	0.011364			
10	195	1	0.005128			
54-1						
1	319	14	0.043887	2586	79	0.03
2	269	25	0.092937			
3	426	15	0.035211			
4	195	0	0			
5	209	0	0			
6	207	1	0.004831			
7	138	0	0			
8	234	8	0.034188			
9	275	5	0.018182			
10	314	11	0.035032			
54-3						
1	163	26	0.159509	1176	253	0.22
2	134	39	0.291045			
3	150	32	0.213333			
4	94	23	0.244681			
5	67	51	0.761194			
6	82	34	0.414634			
7	105	21	0.2			
8	113	5	0.044248			

Patient	Cell Total	Apoptotic Cell Total	Apoptotic Index	Total Cells/10 fields	Total Apoptotic Cells	Apop Index
9	119	8	0.067227			
10	149	14	0.09396			
55-5						
1	87	0	0	1613	0	0.00
2	142	0	0			
3	118	0	0			
4	199	0	0			
5	269	0	0			
6	167	0	0			
7	129	0	0			
8	226	0	0			
9	151	0	0			
10	125	0	0			
55-6						
1	361	0	0	3403	1	0.00
2	364	0	0			
3	331	1	0.003021			
4	394	0	0			
5	361	0	0			
6	379	0	0			
7	348	0	0			
8	296	0	0			
9	421	0	0			
10	148	0	0			
67-3						
1	165	0	0	1366	1	0.00
2	169	0	0			
3	118	0	0			
4	146	0	0			
5	134	0	0			
6	150	0	0			
7	166	0	0			
8	156	1	0.00641			
9	49	0	0			
10	113	0	0			
67-5						
1	279	0	0	2563	0	0.00
2	189	0	0			
3	289	0	0			
4	228	0	0			
5	290	0	0			
6	268	0	0			
7	223	0	0			
8	237	0	0			
9	298	0	0			

10	262	0	0			

TURP patients taking Alfuzosin

Image	Cell Total	Apoptotic Cell Total	Apoptotic Index	Total Cells/6 fields	Total Apoptotic Cells	% Apoptosis
3						
1	120	0	0	1910	369	0.19
2	269	42	0.156134			
3	140	67	0.478571			
4	143	74	0.517483			
5	268	87	0.324627			
6	178	13	0.073034			
7	262	0	0			
8	146	0	0			
9	186	62	0.333333			
10	198	24	0.121212			
30-2						
1	163	41	0.251534	1933	538	0.28
2	145	86	0.593103			
3	147	73	0.496599			
4	260	25	0.096154			
5	265	36	0.135849			
6	191	72	0.376963			
7	190	62	0.326316			
8	179	21	0.117318			
9	171	81	0.473684			
10	222	41	0.184685			
30-3						
1	238	95	0.39916	1868	937	0.50
2	197	98	0.497462			
3	135	112	0.82963			
4	221	86	0.38914			
5	182	159	0.873626			
6	171	109	0.637427			
7	181	54	0.298343			
8	239	63	0.263598			
9	130	53	0.407692			
10	174	108	0.62069			
74-3						
1	124	43	0.346774	1110	198	0.18
2	39	10	0.25641			
3	94	29	0.308511			
4	54	12	0.222222			
5	161	1	0.006211			
6	167	0	0			
7	187	18	0.096257			

Image	Cell Total	Apoptotic Cell Total	Apoptotic Index	Total Cells/6 fields	Total Apoptotic Cells	% Apoptosis
8	67	19	0.283582			
9	133	35	0.263158			
10	84	31	0.369048			
74-4						
1	204	42	0.205882	1892	858	0.45
2	165	89	0.539394			
3	230	124	0.53913			
4	192	94	0.489583			
5	178	92	0.516854			
6	206	89	0.432039			
7	209	102	0.488038			
8	145	111	0.765517			
9	163	59	0.361963			
10	200	56	0.28			
76-5						
1	238	14	0.058824	1981	51	0.03
2	200	7	0.035			
3	236	6	0.025424			
4	149	0	0			
5	202	0	0			
6	232	2	0.008621			
7	195	4	0.020513			
8	212	0	0			
9	128	2	0.015625			
10	189	16	0.084656			
76-8						
1	216	3	0.013889	1839	132	0.07
2	203	0	0			
3	232	6	0.025862			
4	209	2	0.009569			
5	234	8	0.034188			
6	179	3	0.01676			
7	183	12	0.065574			
8	131	37	0.282443			
9	128	0	0			
10	124	61	0.491935			

TURP patients taking no medications

Image	Cell Total	Apoptotic Cell Total	Apoptotic Index	Total Cells/6 fields	Total Apoptotic Cells	% Apoptosis
24-2						
1	101	1	0.009901	902	15	0.02
2	95	0	0			
3	58	0	0			
4	101	3	0.029703			
5	62	0	0			
6	94	0	0			
7	53	0	0			
8	93	1	0.010753			
9	135	5	0.037037			
10	110	5	0.045455			
51-5						
1	266	0	0	1871	0	0.00
2	182	0	0			
3	171	0	0			
4	168	0	0			
5	243	0	0			
6	198	0	0			
7	135	0	0			
8	228	0	0			
9	174	0	0			
10	106	0	0			
53-4						
1	185	2	0.010811	1859	3	0.00
2	207	0	0			
3	176	0	0			
4	127	0	0			
5	184	0	0			
6	179	1	0.005587			
7	245	0	0			
8	238	0	0			
9	138	0	0			
10	180	0	0			
56-4						
1	268	0	0	1845	0	0.00
2	212	0	0			
3	227	0	0			
4	147	0	0			
5	215	0	0			
6	168	0	0			
7	145	0	0			
8	162	0	0			
9	169	0	0			
10	132	0	0			

Image	Cell Total	Apoptotic Cell Total	Apoptotic Index	Total Cells/6 fields	Total Apoptotic Cells	% Apoptosis
63-3						
1	226	0	0	1808	0	0.00
2	106	0	0			
3	132	0	0			
4	141	0	0			
5	218	0	0			
6	188	0	0			
7	172	0	0			
8	206	0	0			
9	231	0	0			
10	188	0	0			
63-4						
1	90	4	0.044444	1803	39	0.02
2	231	0	0			
3	167	1	0.005988			
4	209	5	0.023923			
5	173	5	0.028902			
6	168	9	0.053571			
7	176	3	0.017045			
8	225	1	0.004444			
9	203	6	0.029557			
10	161	5	0.031056			
75-1						
1	176	2	0.011364	1818	14	0.01
2	144	2	0.013889			
3	226	0	0			
4	236	1	0.004237			
5	122	2	0.016393			
6	239	0	0			
7	153	2	0.013072			
8	150	3	0.02			
9	154	0	0			
10	218	2	0.009174			
75-4						
1	158	0	0	2136	2	0.00
2	156	0	0			
3	224	0	0			
4	202	0	0			
5	214	0	0			
6	239	0	0			
7	198	0	0			
8	324	0	0			
9	247	1	0.004049			
10	174	1	0.005747			

RRP patients taking Tamsulosin

Image	Cell Total	Apoptotic Cell Total	Apoptotic Index	Total Cells/10 fields	Total Apoptotic Cells	% Apoptosis
12097K						
1	188	1	0.005319	1954	4	0.00
2	205	1	0.004878			
3	274	0	0			
4	259	1	0.003861			
5	156	0	0			
6	174	0	0			
7	181	0	0			
8	131	0	0			
9	185	0	0			
10	201	1	0.004975			
3800F						
1	203	3	0.014778	1915	9	0.00
2	238	3	0.012605			
3	205	2	0.009756			
4	237	0	0			
5	228	0	0			
6	158	0	0			
7	174	1	0.005747			
8	201	0	0			
9	162	0	0			
10	109	0	0			
799K	Updated counting					
1	155	1	0.006452	1718	31	0.02
2	181	3	0.016575			
3	111	0	0			
4	235	9	0.038298			
5	141	3	0.021277			
6	210	2	0.009524			
7	182	2	0.010989			
8	216	6	0.027778			
9	190	3	0.015789			
10	97	2	0.020619			
1070L	Updated counting					
1	168	0	0	2162	35	0.02
2	199	0	0			
3	227	0	0			
4	256	15	0.058594			
5	218	7	0.03211			
6	171	3	0.017544			
7	191	1	0.005236			
8	264	6	0.022727			
9	273	0	0			
10	195	3	0.015385			

Image	Cell Total	Apoptotic Cell Total	Apoptotic Index	Total Cells/10 fields	Total Apoptotic Cells	% Apoptosis
8324E						
1	124	0	0	1272	3	0.00
2	127	0	0			
3	144	0	0			
4	124	0	0			
5	115	0	0			
6	161	0	0			
7	131	0	0			
8	119	1	0.008403			
9	102	1	0.009804			
10	125	1	0.008			
8324I						
1	153	0	0	1550	5	0.00
2	168	0	0			
3	179	0	0			
4	198	2	0.010101			
5	227	2	0.008811			
6	142	0	0			
7	113	0	0			
8	149	1	0.006711			
9	164	0	0			
10	57	0	0			
1070J						
1	208	0	0	1569	3	0.00
2	214	0	0			
3	209	0	0			
4	164	0	0			
5	113	0	0			
6	115	0	0			
7	151	0	0			
8	144	0	0			
9	133	3	0.022556			
10	118	0	0			
12097J						
1	123	0	0	1608	10	0.01
2	146	0	0			
3	155	0	0			
4	185	1	0.005405			
5	219	6	0.027397			
6	198	2	0.010101			
7	175	1	0.005714			
8	143	0	0			
9	136	0	0			
10	128	0	0			

Image	Cell Total	Apoptotic Cell Total	Apoptotic Index	Total Cells/10 fields	Total Apoptotic Cells	% Apoptosis
3800I						
1	175	0	0	1449	6	0.00
2	144	1	0.006944			
3	143	0	0			
4	155	1	0.006452			
5	161	2	0.012422			
6	157	0	0			
7	145	0	0			
8	161	2	0.012422			
9	132	0	0			
10	76	0	0			
799N						
1	141	0	0	1609	5	0.00
2	132	0	0			
3	187	0	0			
4	172	0	0			
5	129	0	0			
6	185	1	0.005405			
7	165	3	0.018182			
8	180	0	0			
9	161	0	0			
10	157	1	0.006369			

RRP patients taking Alfuzosin

Image	Cell Total	Apoptotic Cell Total	Apoptotic Index	Total Cells/6 fields	Total Apoptotic Cells	% Apoptosis
105719K						
1	131	1	0.007634	1465	9	0.01
2	74	3	0.040541			
3	113	0	0			
4	114	0	0			
5	144	4	0.027778			
6	197	0	0			
7	143	0	0			
8	147	0	0			
9	217	1	0.004608			
10	185	0	0			
13566J						
1	161	0	0	1438	1	0.00
2	168	0	0			
3	128	0	0			
4	195	0	0			
5	151	0	0			
6	126	0	0			
7	115	1	0.008696			
8	130	0	0			
9	136	0	0			
10	128	0	0			
13566K						
1	126	1	0.007937	1536	2	0.00
2	158	0	0			
3	124	1	0.008065			
4	140	0	0			
5	166	0	0			
6	195	0	0			
7	179	0	0			
8	181	0	0			
9	148	0	0			
10	119	0	0			
17962O						
1	98	1	0.010204	1451	17	0.01
2	226	3	0.013274			
3	205	6	0.029268			
4	195	3	0.015385			
5	138	0	0			
6	128	0	0			
7	81	0	0			
8	79	0	0			
9	189	2	0.010582			
10	112	2	0.017857			

Image	Cell Total	Apoptotic Cell Total	Apoptotic Index	Total Cells/6 fields	Total Apoptotic Cells	% Apoptosis
17962P						
1	202	0	0	1607	7	0.00
2	235	2	0.008511			
3	167	1	0.005988			
4	236	0	0			
5	149	1	0.006711			
6	104	0	0			
7	76	1	0.013158			
8	109	0	0			
9	159	0	0			
10	170	2	0.011765			
3574I						
1	193	1	0.005181	1855	3	0.00
2	224	0	0			
3	243	0	0			
4	137	0	0			
5	119	0	0			
6	206	0	0			
7	207	0	0			
8	198	1	0.005051			
9	185	1	0.005405			
10	143	0	0			
524L						
1	131	2	0.015267	1353	7	0.01
2	83	0	0			
3	129	2	0.015504			
4	151	1	0.006623			
5	143	0	0			
6	135	1	0.007407			
7	157	0	0			
8	133	1	0.007519			
9	154	0	0			
10	137	0	0			
524M						
1	192	0	0	1753	15	0.01
2	268	4	0.014925			
3	253	6	0.023715			
4	265	3	0.011321			
5	84	0	0			
6	175	0	0			
7	109	0	0			
8	157	0	0			
9	128	2	0.015625			
10	122	0	0			

Image	Cell Total	Apoptotic Cell Total	Apoptotic Index	Total Cells/6 fields	Total Apoptotic Cells	% Apoptosis
105719J						
1	119	1	0.008403	1281	8	0.01
2	107	3	0.028037			
3	121	2	0.016529			
4	134	0	0			
5	145	1	0.006897			
6	101	1	0.009901			
7	123	0	0			
8	112	0	0			
9	159	0	0			
10	160	0	0			
3574L						
1	152	0	0	1780	7	0.00
2	172	1	0.005814			
3	179	0	0			
4	174	1	0.005747			
5	170	0	0			
6	152	0	0			
7	224	3	0.013393			
8	203	2	0.009852			
9	178	0	0			
10	176	0	0			

RRP patients taking no medications

Image	Cell Total	Apoptotic Cell Total	Apoptotic Index	Total Cells/6 fields	Total Apoptotic Cells	% Apoptosis
11442O						
1	130	3	0.023077	1581	12	0.01
2	188	1	0.005319			
3	86	0	0			
4	304	1	0.003289			
5	156	0	0			
6	170	4	0.023529			
7	196	1	0.005102			
8	118	0	0			
9	94	1	0.010638			
10	139	1	0.007194			
16921N						
1	186	3	0.016129	1415	12	0.01
2	145	0	0			
3	134	0	0			
4	161	3	0.018634			
5	130	4	0.030769			
6	141	0	0			
7	143	2	0.013986			
8	120	0	0			
9	112	0	0			
10	143	0	0			
2153G						
1	108	0	0	1390	16	0.01
2	171	3	0.017544			
3	170	4	0.023529			
4	135	3	0.022222			
5	199	1	0.005025			
6	173	2	0.011561			
7	110	0	0			
8	110	0	0			
9	125	2	0.016			
10	89	1	0.011236			
4559N						
1	238	1	0.004202	1659	4	0.00
2	227	0	0			
3	134	0	0			
4	195	1	0.005128			
5	161	1	0.006211			
6	69	0	0			
7	174	0	0			
8	200	0	0			
9	135	1	0.007407			
10	126	0	0			

Image	Cell Total	Apoptotic Cell Total	Apoptotic Index	Total Cells/6 fields	Total Apoptotic Cells	% Apoptosis
5359L						
1	172	2	0.011628	1539	50	0.03
2	114	3	0.026316			
3	222	10	0.045045			
4	153	8	0.052288			
5	181	9	0.049724			
6	176	8	0.045455			
7	99	1	0.010101			
8	98	3	0.030612			
9	135	3	0.022222			
10	189	3	0.015873			
8489W						
1	91	0	0	1249	4	0.00
2	149	1	0.006711			
3	161	1	0.006211			
4	118	2	0.016949			
5	59	0	0			
6	85	0	0			
7	143	0	0			
8	146	0	0			
9	154	0	0			
10	143	0	0			
11442S						
1	110	0	0	1416	3	0.00
2	123	0	0			
3	84	0	0			
4	168	0	0			
5	207	0	0			
6	187	2	0.010695			
7	149	1	0.006711			
8	114	0	0			
9	126	0	0			
10	148	0	0			
16921M						
1	90	0	0	942	1	0.00
2	82	0	0			
3	92	0	0			
4	122	1	0.008197			
5	124	0	0			
6	106	0	0			
7	62	0	0			
8	63	0	0			
9	95	0	0			
10	106	0	0			

Appendix V – Presentations arising from this work

April 2006	"Morphometric analysis of the prostate demonstrates the importance of the loco-regional morphology to the mechanical characteristics of the gland. European Association of Urology Annual Meeting, Paris
April 2006	"The relationship between loco-regional morphology and the mechanical characteristics of benign prostate tissue" Scottish Urological Society, Edinburgh
June 2006	"Structure-property relationships for assessing tissue quality to aid diagnosis of prostate disease" Postgraduate Research Conference, Heriot-Watt University, Edinburgh
Sept 2006	"The relationship between the mechanical and morphological characteristics of hyperplastic glandular nodules and stroma British Prostate Group, Cardiff
Oct 2006	"The differences in morphological and mechanical characteristics between glandular nodules and stroma in benign prostate tissue" The Royal College of Surgeons of Edinbugh and the College of Surgeons Hong Kong, Cojoint Scientific Congress, Hong Kong
May 2008	"The relationship between alpha blocker therapy, apoptosis and the morphometric and mechanical properties of prostate tissue" American Urological Association Annual Meeting, Florida